Effect of Fiber Morphology on Composite Properties

by

Tamara Wright Knoll

Thesis submitted to the Faculty of the

Virginia Polytechnic Institute and State University

in partial fulfillment of the requirements for the degree of

Master of Science

in

Engineering Mechanics

APPROVED:

C. T. Herakovich, Chairman

C. H. Griffin, Jr.

M. J. Pindera

May 1988

Blacksburg, Virginia

Effect of Fiber Morphology on Composite Properties

by

Tamara Wright Knott

C. T. Herakovich, Chairman

Engineering Mechanics

(ABSTRACT)

The effect of the cylindrically orthotropic morphology known to exist in graphite fibers on the effective properties of a composite material was studied using the composite cylinder assemblage model. The cylindrical orthotropy of the fibers was found to have no effect on the properties of a composite with purely orthotropic fibers. For fibers with a transversely isotropic core both the size of the core and the morphology of the sheath were found to have an effect on the composite properties.

The stress states resulting in the composite cylinder for axial, radial, axial shear, and thermal loads were examined. Singular stresses were observed to occur at $r=0$ in some fibers in some load conditions. The presence of a transversely isotropic core, which must exist in a real fiber, removed this singularity.

The strength of the composite cylinder was found to depend on fiber morphology. The size of the transversely isotropic core within the fiber also affected the strength. The strength of the fiber increased with increasing transversely isotropic core size in some instances. In general, for axial loading failure is expected to be caused by fiber breakage. For radial, axial shear, and thermal loading the failure mode is fiber splitting.

Acknowledgements

This work was supported by National Science Foundation Grant MSM86113090. The author wishes to thank Prof. C. T. Herakovich for his guidance and support during the course of this work. The author would also like to thank Prof. M. J. Pindera and Prof. J. Aboudi for enhancing the author's understanding of the principles of elasticity used in this work. The understanding and patience of Profs. O. H. Griffin, Jr., M. W. Hyer, and Z. Gurdal is also greatly appreciated. The author also thanks the friends who always had a word of encouragement when things got rough, especially who also helped type the manuscript.

Last but definitely not least, the author wishes to thank her husband for his unending love, support, and assistance throught out this effort.

Table of Contents

List of Illustrations

List of Tables

1.0 Introduction and Literature Review

1.1 Introduction

Just as the properties of a composite laminate can be tailored by varying fiber angles and stacking sequence, there is evidence that the properties of the fibers themselves can be tailored by controlling the fiber morphology through the manufacturing process. In most analyses a fiber is considered to be transversely isotropic. However, if the crystals that make up the fiber are aligned by the manufacturing process, the fibers can exhibit some degree of orthotropy. In particular, graphite fibers are known to exhibit circumferential or radial orthotropy in at least part of their cross-section. This study will examine the effect of idealized fiber morphologies on the thermoelastic properties of a composite material and on the stress distributions in the fiber and surrounding matrix. The effect of morphology on composite strength will also be examined.

1.2 Literature Review

1.2.1 Morphology of graphite fibers

Graphite fibers are attractive for use in composite materials partially due to their high axial stiffness. This high axial stiffness results from the alignment of the stiff basal planes of the graphite crystals along the fiber axis during processing[1 2 3 4]. The more highly aligned the basal planes are with the fiber axis, the stiffer the fiber. The alignment of the graphite crystal basal planes along the axis of the fiber produces three distinct configurations of graphite basal planes in the transverse plane of the fiber, 1) circumferential alignment (Fig. 1a), 2) radial alignment (Fig. 1b), and 3) random orientation (Fig. 1c)[5 6 7 8 9]. Micrographs indicate that most fibers exhibit more than one type of morphology in their cross-section [5].

Although partially dependent on the fiber precursor, polyacronitrile-based fibers fiber typically have circumferential alignment of basal planes while pitch-based fibers typically have radial alignment [4 7], the orientation of the basal planes can be controlled through the processing method. For example when pitch fibers are spun, depending on the temperature at which spinning takes place, either radial or circumferential and random structures form[2]. Likewise the amount of oxygen present during early processing affects the thickness of the various structural regions within the fiber[5]. Therefore, if a specific type of morphology can be shown to provide beneficial composite properties, processing methods can be altered to produce fibers with that microstructure.

1.2.2 Methods and Models

The prediction of the effective properties of long fiber composite materials has been accomplished by several methods[10] [11]. These methods include the composite cylinder model, self consistent models, and three phase models. The effective properties of composite materials have also been analyzed using square and hexagonal arrays of fibers with both analytical and numerical techniques. Most analyses have considered the properties of the fiber and matrix phases to be isotropic or at most transversely isotropic. A few have considered a fiber with rectilinear orthotropy, but none have considered cylindrical orthotropy such as that noted in the previous section. All methods for computing effective moduli consider the composite to be an effectively transversely isotropic (or square symmetric) homogeneous material.

The composite cylinder assemblage model was developed by Hashin and Rosen[12] [13] based on Hashin's composite sphere model. In this method a composite is considered to consist of a random assemblage of composite cylinders. Each composite cylinder is composed of a circular fiber of radius b surrounded by a matrix annulus of outer radius c. The volume of a composite is filled with these composite cylinders, each having the same fiber-matrix ratio b/c, but various sizes such that the entire volume of the composite is filled with non-overlapping composite cylinders. The determination of effective moduli is accomplished by defining the elastic moduli in terms of strain energy and determining the upper and lower bounds on the strain energy for simple applied average stress and strain fields. Equivalently, the effective moduli are determined through the requirement that a composite cylinder within the composite and a similar cylinder of the equivalent homogeneous medium possess the same amount of stored energy for a given load state. In other words, the average stress and strain in the composite are equal to the stress and strain in the homogeneous material for a given load. For four of the five fiber moduli needed to fully characterize the effective composite material the upper and lower bounds on the strain energy of the composite coincide and exact

expressions for the moduli are obtained. Only the bounds on the fifth property can be determined with this model.

The self-consistent model is often applied to determine the effective properties of composite materials. Devised by Hershey and Kroner (see [11]) for crystalline materials, Hill[14] and Budiansky[15] extended the theory to multiphase materials. In this method the composite is analyzed by lumping one phase into an inclusion in an infinite body of the effective homogeneous material. The average stress and strain conditions in the inclusion, in terms of the effective moduli of the composite and the phase properties, are determined by applying uniform stress and stain to the system. This is repeated for each phase. Once the average conditions of stress and strain are known the effective moduli can be calculated. This method is not particularly successful for multiphase materials, but is often used due to its simplicity.

An extension of the self consistent model, the three-phase model, has been used with success[16] [17]. The composite is analyzed by considering a circular fiber surrounded by an annulus of matrix imbedded in an infinite body of the effective material. The effective moduli are determined by requiring that the effective homogeneous medium contain the same average stress and strain as the model for a given load. This is accomplished using Eshelby's result that the strain energy of a homogeneous medium with an inclusion can be determined from the strain energy of the same medium without an inclusion and the tractions and displacements in the two media. Christensen and Lo[16] used this method to determine the transverse shear modulus of a composite, a property that Hashin was not able to determine exactly with the composite cylinder assemblage.

Other methods of determining effective moduli model the composite as a square or hexagonal array of fibers in matrix. Many of these analyses resort to numerical techniques to solve the problem. Aboudi[18], however, uses a high order continuum theory in a square array to analytically determine the effective moduli. For fibers with square cross-section the first order reduction of the theory yields the elastic properties of the composite. The theory is based on

the expansion of displacements within a subcell (the repeating cell, which is one quarter of a square fiber surrounded by a square of matrix, is divided into three subcells of matrix and one of fiber) are expressed in terms of distance from the center of the subcell. The average behavior of the composite under various loads can be determined and from this five of the six moduli needed to characterize the effective square symmetric can be material computed. The geometry of the model provides an easy means to analyze rectilinear anisotropy. Cylindrical anisotropy, however, is not easily handled by this model.

Numerical analyses include work by Adams and Doner[19 20]. They study a doubly periodic array of circular filaments in an infinite matrix. Solutions to displacement boundary value problems are obtained with finite difference techniques and result in the determination of the effective moduli of the composite.

1.3 Approach

This study uses the composite cylinder assemblage model developed by Hashin[13 12] to investigate the effect of fiber morphology on the material properties of a composite. This method is chosen as a first approach due to its simple yet effective ability to predict the effective moduli of composites with transversely isotropic fibers. Because of the model's cylindrical geometry the method can be easily adapted to account for the cylindrical orthotropy examined in this work. Recall that in this method a unidirectional composite material is modeled as an assemblage of composite cylinders. The center of each cylinder is a fiber, exhibiting morphology similar to one of the types shown in Figure 1. Each fiber is surrounded by a matrix annulus. The volume ratio of fiber to matrix in each composite cylinder is constant and equal to the fiber volume fraction of the overall composite. The volume of the composite

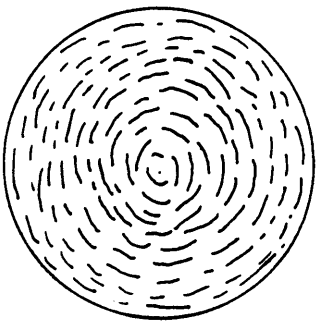

a) Circumferentially Orthotropic

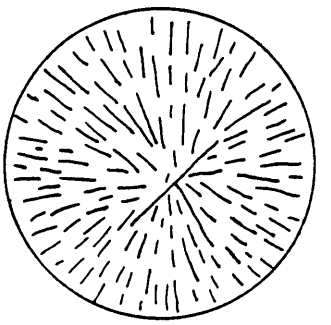

b) Radially Orthotropic

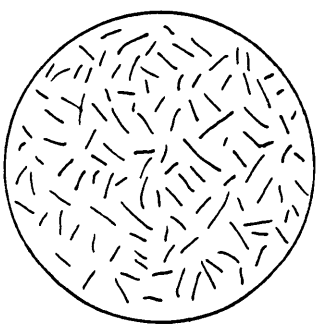

c) Transversely Isotropic

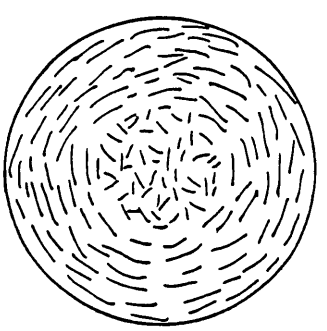

d) Circumferentially Orthotropic with Transversely Isotropic Core

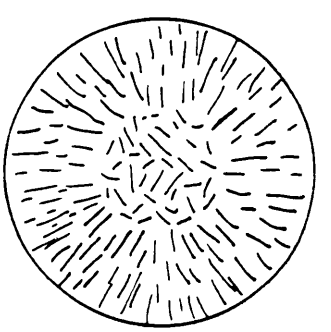

e) Radially Orthotropic with Transversely Isotropic Core

Figure 1. Transverse Microstructure of Graphite Fibers

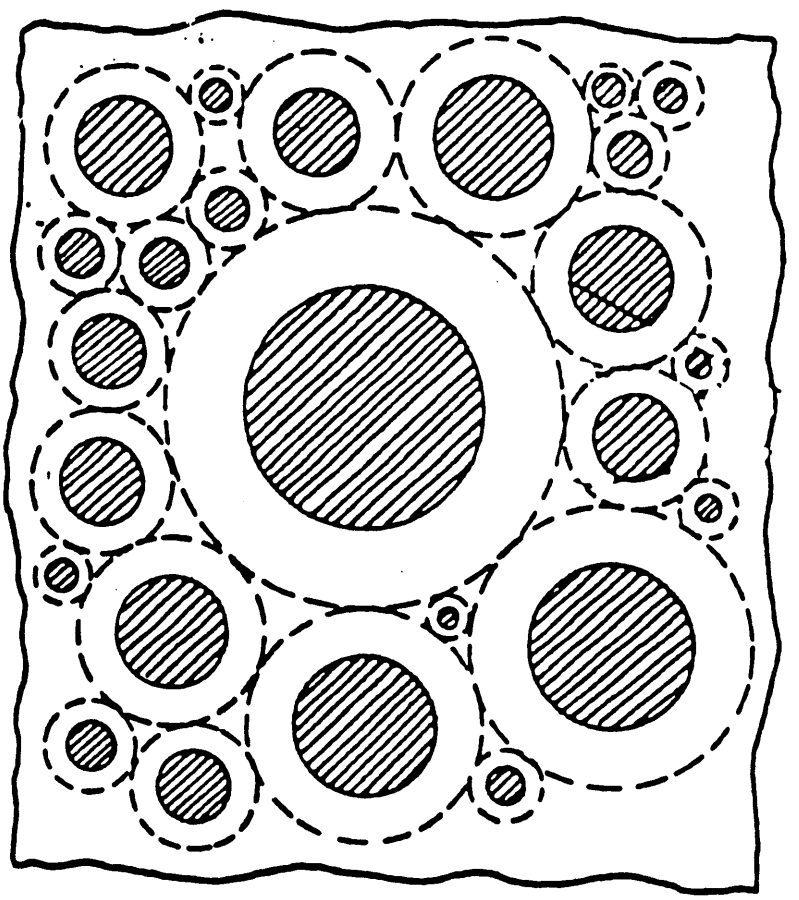

Figure 2. The Composite Cylinder Assemblage Model [13]

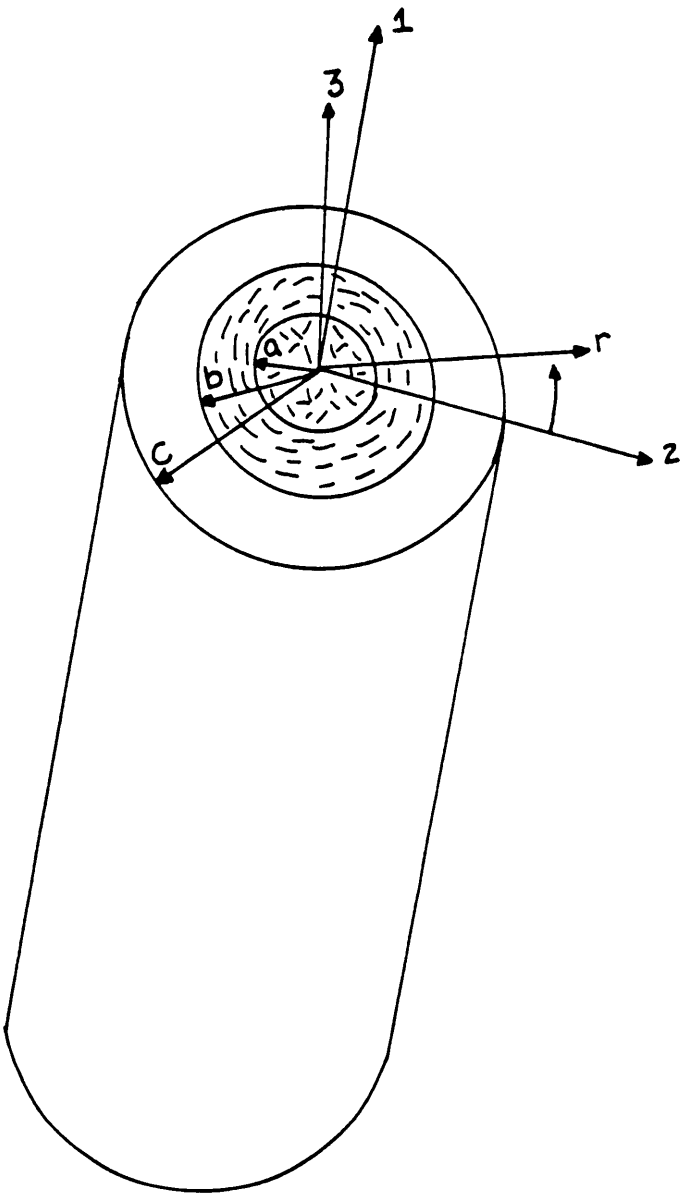

Figure 3. Composite Cylinder Geometry and Coordinate System

material is filled with composite cylinders of various sizes, such that in the limit, the entire volume of the composite is filled (Figure 2). The randomness of this arrangement dictates that the overall composite material exhibit transverse isotropy. As such, five independent elastic properties and two thermal properties are needed to fully characterize the material.

The analysis of the effect of fiber morphology on the effective moduli will be simplified by considering only the simple morphologies shown in Figures 1a, 1b, and 1c, in the determination of expressions for the moduli. The morphology of a fiber is determined by the orientation of the crystal basal planes. In this analysis the stiff basal plane of the graphite crystal is always considered to be parallel to the longitudinal axis of the fiber. In the transverse plane of the fiber the basal planes are either arranged circumferentially (Fig. 1a), radially (Fig. 1b), or randomly (Fig. 1c). If the basal planes are oriented circumferentially, as in a circumferentially orthotropic (CO) fiber, $E_\theta > E_r$, while if the basal planes are oriented radially, as in a radial orthotropic (RO) fiber, $E_r > E_\theta$. In the transversely isotropic (TI) fiber the basal planes are randomly oriented in the transverse plane and $E_r = E_\theta$. For the purpose of this study the properties of the basal plane are taken to be the same in all fibers types. The properties transverse to the basal plane are also constant in this study, but different than the basal in-plane properties. Thus E_r, E_θ, and E_x of the RO fiber will equal E_θ, E_r , and E_x of the CO fiber, respectively. The axial properties of a TI fiber are taken to be the same as the axial properties of the CO and RO fibers. The transverse properties are taken as an average of the transverse properties of the CO and RO fibers. For comparison, three TI fibers are considered, having different transverse properties. The material properties used for all five fibers are given in Table 1. These are ideal properties for a graphite fiber. Since transverse and shear properties are not readily available, the properties used in this study were chosen to emphasize the geometric relationship between the different crystal arrangements in the fibers, and to be thermodynamically admissible. The shear modulus of the basal plane is determined using the relation between E, ν, and G for an isotropic material since the basal plane is itself isotropic.

The elasticity solution used to determine the effective moduli of the composite cylinder assemblage also yields expressions for the stresses in each of the phases of the composite cylinder. The stress distributions for the various ideal morphologies are discussed. Actual fibers, however, do not possess the simple morphologies used in the determination of the expression for the thermoelastic moduli of composites with orthotropic fibers, rather one fiber will exhibit layers of the different morphologies, as shown in Figs. 1d,e. Therefore the effect of a transversely isotropic core within the orthotropic fiber on the effective moduli and the stress distributions is considered. The relative strength of the composites due to fiber morphology and based on an analysis of the stress distributions resulting in the composite cylinders is also made.

2.0 Effective Moduli

2.1 Orthotropic Elasticity

The effective elastic and thermal properties of the transversely isotropic composite are determined from the average stress and strain states in the composite for appropriate loading conditions The applied conditions necessary to determine the moduli fall into two categories, axisymmetric loading and axial shear loading. For both types of loading the average states of stress and strain are determined from the elasticity solution. For axisymmetric loading the solution is determined using a displacement formulation and examining all the equations of elasticity. The shear solution is obtained using a semi-inverse method in which the form of the displacements is assumed.

2.1.1 Solution for Axisymmetric Loading

The elasticity formulation used to study the axisymmetric problem follows the works of Lekhnitskii [21] [22], Cohen et al. [23] [24] [25], Rousseau and Hyer [26], and Avery and Herakovich [27].

Lekhnitskii discusses the form of the solution for a variety of loading conditions. Cohen et. al and Rousseau and Hyer provide explicit forms of the solution for laminated composite tubes. Avery and Herakovich examine the solution for composite materials with orthotropic and transversely isotropic phases.

The solution to the problem of a composite cylinder subjected to an axisymmetric loading is facilitated by examining the equations of elasticity in cylindrical coordinates. The displacements in the axial, circumferential, and radial directions u,v,and w, respectively, are in general functions of x, θ, and r. However, in the axisymmetric case, displacements are independent of θ. In addition away from the ends it can be assumed that the radial displacement is a function of r only. Thus,

$$u = u(x,r) \tag{2.1.1a}$$

$$v = v(x,r) \tag{2.1.1b]}$$

$$w = w(r). \tag{2.1.1c}$$

Using the assumption of generalized plane strain, stresses and strains are independent of the axial coordinate, as well as being independent of θ due to the axisymmetry. Thus, the strain-displacement relations for the axisymmetric loading reduce to

$$\varepsilon_x = \frac{\partial u}{\partial x} \tag{2.1.2a}$$

$$\varepsilon_\theta = \frac{w}{r} \tag{2.1.2b}$$

$$\varepsilon_r = \frac{\partial w}{\partial r} \tag{2.1.2c}$$

$$\gamma_{\theta r} = \frac{\partial v}{\partial r} - \frac{v}{r} \tag{2.1.2d}$$

$$\gamma_{xr} = \frac{\partial u}{\partial r} \tag{2.1.2e}$$

$$\gamma_{x\theta} = \frac{\partial v}{\partial x}. \tag{2.1.2f}$$

Axisymmetric loading causes three of the compatibility equations to be identically satisfied. The remaining three simplify to

$$\frac{\partial^2 \varepsilon_x}{\partial r^2} = 0 \tag{2.1.3a}$$

$$\frac{1}{r}\ \frac{\partial \varepsilon_x}{\partial r} = 0 \tag{2.1.3b}$$

$$\frac{\partial}{\partial r}\left[\frac{1}{r}\ \frac{\partial}{\partial r}\ (r\gamma_{x\theta})\right] = 0. \tag{2.1.3c}$$

The thermoelastic stress-strain relation for an orthotropic material whose principal material directions are x, θ, and r, is given by

$$\begin{Bmatrix} \sigma_x \\ \sigma_\theta \\ \sigma_r \\ \tau_{\theta r} \\ \tau_{xr} \\ \tau_{x\theta} \end{Bmatrix} = \begin{bmatrix} C_{xx} & C_{x\theta} & C_{xr} & 0 & 0 & 0 \\ C_{x\theta} & C_{\theta\theta} & C_{\theta r} & 0 & 0 & 0 \\ C_{xr} & C_{\theta r} & C_{rr} & 0 & 0 & 0 \\ 0 & 0 & 0 & G_{\theta r} & 0 & 0 \\ 0 & 0 & 0 & 0 & G_{xr} & 0 \\ 0 & 0 & 0 & 0 & 0 & G_{x\theta} \end{bmatrix} \begin{Bmatrix} \varepsilon_x - \alpha_x \Delta T \\ \varepsilon_\theta - \alpha_\theta \Delta T \\ \varepsilon_r - \alpha_r \Delta T \\ \gamma_{\theta r} \\ \gamma_{xr} \\ \gamma_{x\theta} \end{Bmatrix} \tag{2.1.4}$$

where C_{ij} are the stiffness coefficients, α_i are the coefficients of thermal expansion, and ΔT is a uniform temperature change. Due to the axisymmetric condition the equilibrium equations in cylindrical coordinates simplify to

$$\frac{\partial \sigma_r}{\partial r} + \frac{\sigma_r - \sigma_\theta}{r} = 0 \tag{2.1.5a}$$

$$\frac{\partial \tau_{\theta r}}{\partial r} + \frac{2\tau_{\theta r}}{r} = 0 \qquad (2.1.5b)$$

$$\frac{\partial \tau_{xr}}{\partial r} + \frac{\tau_{xr}}{r} = 0. \qquad (2.1.5c)$$

Examining these equations of elasticity, it is required from Equations 2.1.3a and 2.1.3b that

$$\varepsilon_x(r) = \varepsilon^o. \qquad (2.1.6)$$

From equations 2.1.3c and the fact that $\frac{\partial \varepsilon_i}{\partial x} = 0$,

$$\gamma_{x\theta} = Cr + \frac{D}{r}. \qquad (2.1.7)$$

Integrating 2.1.2a and 2.1.2f yields

$$u(x,r) = \varepsilon^o x + f(r) \qquad (2.1.8)$$

and,

$$v(x,r) = \left(Cr + \frac{D}{r}\right)x + p(r). \qquad (2.1.9)$$

The equilibrium equations 2.1.5b and 2.1.5c integrate to

$$\tau_{\theta r} = \frac{E}{r^2} \qquad (2.1.10)$$

and,

$$\tau_{xr} = \frac{F}{r}. \qquad (2.1.11)$$

Using the strain displacement relation 2.1.2e and the stress strain relations 2.1.4, f and p in 2.1.8 and 2.1.9 are found to be

$$f(r) = S_{55}F\,\ell n\, r + F_1 \tag{2.1.12}$$

$$p(r) = \frac{-S_{44}E}{r^2} + P_1 r \tag{2.1.13}$$

where F_1 and P_1 represent rigid body displacement and rotation, respectively, and S_{ij} are elements of the compliance matrix (i.e., the inverse of the stiffness matrix given in equation 2.4). Thus the expressions for the axial and circumferential displacements are

$$u(x,r) = \varepsilon^{o}x + S_{55}F\,\ell n\, r + F_1 \tag{2.1.14}$$

$$v(x,r) = \gamma^{o}_{rx} - \frac{S_{44}E}{r^2} + P_1 r. \tag{2.1.15}$$

Expressing the stresses in terms of displacements, the first equilibrium equation 2.1.5a becomes

$$C_{rr}\left[\frac{\partial^2 w}{\partial r^2} + \frac{1}{r}\,\frac{\partial w}{\partial r}\right] - C_{\theta\theta}\,\frac{w}{r^2} = \frac{1}{r}\,(C_{x\theta} - C_{xr})\varepsilon^{0} + \frac{1}{r}\,(C_{rj} - C_{\theta j})\,\alpha_j \Delta T. \tag{2.1.16}$$

The repeated subscripts i and j are summed over x, θ, and r. The solution to this equation as discussed by Avery and Herakovich[27] is:

a) for an orthotropic material ($C_{\theta\theta} \neq C_{rr}$)

$$w(r) = A_1 r^{\lambda} + A_2 r^{-\lambda} + H_1 \varepsilon^{o} r + H_2 \Delta T r \tag{2.1.17a}$$

where,

$$H_1 = \frac{C_{x\theta} - C_{xr}}{C_{rr} - C_{\theta\theta}} \tag{2.1.17b}$$

$$H_2 = \frac{(C_{rj} - C_{\theta j})\alpha_j}{C_{rr} - C_{\theta\theta}}, \tag{2.1.17c}$$

b) for a transversely isotropic material ($C_{\theta\theta} = C_{rr}$)

$$w(r) = A_1 r^{\lambda} + A_2 r^{-\lambda} + G_1 \varepsilon^0 r \ell n\, r + G_2 \Delta T\, r \ell n\, r \tag{2.1.18a}$$

where,

$$G_1 = \frac{C_{x\theta} - C_{xr}}{2C_{\theta\theta}} \tag{2.1.18b}$$

$$G_2 = \frac{(C_{ri} - C_{\theta i})\alpha_i}{2C_{\theta\theta}}, \tag{2.1.18c}$$

and for both types of fibers,

$$\lambda = \sqrt{\frac{C_{\theta\theta}}{C_{rr}}}. \tag{2.1.19}$$

For the composite cylinder the solutions for u(x,r), v(x,r), w(r), $\tau_{\theta r}(r)$, and $\tau_{xr}(r)$ require a different set of constants F, E, F_1 , P_1 , A_1 , A_2 , ε^o , and γ^o in each phase of fiber and matrix. In addition λ may be different in each phase. Thus for the kth phase the displacements are as follows:

$$u^k(x,r) = \varepsilon^{ok} x + S^k_{55} F^k \ell n\, r + F^k_1 \tag{2.1.20}$$

$$v^k(x,r) = \gamma^{ok} xr - \frac{S^k_{44} E^k}{2r} + P^k_1 \tag{2.1.21}$$

$$w^k(r) = A^k_1 r^{\lambda_k} + A^k_2 r^{-\lambda_k} + H^k_1 \varepsilon^{ok} r + H^k_2 \Delta T r \tag{2.1.22a}$$

where,

$$H^k_1 = \frac{C^k_{x\theta} - C^k_{xr}}{C^k_{rr} - C^k_{\theta\theta}} \tag{2.1.22b}$$

$$H_2^k = \frac{\left(C_{ri}^k - C_{\theta i}^k\right)\alpha_i^k}{C_{rr}^k - C_{\theta\theta}^k} \tag{2.1.22c}$$

if the phase is orthotropic, or

$$w^k(r) = A_1^k r^{\lambda_k} + A_2^k r^{-\lambda k} + G_1^k \varepsilon^k\, r\, \ell n\, r + G_2^k \Delta T\, r\, \ell n\, r \tag{2.1.23a}$$

where,

$$G_1^k = \frac{C_{x\theta}^k - C_{xr}^k}{2C_{\theta\theta}^k} \tag{2.1.23b}$$

$$G_2^k = \frac{\left(C_{ri}^k - C_{\theta i}^k\right)\alpha_i^k}{2C_{\theta\theta}^k} \tag{2.1.23c}$$

if the layer is transversely isotropic, with

$$\lambda_k = \sqrt{\frac{C_{\theta\theta}^k}{C_{rr}^k}} \tag{2.1.24}$$

for either type of material.

The stresses are

$$\sigma_i = A_i^k\left(C_{i\theta}^k + C_{ir}^k\lambda_k\right)r^{\lambda_k - 1} + A_2^k\left(C_{i\theta}^k - C_{ir}^k\lambda_k\right)r^{-\lambda_k - 1} + L_i^k \varepsilon^{ok} + N_i^k \Delta T \tag{2.1.25a}$$

where,

$$L_i^k = C_{ix}^k + H_1^k\left(C_{i\theta}^k + C_{ir}^k\right) \tag{2.1.25b}$$

$$N_i^k = H_2^k\left(C_{i\theta}^k + C_{ir}^k\right) - C_{ij}^k\alpha_j^k \tag{2.1.25c}$$

if the layer is orthotropic, and

$$\sigma_i^k = A_1^k\left(C_{i\theta}^k + C_{ir}^k\right) + A_2^k\left(C_{i\theta}^k - C_{ir}^k\right)\frac{1}{r^2} + C_{ix}^k\varepsilon^{ok} - C_{ij}^k\alpha_j^k\Delta T \qquad (2.1.26)$$

if the layer is transversely isotropic, where $i = x, \theta, r$, and

$$\tau_{\theta r}^k = \frac{E^k}{r^2} \qquad (2.1.27)$$

$$\tau_{xr}^k = \frac{F^k}{r} \qquad (2.1.28)$$

$$\tau_{x\theta}^k = G_{x\theta}^k\gamma^{ok}r \qquad (2.1.29)$$

Boundary conditions and continuity conditions for each axisymmetric loading case of interest can be applied to solve for the unknowns, and complete the solution of the axisymmetric elasticity problem.

2.1.2 Solution for Axial Shear Loading

Also of interest in this study is the application of an axial shear loading. This problem is solved using a semi-inverse method, in the cartesian coordinate system. Following Hashin[13], displacements are assumed to have the form:

$$u_1 = u(x_2, x_3) \qquad (2.1.30a)$$

$$u_2 = \varepsilon_{12}^o x_1 \qquad (2.1.30b)$$

$$u_3 = \varepsilon_{13}^o x_1. \qquad (2.1.30c)$$

A function ϕ is then defined such that

$$u_1 = \phi - \varepsilon^{o}_{12} x_2 - \varepsilon^{o}_{13} x_3. \tag{2.1.31}$$

From the strain-displacement relations the strains are thus

$$\varepsilon_{11} = \varepsilon_{22} = \varepsilon_{33} = \gamma_{23} = 0 \tag{2.1.32a}$$

$$\gamma_{12} = \frac{\partial \phi}{\partial x_2} \tag{2.1.32b}$$

and

$$\gamma_{13} = \frac{\partial \phi}{\partial x_3}. \tag{2.1.32c}$$

The stresses can be determined from the strains using Hooke's law in cartesian coordinates. Note that for a circumferentially or radially orthotropic material Hooke's law is given by

$$\begin{Bmatrix} \sigma_1 \\ \sigma_2 \\ \sigma_3 \\ \sigma_{12} \\ \sigma_{23} \\ \sigma_{31} \end{Bmatrix} = \begin{bmatrix} C_{11} & C_{12} & C_{13} & 0 & C_{15} & 0 \\ C_{12} & C_{22} & C_{23} & 0 & C_{25} & 0 \\ C_{13} & C_{23} & C_{33} & 0 & C_{35} & 0 \\ 0 & 0 & 0 & C_{44} & 0 & C_{46} \\ C_{15} & C_{25} & C_{35} & 0 & C_{55} & 0 \\ 0 & 0 & 0 & C_{46} & 0 & C_{66} \end{bmatrix} \begin{Bmatrix} 0 \\ 0 \\ 0 \\ \dfrac{\partial \phi}{\partial x_2} \\ 0 \\ \dfrac{\partial \phi}{\partial x_3} \end{Bmatrix} \tag{2.1.33}$$

where each term of the stiffness matrix $\overline{C}_{ijkl}$ in the cartesian coordinate system is a function of the stiffnesses C_{mnpr} in the r-θ coordinate system and of θ, as determined by the tensor transformation

$$\overline{C}_{ijkl} = a_{im} a_{jn} a_{kp} a_{lr} C_{mnpr}. \tag{2.1.34}$$

For an isotropic or transversely isotropic material the stiffness matrix is the same in the cartesian and cylindrical coordinate systems, with $C_{46} = C_{15} = C_{25} = C_{35} = 0$, and $C_{44} = C_{66} = G_a$.

From 2.1.33, the non-zero stresses for an orthotropic material with the applied boundary conditions 2.1.30, are

$$\sigma_{12} = C_{44} \frac{\partial \phi}{\partial x_2} + C_{46} \frac{\partial \phi}{\partial x_3} \tag{2.1.35}$$

and,

$$\sigma_{13} = C_{46} \frac{\partial \phi}{\partial x_2} + C_{66} \frac{\partial \phi}{\partial x_3} . \tag{2.1.36}$$

For an isotropic or transversely isotropic material the non-zero stresses are

$$\sigma_{12} = G_a \frac{\partial \phi}{\partial x_2} \tag{2.1.37}$$

and,

$$\sigma_{13} = G_a \frac{\partial \phi}{\partial x_3} . \tag{2.1.38}$$

Because the normal (σ_{11}, σ_{22}, σ_{33}) and transverse shear (σ_{23}) stresses are zero, the only equilibrium equation not identically satisfied is

$$\frac{\partial \sigma_{12}}{\partial x_2} + \frac{\partial \sigma_{13}}{\partial x_3} = 0. \tag{2.1.39}$$

For an orthotropic material, when expressions 2.1.35 and 2.1.36 are substituted for the stresses, this equilibrium equation becomes

$$\frac{\partial}{\partial x_2}\left(C_{44}\frac{\partial \phi}{\partial x_2}+C_{46}\frac{\partial \phi}{\partial x_3}\right)+\frac{\partial}{\partial x_3}\left(C_{46}\frac{\partial \phi}{\partial x_2}+C_{66}\frac{\partial \phi}{\partial x_3}\right)=0. \qquad (2.1.40)$$

Since C_{44}, C_{46}, and C_{66} are functions of θ , they are also functions of x_2 and x_3. After taking derivatives of the stresses and transforming the resulting equation into cylindrical coordinates the equilibrium equation for an orthotropic material becomes

$$G_{x\theta}\frac{\partial^2 \phi}{\partial r^2}+\frac{1}{r}\,G_{x\theta}\frac{\partial \phi}{\partial r}+\frac{1}{r^2}\,G_{xr}\frac{\partial^2 \phi}{\partial \theta^2}=0 \qquad (2.1.41)$$

For a transversely isotropic material, substituting from expressions 2.1.37 and 2.1.38, the equilibrium equation becomes

$$\frac{\partial^2 \phi}{\partial x_2^2}+\frac{\partial^2 \phi}{\partial x_3^2}=0. \qquad (2.1.42)$$

In cylindrical coordinates this is written

$$\frac{\partial^2 \phi}{\partial r^2}+\frac{1}{r}\,\frac{\partial \phi}{\partial r}+\frac{1}{r^2}\,\frac{\partial^2 \phi}{\partial \theta^2}=0. \qquad (2.1.43)$$

Using a separation of variables technique, the equilibrium equation can be solved for either type of material. For a transversely isotropic material the solution has the form

$$\phi(r,\theta)=a_o+\sum_{n=1}^{\infty}(A_n r^n+B_n r^{-n})(C_n \sin(n\theta)+D_n \cos(n\theta)) \qquad (2.1.44)$$

and for a cylindrically orthotropic material the solution is

$$\phi(r,\theta) = a_o + \sum_{n=1}^{\infty}\left(A_n r^{\gamma n} + B_n r^{-\gamma n}\right)\left(C_n \sin(n\theta) + D_n \cos(n\theta)\right). \qquad (2.1.45a)$$

where,

$$\gamma = \sqrt{\frac{G_{xr}}{G_{x\theta}}}. \qquad (2.1.45b)$$

The elasticity problem for axial shear loading in a multi-layered cylindrical body is therefore defined by the assumed displacements

$$u_1^k = \phi^k - \varepsilon_{12}^{ok} x_2 - \varepsilon_{13}^{ok} x_3 \qquad (2.1.46)$$

$$u_2^k = \varepsilon_{12}^{ok} x_1 \qquad (2.1.47)$$

$$u_3^k = \varepsilon_{13}^{ok} x_1 \qquad (2.1.48)$$

and,

$$\phi^k(r,\theta) = a_o^k + \sum_{n=1}^{\infty}\left(A_n^k r^n + B_n^k r^{-n}\right)\left(C_n^k \sin(n\theta) + D_n^k \cos(n\theta)\right) \qquad (2.1.49)$$

in transversely isotropic materials, and

$$\phi^k(r,\theta) = a_o^k + \sum_{n=1}^{\infty}\left(A_n^k r^{\gamma_n^k} + B_n^k r^{-\gamma_n^k}\right)\left(C_n^k \sin(n\theta) + D_n^k \cos(n\theta)\right) \qquad (2.1.50a)$$

$$\gamma^k = \sqrt{\frac{G^k_{xr}}{G^k_{x\theta}}} \tag{2.1.50b}$$

in cylindrically orthotropic materials, where k indicates the layer. Boundary conditions on the surface and continuity conditions between the layers complete the problem.

2.2 Axial Modulus

In order to determine the axial modulus of the composite material, an axial extension is applied to a single composite cylinder with fiber radius b, and outer radius c (see Figure 3) The boundary conditions are

$$u_x = \varepsilon^o x \tag{2.2.1}$$

$$T_r(c) = T_\theta(c) = 0 \tag{2.2.2}$$

where T_i is the boundary traction in the *i* direction. From Section 2.1.1, the equations of elasticity are

$$u^m(x,r) = \varepsilon^m x + S^m_{55} F^m \ell n\, r + F^m_1 \tag{2.2.3}$$

$$v^m(x,r) = \gamma^m x r - \frac{S^m_{44} E^m}{2r} + D^m_1 \tag{2.2.4}$$

$$\begin{aligned} w^m(r) = {} & A^m_1 r^{\lambda m} + A^m_2 r^{-\lambda m} + G^m_1 \varepsilon^{om}\, r \ell n\, r \\ & + G^m_2 \Delta T\, r \ell n\, r \end{aligned} \tag{2.2.5}$$

$$\tau^m_{\theta r} = \frac{E^m}{r^2} \tag{2.2.6}$$

$$\tau_{xr}^{m} = \frac{F^{m}}{r} \tag{2.2.7}$$

and,

$$u^{f}(x,r) = \varepsilon^{of}x + S_{55}^{f}F^{1}\,\ell n\, r + F_{1}^{f} \tag{2.2.8}$$

$$v^{f}(x,r) = \gamma^{of}xr - \frac{S_{44}^{f}E^{f}}{2r} + D_{1}^{f} \tag{2.2.9}$$

$$w^{f}(r) = A_{1}^{f}r^{\lambda f} + A_{2}^{f}r^{-\lambda f} + H_{1}^{f}\varepsilon^{of}r + H_{2}^{f}\Delta Tr \tag{2.2.10}$$

$$\tau_{\theta r}^{f} = \frac{E^{f}}{r^{2}} \tag{2.2.11}$$

$$\tau_{xr}^{f} = \frac{F^{f}}{r} \tag{2.2.12}$$

where m and f signify matrix and fiber, respectively, and where G_1^m, G_2^m, H_1^f, and H_2^f are defined by 2.1.17a,b and 2.1.18a,b. Stress continuity at the interface between the fiber and matrix requires,

$$\sigma_{r}^{m}(b) = \sigma_{r}^{f}(b) \tag{2.2.13a}$$

$$\tau_{\theta r}^{m}(b) = \tau_{\theta r}^{f}(b) \tag{2.2.13b}$$

$$\tau_{xr}^{m}(b) = \tau_{xr}^{f}(b). \tag{2.2.13c}$$

and displacement continuity requires

$$u^{m}(x,b) = u^{f}(x,b) \tag{2.2.14a}$$

$$v^{m}(x,b) = v^{m}(x,b) \tag{2.2.14b}$$

$$w^{m}(b) = w^{f}(b). \tag{2.2.14c}$$

In determining the axial modulus no temperature change is applied, thus $\Delta T = 0$. From the boundary conditions 2.2.1 and 2.2.2 and the continuity conditions 2.2.13b,c,

$$F^f = F^m = E^f = E^m = 0. \tag{2.2.15}$$

From 2.2.14a with 2.2.3, 2.2.8, and 2.2.15

$$\varepsilon^{om}x + F_1^m = \varepsilon^{of}x + F_1^f. \tag{2.2.16}$$

Thus,

$$\varepsilon^{om} = \varepsilon^{of} = \varepsilon^o \tag{2.2.17}$$

is the constant axial strain, and $F_1^m = F_1^f$ can be taken as zero if rigid body displacements are ignored. Likewise, from Eqns 2.2.14b, 2.2.4, 2.2.9, and 2.2.15

$$\gamma^{om} = \gamma^{of} = \gamma^o. \tag{2.2.18}$$

Eliminating rigid body rotation, $D_1^m = D_1^f = 0$. In the case of axial extension the net torsion on the cross-section A of the composite cylinder is 0 thus

$$\int_A \tau_{x\theta} r^2 d\theta dr = 0 \tag{2.2.19a}$$

and therefore,

$$\gamma^o = 0 \tag{2.2.19b}$$

The remaining boundary conditions to be satisfied are (for a solid fiber):

1) finite displacements at r=0

$$A_1^f r^\lambda + A_2^f r^{-\lambda} + H_1^f \varepsilon^o r \quad \text{is finite} \tag{2.2.20}$$

2) continuity of radial stress at r=b

$$A_1^m(C_{\theta r}^m + C_{rr}^m) + A_2^m(C_{\theta r}^m - C_{rr}^m)\frac{1}{b^2} + C_{xr}^m\varepsilon^o$$
$$= A_1^f(C_{\theta r}^f + C_{rr}^f\lambda)b^{\lambda-1} + A_2^f(C_{\theta r}^f - C_{rr}^f\lambda)r^{-\lambda-1} + L_r^f\varepsilon^o \qquad (2.2.21)$$

where

$$L_i^f = C_{ix}^f + H_1^f(C_{i\theta}^f + C_{ir}^f) \qquad (2.2.22)$$

3) continuity of radial displacements at r=b

$$A_1^m b + A_2^m\frac{1}{b} = A_1^f b^{\lambda} + A_2^f b^{-\lambda} + H_1^f\varepsilon^o b \qquad (2.2.23)$$

and

4) stress free boundary conditions at r=c

$$A_1^m(C_{\theta r}^m + C_{rr}^m) + A_2^m(C_{\theta r}^m - C_{rr}^m)\frac{1}{c^2} + C_{xr}^m\varepsilon^o = 0. \qquad (2.2.24)$$

From 2.2.20 it is concluded that

$$A_2^f = 0 \qquad (2.2.25)$$

for both transversely isotropic and transversely orthotropic solid fibers.

Solving the system of equations that result from the remaining boundary and continuity conditions we find that

$$A_1^f = \frac{1}{DET}\left\{ -\frac{C_{xr}^m \varepsilon^o}{b}\left[(C_{\theta r}^m - C_{rr}^m) - (C_{\theta r}^m + C_{rr}^m)\right] \right.$$
$$- \frac{(C_{\theta r}^m + C_{rr}^m)\varepsilon^o}{b}\left[H_1^f(C_{\theta r}^m - C_{rr}^m) - \left(C_{xr}^f + H_1^f\left(C_{\theta r}^f + C_{rr}^f\right)\right) + C_{xr}^m\right] \qquad (2.2.26)$$
$$\left. + \frac{(C_{\theta r}^m - C_{rr}^m)b^\lambda}{c^2}\left[H_1^f(C_{\theta r}^m + C_{rr}^m) - \left(C_{xr}^f + H_1^f\left(C_{\theta r}^f + C_{rr}^f\right)\right) + C_{xr}^m\right]\right\}$$

$$A_1^m = \frac{1}{DET}\left\{ \frac{-C_{xr}^m \varepsilon^o b^\lambda}{b^2}\left[(C_{\theta r}^m - C_{rr}^m) - (C_{\theta r}^m + C_{rr}^m)\right] \right.$$
$$\left. \frac{-(C_{\theta r}^m - C_{rr}^m)\varepsilon^o b^\lambda}{c^2}\left[-\left(C_{xr}^f + H_1^f\left(C_{\theta r}^f + C_{rr}^f\right)\right) + C_{xr}^m + H_1^f\left(C_{\theta r}^f + C_{rr}^f\lambda\right)\right]\right\} \qquad (2.2.27)$$

and,

$$A_2^m = \frac{1}{DET}\left\{-(C_{r\theta}^m + C_{rr}^m)\varepsilon^o b^\lambda\left[-\left(C_{rx}^f + H_1^f\left(C_{r\theta}^f + C_{rr}^f\right)\right) + C_{rx}^m + H_1^f\left(C_{r\theta}^f + C_{rr}^f\lambda\right)\right]\right.$$
$$\left. - C_{rx}^m \varepsilon^o b^\lambda\left[-(C_{r\theta}^m + C_{rr}^m) + \left(C_{r\theta}^f + C_{rr}^f\lambda\right)\right]\right\} \qquad (2.2.28)$$

where,

$$DET = \frac{-(C_{\theta r}^m + C_{rr}^m)b^\lambda}{b^2}\left[-(C_{\theta r}^m - C_{rr}^m) + \left(C_{\theta r}^f + C_{rr}^f\lambda\right)\right]$$
$$+ \frac{(C_{\theta r}^m - C_{rr}^m)b^\lambda}{c^2}\left[-(C_{\theta r}^m + C_{rr}^m) + \left(C_{\theta r}^f + C_{rr}^f\lambda\right)\right] \qquad (2.2.29)$$

The average axial stress in the composite cylinder can now be determined. It is

$$\bar{\sigma}_x = \int_0^{2\pi}\int_0^c \sigma_x r dr d\theta$$
$$= 2\pi\left[\int_0^b \sigma_x^f r dr + \int_b^c \sigma_x^m r dr\right] \qquad (2.2.30)$$

and can be expressed as

$$\bar{\sigma}_x = E_A^* \varepsilon^o \tag{2.2.31}$$

where E_A^*, the apparent Young's modulus of the composite cylinder is given by

$$E_A^* = v_m C_{xx}^m + v_f C_{xx}^f + v_f \frac{(C_{x\theta}^f - C_{xr}^f)(C_{x\theta}^f - C_{xr}^f)}{(C_{rr}^f - C_{\theta\theta}^f)} + \frac{\delta_1}{\delta_2} \tag{2.2.32a}$$

with,

$$\begin{aligned}
\delta_1 = {} & v_f \frac{2}{\lambda+1}(C_{x\theta}^f + C_{xr}^f\lambda)\{-C_{xr}^m[(C_{\theta r}^m - C_{rr}^m) - (C_{\theta r}^m + C_{rr}^m)] \\
& - (C_{\theta r}^m + C_{rr}^m)[H_1^f(C_{\theta r}^m - C_{rr}^m) - (C_{xr}^f + H_1^f(C_{\theta r}^f + C_{rr}^f)) + C_{xr}^m]\} \\
& + v_f^2 \frac{2}{\lambda+1}(C_{x\theta}^f + C_{xr}^f\lambda)(C_{\theta r}^m - C_{rr}^m)[H_1^f(C_{\theta r}^m + C_{rr}^m) - (C_{xr}^f + H_1^f(C_{\theta r}^f + C_{rr}^f)) + C_{xr}^m] \\
& + v_m(C_{x\theta}^m + C_{xr}^m)\{C_{xr}^m[(C_{rr}^m - C_{\theta r}^m) + (C_{\theta r}^f + C_{rr}^f\lambda)] \\
& + v_f(C_{\theta r}^m - C_{rr}^m)[H_1^f(C_{\theta r}^f + C_{rr}^f\lambda) - (C_{xr}^f + H_1^f(C_{\theta r}^f + C_{rr}^f)) + C_{xr}^m]\} \\
& + 2v_f(\ell nc - \ell nb)(C_{x\theta}^m - C_{xr}^m)\{C_{xr}^m[(C_{\theta r}^m + C_{rr}^m) - (C_{\theta r}^f + C_{rr}^f\lambda)] \\
& - (C_{\theta r}^m + C_{rr}^m)[H_1^f(C_{\theta r}^f + C_{rr}^f\lambda) - (C_{xr}^f + H_1^f(C_{\theta r}^f + C_{rr}^f)) + C_{xr}^m]\}
\end{aligned} \tag{2.2.32b}$$

and,

$$\delta_2 = v_m(C_{\theta r}^m + C_{rr}^m)(C_{\theta r}^m - C_{rr}^m) - (C_{\theta r}^m + C_{rr}^m)(C_{\theta r}^f + C_{rr}^f\lambda) + v_f(C_{\theta r}^m - C_{rr}^m)(C_{\theta r}^f - C_{rr}^f\lambda). \tag{2.2.32c}$$

In the above expressions v_f is the fiber volume fraction given by

$$v_f = \frac{b^2}{c^2} \tag{2.2.33a}$$

where b is the radius of the fiber and c is the radius of the composite cylinder, and the matrix volume fraction, v_m is given by

$$v_m = 1 - v_f. \tag{2.2.33b}$$

The radial displacement at the outer radius of the matrix is

$$\begin{aligned} w_m(c) &= A_1^m r + A_2^m \frac{1}{r} \\ &= -\nu_A^* \varepsilon^o c \end{aligned} \tag{2.2.34}$$

where ν_A^* is the apparent Poisson's ratio of the composite cylinder given by

$$\begin{aligned} -\nu_A^* = \frac{1}{\delta_2} \Big\{ & C_{xr}^m \Big[(C_{rr}^m - C_{\theta r}^m) + v_f (C_{rr}^m + C_{\theta r}^m) + v_m \left(C_{\theta r}^f + C_{rr}^f \lambda \right) \Big] \\ & + v_f \Big[(C_{\theta r}^m - C_{rr}^m) - (C_{\theta r}^m + C_{rr}^m) \Big] \Big[H_1^f \left(C_{\theta r}^f + C_{rr}^f \lambda \right) - \left(C_{xr}^f + H_1^f \left(C_{\theta r}^f + C_{rr}^f \right) \right) + C_{xr}^m \Big] \Big\} \end{aligned} \tag{2.2.35}$$

It is noted that the tractions resulting on the boundary of the composite cylinder compose a homogeneous traction system with the only non-zero traction being $T_x = \sigma_x n_x = \sigma_x$.

If the boundary conditions 2.2.1 and 2.2.2 are applied to a homogeneous transversely isotropic cylinder of radius c the solution will yield

$$\sigma_x = E_A \varepsilon^o \tag{2.2.36}$$

with,

$$w(c) = -\nu_A \varepsilon^o c \tag{2.2.37}$$

where E_A and ν_A are the axial modulus and Poisson's ratio of the homogeneous material. Thus since the tractions and displacements on the surface of the composite cylinder, 2.2.31 and 2.2.34, are of the same form as those on the homogeneous cylinder, namely 2.2.36 and 2.2.37, the composite cylinder is indistinguishable to an external observer from a homogeneous cylinder having moduli E_A^* and ν_A^*.

In order to show that the apparent moduli of the composite cylinder are the effective moduli of an assemblage of composite cylinders, following the discussion by Hashin[13], consider a

homogeneous cylindrical body of cross-section A subjected to the boundary conditions 2.2.1 and 2.2.2. The displacements of the body are (by the theorem of homogeneous bodies)[13]

$$u_1(\bar{x}) = \varepsilon^o x_1 \tag{2.2.38a}$$

$$u_2(\bar{x}) = -\nu_A \varepsilon^o x_2 \tag{2.2.28b}$$

$$u_3(\bar{x}) = -\nu_A \varepsilon^o x_3 \,. \tag{2.2.28c}$$

The strains in the body are thus

$$\varepsilon_{ij}^o = \begin{bmatrix} \varepsilon^o & 0 & 0 \\ 0 & -\nu_A \varepsilon^o & 0 \\ 0 & 0 & -\nu_A \varepsilon^o \end{bmatrix} \tag{2.2.39}$$

and the stresses

$$\sigma_{ij}^o = \begin{bmatrix} E_A \varepsilon^o & 0 & 0 \\ 0 & 0 & 0 \\ 0 & 0 & 0 \end{bmatrix}. \tag{2.2.40}$$

Consider now any circular cylinder of radius c within the body. If the center of the cylinder is located by (x_2^c, x_3^c), a local coordinate system can be introduced such that

$$x_2 = x_2^c + y_2 \tag{2.2.41a}$$

$$x_3 = x_3^c + y_3. \tag{2.2.41b}$$

The displacements on the surface of the cylinder c from 2.2.38 and 2.2.41 are

$$u_1(c) = \varepsilon^o x_1 \tag{2.2.42a}$$

$$u_2(c) = -\nu_A \varepsilon^o x_2^c - \nu_A \varepsilon^o y_2^c \tag{2.2.42b}$$

and,

$$u_3(c) = -\nu_A \varepsilon^o x_3^c - \nu_A \varepsilon^o y_3^c . \tag{2.2.42c}$$

The first term in 2.2.42b,c is constant and represents rigid body motion, with no effect on the stress or strain in the cylinder. Since the second term is referred to the local coordinate system it is equivalent to 2.2.34 for the composite cylinder. Also since the stresses everywhere in the homogeneous specimen are 2.2.40, the tractions on the surface of the homogeneous cylinder of radius c are the same as on the composite cylinder. Therefore a homogeneous cylinder of radius c within the homogeneous body can be replaced with a composite cylinder of radius c and apparent moduli E_A^* and ν_A^* with no effect on the stress and strain in the remainder of the body. Such replacements can be performed over and over, with varied size composite cylinders as long as the ratio $\frac{b}{c}$ is constant in each of the cylinders. In the limit the entire volume of the body is filled with composite cylinders, and the apparent moduli E_A^* and ν_A^* of the composite cylinder are the effective moduli of the composite body.

Expressing the engineering moduli in terms of the stiffness coefficients as follows:

$$E_x^f = C_{xx}^f + \frac{\left(-C_{\theta\theta}^f C_{xr}^{f\,2} - C_{rr}^f C_{x\theta}^{f\,2} + 2C_{x\theta}^f C_{\theta r}^f C_{xr}^f\right)}{C_{\theta\theta}^f C_{rr}^f - C_{\theta r}^{f\,2}} \tag{2.2.43a}$$

$$E_x^m = C_{xx}^m - \frac{2C_{x\theta}^m}{C_{\theta\theta}^m + C_{\theta r}^m} \tag{2.2.43b}$$

$$k_m = \frac{1}{2}\left(C_{\theta\theta}^m + C_{\theta r}^m\right) \tag{2.2.43c}$$

$$G_m = \frac{1}{2}\left(C_{\theta\theta}^m - C_{\theta r}^m\right) \tag{2.2.43d}$$

$$\nu_m = \frac{C_{x\theta}^m}{2k_m} \tag{2.2.43e}$$

E_A^* from Eqn 2.2.32 can be simplified to

$$E_A^* = v_m E_x^m + v_f E_x^f + v_f \frac{\left(C_{x\theta}^{f\,2} - C_{xr}^{f\,2}\right)}{\left(C_{rr}^f - C_{\theta\theta}^f\right)} + \frac{\mu_1}{\mu_2} \tag{2.2.44a}$$

where,

$$\begin{aligned}\mu_1 = &\left(-2v_m v_f k_m G_m - v_f k_m\left(C_{\theta r}^f + C_{rr}^f\lambda\right) - v_f^2 G_m\left(C_{\theta r}^f + C_{rr}^f\lambda\right)\right)\left(C_{\theta\theta}^f C_{xr}^{f\,2} + C_{rr}^f C_{x\theta}^{f\,2} - 2C_{x\theta}^f C_{\theta r}^f C_{rr}^f\right)\\ &+ v_m v_f G_m\left\{-C_{x\theta}^{m\,2}\frac{C_{\theta r}^f + C_{rr}^f\lambda}{k_m} + 2C_{x\theta}^m C_{xr}^m + 2C_{x\theta}^m H_1^f\left[\left(C_{\theta r}^f + C_{rr}^f\right) - \left(C_{\theta r}^f - C_{rr}^f\lambda\right)\right]\right.\\ &\left. + \frac{2}{\lambda+1}C_{xr}^m\left(C_{x\theta}^f + C_{xr}^f\lambda\right) + \frac{4}{\lambda+1}k_m H_1^f\left(C_{x\theta}^f + C_{xr}^f\lambda\right)\right\}\left(C_{\theta\theta}^f C_{rr}^f - C_{\theta r}^{f\,2}\right)\\ &+ \frac{2}{\lambda+1}v_f\left\{k_m\left(C_{x\theta}^f + C_{xr}^f\lambda\right)\left(C_{rx}^f + H_1^f\left(C_{\theta r}^f + C_{rr}^f\right)\right)\right.\\ &\left. + v_m G_m\left(C_{x\theta}^f + C_{xr}^f\lambda\right)\left(C_{xr}^f + H_1^f\left(C_{\theta r}^f + C_{rr}^f\right)\right)\right\}\left(C_{\theta\theta}^f C_{rr}^f - C_{\theta r}^{f\,2}\right)\end{aligned} \tag{2.2.44b}$$

and,

$$\mu_2 = \left(-2v_m k_m G_m - k_m\left(C_{\theta r}^f + C_{rr}^f\lambda\right) - v_f G_m\left(C_{\theta r}^f + C_{rr}^f\lambda\right)\right)\left(C_{\theta\theta}^f C_{rr}^f - C_{\theta r}^{f\,2}\right). \tag{2.2.44c}$$

It is noted that if the fiber is taken to be transversely isotropic $C_{rr}^f = C_{\theta\theta}^f$, $C_{xr}^f = C_{\theta x}^f$, $H_1^f = 0$ and $\lambda = 1$, thus the above expression reduces to

$$\begin{aligned}E_A^* &= v_m E_x^m + v_f E_x^f + \frac{\left(-2v_m v_f G_m k_m C_{xr}^{f\,2} - 2v_m v_f G_m C_{x\theta}^{m\,2}\dfrac{k_f^2}{k_m^2} + 2v_m v_f G_m C_{x\theta}^m C_{xr}^f k_f\right)}{\left(-v_m k_m G_m - k_m k_f - v_m G_m k_f\right)2k_f}\\ &= v_m E_x^m + v_f E_x^f + \frac{4(\nu_f - \nu_m)^2 v_m v_f}{\dfrac{v_m}{k_f} + \dfrac{v_f}{k_m} + \dfrac{1}{G_m}}\end{aligned} \tag{2.2.45a}$$

which is precisely the expression determined by Hashin for a transversely isotropic fiber composite.

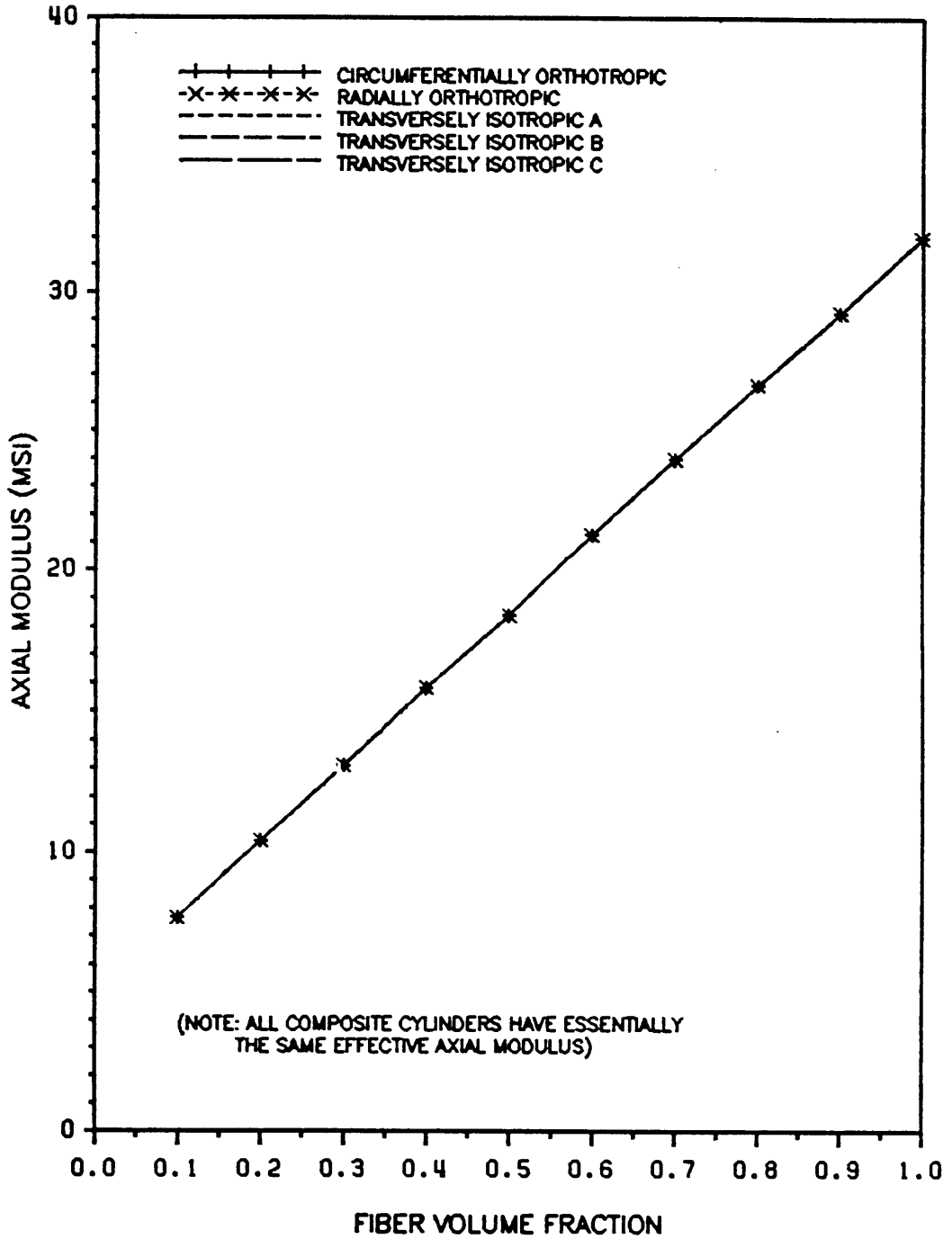

Figure 4. Effective Axial Modulus vs. Fiber Volume Fraction

Table 1. Phase Properties

Material Properties of fiber and matrix constituents

Property	Cylindrically Orthotropic Fiber	Radially Orthotropic Fiber	Transverse Isotropic Fiber 1	Transverse Isotropic Fiber 2	Isotropic Fiber 3	Isotropic Matrix
E_x(Msi)	32	32	32	32	32	5
E_θ(Msi)	32	4	4	18	32	5
E_r(Msi)	4	32	4	18	32	5
$\nu_{x\theta}$	0.15	0.25	0.25	0.20	0.15	0.12
ν_{xr}	0.25	0.15	0.25	0.20	0.15	0.12
$\nu_{\theta r}$	0.25	0.25	0.3	0.15	0.15	0.12
$G_{x\theta}$(Msi)	13.91	1.0	3.0	9.0	13.91	2.23
G_{xr}(Msi)	1.0	13.91	3.0	9.0	13.91	2.23
$G_{\theta r}$(Msi)	1.0	1.0	1.54	7.83	13.91	2.23
α_x $\mu\varepsilon$/°F	0.5	0.5	0.5	0.5	0.5	2
α_θ $\mu\varepsilon$/°F	0.5	10	10	5.25	0.5	2
α_r $\mu\varepsilon$/°F	10	0.5	10	5.25	0.5	2

The effect of the fiber morphology of the fiber types shown in Figure 1 on the effective axial modulus of the composite material is shown in Figure 4. The phase properties used in the analysis are given in Table 1. It is found that the axial modulus is not greatly affected by the fiber morphology when the axial modulus of the fiber phase is the same in all morphologies. This is because the terms in addition to the rule of mixtures terms are quite small. In addition it is found that when the properties are taken as in Table 1 the effect of circumferential orthotropy in a fiber is the same as the effect of radial orthotropy in the fiber. Examining this closer, when the properties of the CO and RO fibers are such that $C_{xx}(CO) = C_{xx}(RO)$, $C_{xr}(CO) = C_{x\theta}(RO)$, $C_{x\theta}(CO) = C_{xr}(RO)$, $C_{\theta\theta}(CO) = C_{rr}(RO)$, $C_{rr}(CO) = C_{\theta\theta}(CO)$, and $C_{\theta r}(CO) = C_{\theta r}(RO)$ then,

$$E_x^f(CO) = E_x^f(CO) \tag{2.2.46a}$$

$$\frac{C_{x\theta}^{f\,2} - C_{xr}^{f\,2}}{C_{rr}^f - C_{\theta\theta}^f}(CO) = \frac{C_{x\theta}^{f\,2} - C_{xr}^{f\,2}}{C_{rr}^f - C_{\theta\theta}^f}(RO) \tag{2.2.46b}$$

$$\left(C_{\theta r}^f + C_{rr}^f\lambda\right)(CO) = \left(C_{\theta r}^f + C_{rr}^f\lambda\right)(RO) \tag{2.2.46c}$$

$$\left(C_{xr}^f + H_1^f\left(C_{\theta r}^f + C_{rr}^f\right)\right)(CO) = \left(C_{xr}^f + H_1^f\left(C_{\theta r}^f + C_{rr}^f\right)\right)(RO) \tag{2.2.46d}$$

$$\frac{1}{\lambda+1}\left(C_{x\theta}^f + C_{xr}^f\lambda\right)(CO) = \frac{1}{\lambda+1}\left(C_{x\theta}^f + C_{xr}^f\lambda\right)(RO) \tag{2.2.46e}$$

$$\left(C_{\theta\theta}^f C_{rr}^f - C_{\theta r}^{f\,2}\right)(CO) = \left(C_{\theta\theta}^f C_{rr}^f - C_{\theta r}^{f\,2}\right)(RO) \tag{2.2.46f}$$

and,

$$\left(C_{\theta\theta}^f C_{xr}^{f\,2} + C_{rr}^f C_{x\theta}^{f\,2} - 2C_{x\theta}^f C_{\theta r}^f C_{xr}^f\right)(CO) = \left(C_{\theta\theta}^f C_{xr}^{f\,2} + C_{rr}^f C_{x\theta}^{f\,2} - 2C_{x\theta}^f C_{\theta r}^f C_{xr}^f\right)(RO). \tag{2.2.46g}$$

Thus it is seen from Eqn 2.2.44 that

$$E_A^*(RO) = E_A^*(CO) \tag{2.2.47}$$

and circumferential and radial orthotropy in the fiber have the same effect on the effective axial modulus of the composite.

2.3 Axial Poisson's Ratio

The loading necessary to determine the axial Poisson's ratio is the same as that to determine the axial Youngs modulus, namely Eqns 2.2.1, and 2.2.2. In the previous section, the solution for these boundary conditions was determined. The expression for the radial displacement at the outer radius (c) of the composite cylinder was determined to be

$$u_r^m(c) = -\nu_A^* \varepsilon^o c \tag{2.3.1}$$

Since the tractions and displacements on the surface of the composite cylinder are of the form that would exist on a homogeneous cylinder subjected to the same stress state, it was shown in the previous section that cylindrical regions in a homogeneous body can be replaced successively with composite cylinders of apparent moduli E_A^* and ν_A^* with no effect on the state of stress and strain in the remainder of the body. Thus the apparent moduli of the composite cylinder are the effective moduli of the effectively transversely isotropic composite material.

Using the results from the previous section the effective Poisson's ratio of the composite material is

$$\begin{aligned} \nu_A^* &= \frac{-w(c)}{\varepsilon^o c} \\ &= \frac{1}{\varepsilon^o}\left(-A_1^m - \frac{A_2^m}{c^2}\right) \\ &= \frac{\rho}{\delta_2} \end{aligned} \tag{2.3.2a}$$

with,

$$\rho = -v_m C^m_{xr}\left[-\left(C^m_{\theta r} - C^m_{rr}\right) + \left(C^f_{\theta r} + C^f_{rr}\lambda\right)\right] + 2v_f C^m_{rr}\left[H^f_1\left(C^f_{\theta r} + C^f_{rr}\lambda\right) - \left(C^f_{xr} + H^f_1\left(C^f_{\theta r} + C^f_{rr}\right)\right) + C^m_{xr}\right] \tag{2.3.2b}$$

and δ_2 given by 2.2.32c. As with the expression for E^*_A, this expression can be simplified using the relations 2.2.43, and

$$\nu^f_{xr} = \frac{C^f_{xr}C^f_{\theta\theta} - C^f_{x\theta}C^f_{\theta r}}{C^f_{rr}C^f_{\theta\theta} - C^{f\,2}_{\theta r}} \tag{2.3.3a}$$

$$\nu^f_{x\theta} = \frac{C^f_{x\theta}C^f_{rr} - C^f_{x\theta}C^f_{\theta r}}{C^f_{rr}C^f_{\theta\theta} - C^{f\,2}_{\theta r}} \tag{2.3.3b}$$

to

$$\nu^*_A = v_m\nu_m + \frac{v_f}{2}\left(\nu^f_{xr} + \nu^f_{x\theta}\right) + \frac{\zeta_1}{\zeta_2} \tag{2.3.4a}$$

with,

$$\zeta_1 = \left[v_m v_f 2k_m G_m + v_f k_m\left(C^f_{\theta r} + C^f_{rr}\lambda\right) + v_f^2 G_m\left(C^f_{\theta r} + C^f_{rr}\lambda\right)\right]\left[\frac{C^f_{x\theta}\left(C^f_{rr} - C^f_{\theta r}\right) + C^f_{xr}\left(C^f_{\theta\theta} - C^f_{\theta r}\right)}{\left(C^f_{rr}C^f_{\theta\theta} - C^{f\,2}_{\theta r}\right)}\right] - 2(v_m G_m + v_f k_m)\left(C^f_{xr} + H^f_1\left(C^f_{\theta r} + C^f_{rr}\right)\right) + 2v_f(G_m + k_m)\left(H^f_1\left(C^f_{\theta r} + C^f_{rr}\lambda\right)\right) - 2v_m v_f C^m_{xr} G_m\left(1 - \frac{\left(C^f_{\theta r} + C^f_{rr}\lambda\right)}{k_m}\right) \tag{2.3.4b}$$

and

$$\zeta_2 = -4v_m k_m G_m - 2k_m\left(C^f_{\theta r} + C^f_{rr}\lambda\right) - 2v_f G_m\left(C^f_{\theta r} + C^f_{rr}\lambda\right). \tag{2.3.4c}$$

If the fiber is transversely isotropic, then $\nu_{xr}^f + \nu_{x\theta}^f = 2\nu_f$, $(C_{\theta r}^f + C_{rr}^f\lambda) = 2k_f$, $H_1^f = 0$, and $\lambda = 1$, and the expression for ν_A^* reduces to

$$\nu_A^* = \nu_m\nu_m + \nu_f\nu_f + \frac{(\nu_f - \nu_m)\left(\frac{1}{k_m} - \frac{1}{k_f}\right)\nu_f\nu_m}{\frac{\nu_m}{k_f} + \frac{\nu_f}{k_m} + \frac{1}{G_m}}, \tag{2.3.5}$$

which is the expression given by Hashin [13] for the effective poisons ration of the composite cylinder assemblage.

In Figure 5 it appears that circumferential orthotropy and radial orthotropy in the fiber have the same effect on the Poisson's ratio. Examining the expression (2.3.4) for ν_A^*, and using the relations 2.2.46 discussed in the previous section, we find that indeed,

$$\nu_A^*(CO) = \nu_A^*(RO). \tag{2.3.6}$$

2.4 Transverse Bulk Modulus

The third effective elastic property of the effectively transversely isotropic composite material to be determined is the transverse bulk modulus k. Consider a single composite cylinder, fiber of radius b, surrounded by matrix of external radius c, subjected to the boundary conditions on the surface S

$$u(S) = 0 \tag{2.4.1a}$$

$$v(S) = 0 \tag{2.4.1b}$$

$$w(S) = \varepsilon_r^o b. \tag{2.4.1c}$$

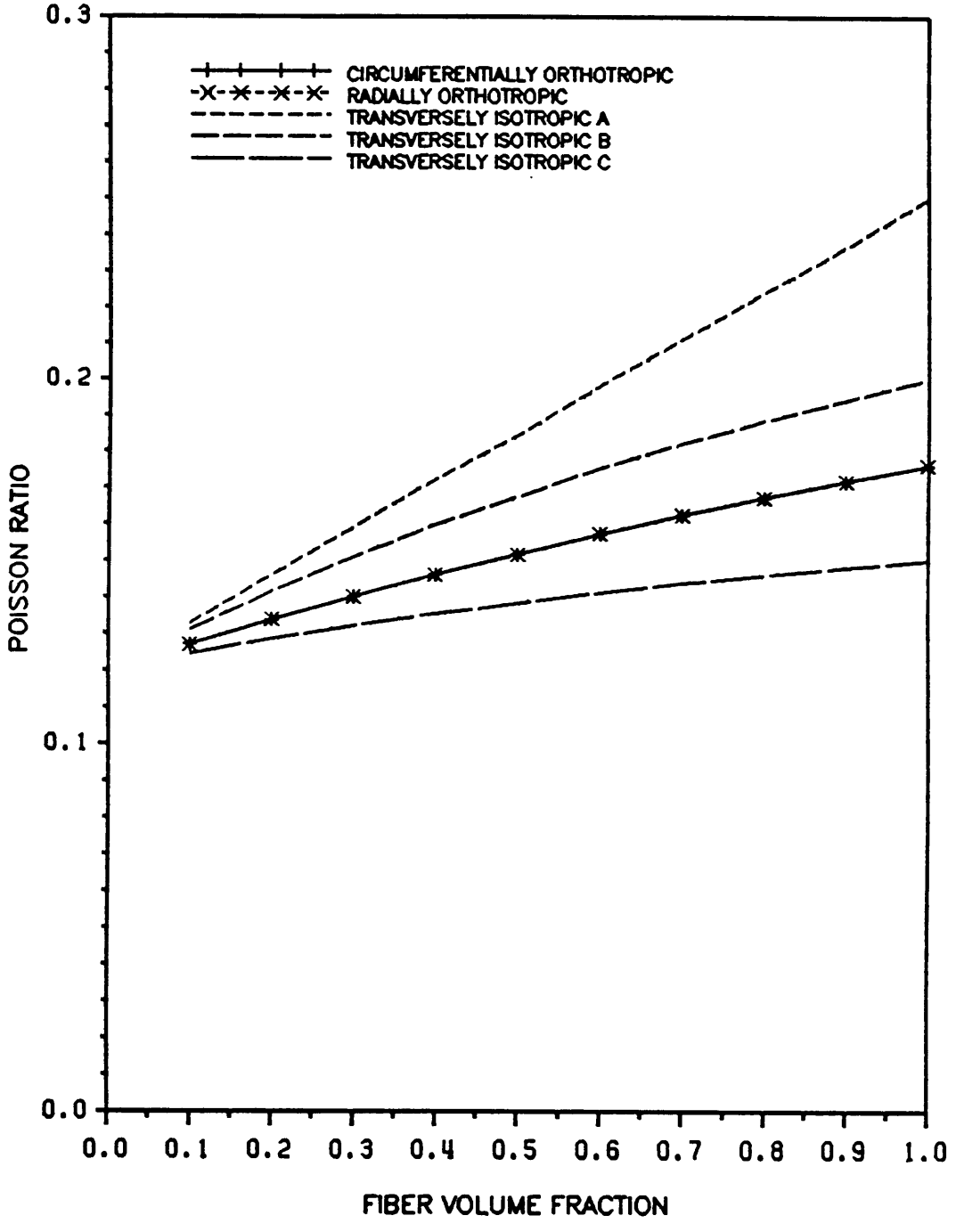

Figure 5. Axial Poisson's Ratio vs. Fiber Volume Fraction

The cylinder is in a state of plane strain, and the stress state is axisymmetric. Thus the elasticity solution of section 2.2.1 can be applied. The boundary conditions correspond to

$$u^m = u^f = 0 \tag{2.4.2a}$$

$$v^m(c) = 0 \tag{2.4.2b}$$

and

$$w^m(c) = \varepsilon_r^o b \tag{2.4.2c}$$

Since there is no applied temperature change all terms involving ΔT will be zero. From the boundary conditions 2.4.2a,b and the continuity of displacements 2.2.14a,b at $r=b$

$$E^m = E^f = F^m = F^f = 0 \tag{2.4.3}$$

$$\text{and} \quad \varepsilon^{of} = \varepsilon^{om} = \gamma^{of} = \gamma^{om} = 0 \tag{2.4.4}$$

Boundary and continuity conditions yet to be satisfied are

1) finite displacement at $r=0$

$$A_1^f r^\lambda + A_2^f r^{-\lambda} \text{ is finite} \tag{2.4.5}$$

2) continuity of radial displacements at $r=b$

$$A_1^f b^\lambda = A_1^m + \frac{A_2^m}{b} \tag{2.4.6}$$

3) continuity of radial stresses at $r=b$

$$A_1^f\left(C_{\theta r}^f + C_{rr}^f \lambda\right) b^{\lambda-1} = A_1^m\left(C_{\theta r} + C_{rr}^m\right) + A_2^m \frac{\left(C_{\theta r}^m - C_{rr}^m\right)}{b^2} \tag{2.4.7}$$

and

4) the applied displacement at $r=c$

$$A_1^m c + \frac{A_2^m}{c} = \varepsilon_r^o c \tag{2.4.8}$$

Solving this system of equations for the four unknowns A_1^f, A_2^f, A_1^m, and A_2^m, we find

$$A_1^f = \frac{\varepsilon^o c^2}{b^{\lambda+1}}\left[1 + v_m \frac{\left[(C_{\theta r}^m - C_{rr}^m) - (C_{\theta r}^f + C_{rr}^f\lambda)\right]}{\frac{b^2}{c^2}\left[(C_{\theta r}^f + C_{rr}^f\lambda) - (C_{\theta r}^m + C_{rr}^m)\right] + \left[(C_{\theta r}^m - C_{rr}^m) - (C_{\theta r}^f + C_{rr}^f\lambda)\right]}\right] \tag{2.4.9}$$

$$A_2^f = 0 \tag{2.4.10}$$

$$A_1^m = \frac{\varepsilon^o\left[(C_{\theta r}^m - C_{rr}^m) - (C_{\theta r}^f + C_{rr}^f\lambda)\right]}{\frac{b^2}{c^2}\left[(C_{\theta r}^f + C_{rr}^f\lambda) - (C_{\theta r}^m + C_{rr}^m)\right] + \left[(C_{\theta r}^m - C_{rr}^m) - (C_{\theta r}^f + C_{rr}^f\lambda)\right]} \tag{2.4.11}$$

and,

$$A_2^m = c^2\varepsilon^o\left[1 - \frac{\left[(C_{\theta r}^m - C_{rr}^m) - (C_{\theta r}^f + C_{rr}^f\lambda)\right]}{\frac{b^2}{c^2}\left[(C_{\theta r}^f + C_{rr}^f\lambda) - (C_{\theta r}^m + C_{rr}^m)\right] + \left[(C_{\theta r}^m - C_{rr}^m) - (C_{\theta r}^f + C_{rr}^f\lambda)\right]}\right]. \tag{2.4.12}$$

Examining the resulting tractions on the composite cylinder surface the only surviving tractions are $T_r = \sigma_r$ on the surface $r=c$, and $T_x = \sigma_x$ on the ends of the cylinder. Using 2.4 11 and 2.4.12, the traction on the lateral surface of the surface of the cylinder is

$$\sigma_r^m(c) = A_1^m(C_{\theta r}^m + C_{rr}^m) + \frac{A_2^m(C_{\theta r}^m - C_{rr}^m)}{c^2} \tag{2.4.13}$$

or

$$\sigma_r^m(c) = 2k^*\varepsilon^o \tag{2.4.14a}$$

where k^* is the apparent transverse bulk modulus of the composite cylinder given by,

$$2k^* = (C^m_{\theta r} - C^m_{rr}) + 2C^m_{rr}\left[\frac{(C^m_{\theta r} - C^m_{rr}) - (C^f_{\theta r} + C^f_{rr}\lambda)}{(C^m_{\theta r} - C^m_{rr}) - v_f(C^m_{\theta r} + C^m_{rr}) - v_m(C^f_{\theta r} + C^f_{rr}\lambda)}\right] \tag{2.4.14b}$$

The average axial stress, which is equivalent to the axial traction can be written in the form

$$\bar{\sigma}_x = 2\ell^* \varepsilon^o \tag{2.4.15a}$$

where ℓ^* is an apparent axial modulus of the composite cylinder given by:

$$2\ell^* = \frac{\frac{2v_f}{\lambda+1}\left[(C^m_{\theta r} - C^m_{rr}) - (C^m_{\theta r} + C^m_{rr})\right](C^f_{x\theta} + C^f_{xr}\lambda) + v_m\left[(C^m_{\theta r} - C^m_{rr}) - (C^f_{\theta r} + C^f_{rr}\lambda)\right](C^m_{x\theta} + C^m_{xr})}{v_m\left[(C^f_{\theta r} + C^f_{rr}\lambda) + (C^m_{\theta r} - C^m_{rr})\right] + v_f\left[(C^m_{\theta r} - C^m_{rr}) - (C^m_{\theta r} + C^m_{rr})\right]}$$

(2.4.15b)

If the boundary conditions 2.4.1 are applied to a homogeneous transversely isotropic cylinder of radius c, the resulting surface tractions would be

$$T_r = \sigma_r = 2k_o\varepsilon^o \tag{2.4.16a}$$

on r=c, and

$$T_x = \sigma_x = 2\ell_o\varepsilon^o \tag{2.4.16b}$$

on the terminal ends. In 2.4.16 k_o and ℓ_o are the transverse bulk modulus and an axial modulus of the the homogeneous cylinder. These surface tractions are of the same form as the tractions of the composite cylinder subjected to 2.4.1. Thus, a composite cylinder is indistinguishable from a homogeneous cylinder with moduli k^* and ℓ^*, and k^* and ℓ^* can be taken to be apparent moduli of the composite cylinder.

As in the case of an axial loading, we can show that the apparent moduli of the composite cylinder are the effective moduli of a composite cylinder assemblage. Consider a homoge-

neous transversely isotropic cylindrical body with moduli k^* and ℓ^*, applying 2.4.1 the following stress and strain states result.

$$\varepsilon_{ij} = \begin{bmatrix} 0 & 0 & 0 \\ 0 & \varepsilon_r^o & 0 \\ 0 & 0 & \varepsilon_r^o \end{bmatrix} \tag{2.4.17}$$

$$\sigma_{ij} = \begin{bmatrix} 2\ell^* \varepsilon_r^o & 0 & 0 \\ 0 & 2k^* \varepsilon_r^o & 0 \\ 0 & 0 & 2k^* \varepsilon_r^o \end{bmatrix}. \tag{2.4.18}$$

Any circular cylinder of radius c extending from end to end with in the homogeneous body can be located by its center (x_2^c, x_3^c) . Any location in the circular cylinder can then be referred to using a local coordinate system y such that

$$x_2 = x_2^c + y_2 \tag{2.4.19a}$$

$$x_3 = x_3^c + y_3 \tag{2.4.19b}$$

On the surface of this cylinder, at r=c, we find

$$u_1(c) = 0 \tag{2.4.20a}$$

$$u_2(c) = \varepsilon_r^o x_2^c + \varepsilon_r^o y_2 \tag{2.4.20b}$$

$$u_3(c) = \varepsilon_r^o x_3^c + \varepsilon_r^o y_3 \tag{2.4.20c}$$

The first terms on the right hand sides of these relations represent rigid body motion. The remaining terms refer to the cylinders local coordinate system, and thus are equivalent to 2.4.2c.

The stresses in the homogeneous cylinder are given by 2.4.18. Thus the tractions on the surface r=c are

$$T_1 = 0 \tag{2.4.21a}$$

$$T_2 = T_r n_2 = 2k^* \varepsilon^o n_2 \tag{2.4.21b}$$

$$T_3 = T_r n_3 = 2k^* \varepsilon^o n_3 \tag{2.4.21c}$$

and on the terminal ends,

$$T_1 = 2\ell^* \varepsilon_r^o \tag{2.4.22a}$$

$$T_2 = T_3 = 0 \tag{2.4.22b}$$

Since the boundary displacements and tractions have the same form in the homogeneous cylinder within the body as does a composite cylinder subjected to 2.4.1, the homogeneous cylinder can be replaced with a composite cylinder of apparent moduli k^* and ℓ^* without affecting the state of stress and strain in the remainder of the specimen. Keeping the ratio $\frac{b}{c}$ in the composite cylinder constant, such replacements can be made until in the limit, the cylindrical body becomes filled with composite cylinders, and k^* and ℓ^* are the effective moduli of the composite specimen. Thus the plane strain bulk modulus given in expression 2.4.14b is the effective plane strain bulk modulus of the composite cylinder.

The expression for k^* can be simplified using the relations 2.2.43 to

$$2k^* = \frac{v_m k_m\left[G_m + \left(C_{\theta r}^f + C_{rr}^f \lambda\right)\right] + v_f\left(C_{\theta r}^f + C_{rr}^f \lambda\right)[G_m + k_m]}{v_f[G_m + k_m] + v_m\left[G_m + \left(C_{\theta r}^f + C_{rr}^f \lambda\right)\right]} \tag{2.4.23}$$

As is the case for E_A^*, and ν_A^* if the fiber is transversely isotropic, i.e., $\lambda = 1$ the expression reduces to the expression for effective bulk modulus given by Hashin [13], namely

$$k^* = \frac{v_m k_m[G_m + k_f] + v_f k_f[k_m + G_m]}{v_m[G_m + k_f] + v_f[G_m + k_m]}. \tag{2.4.24}$$

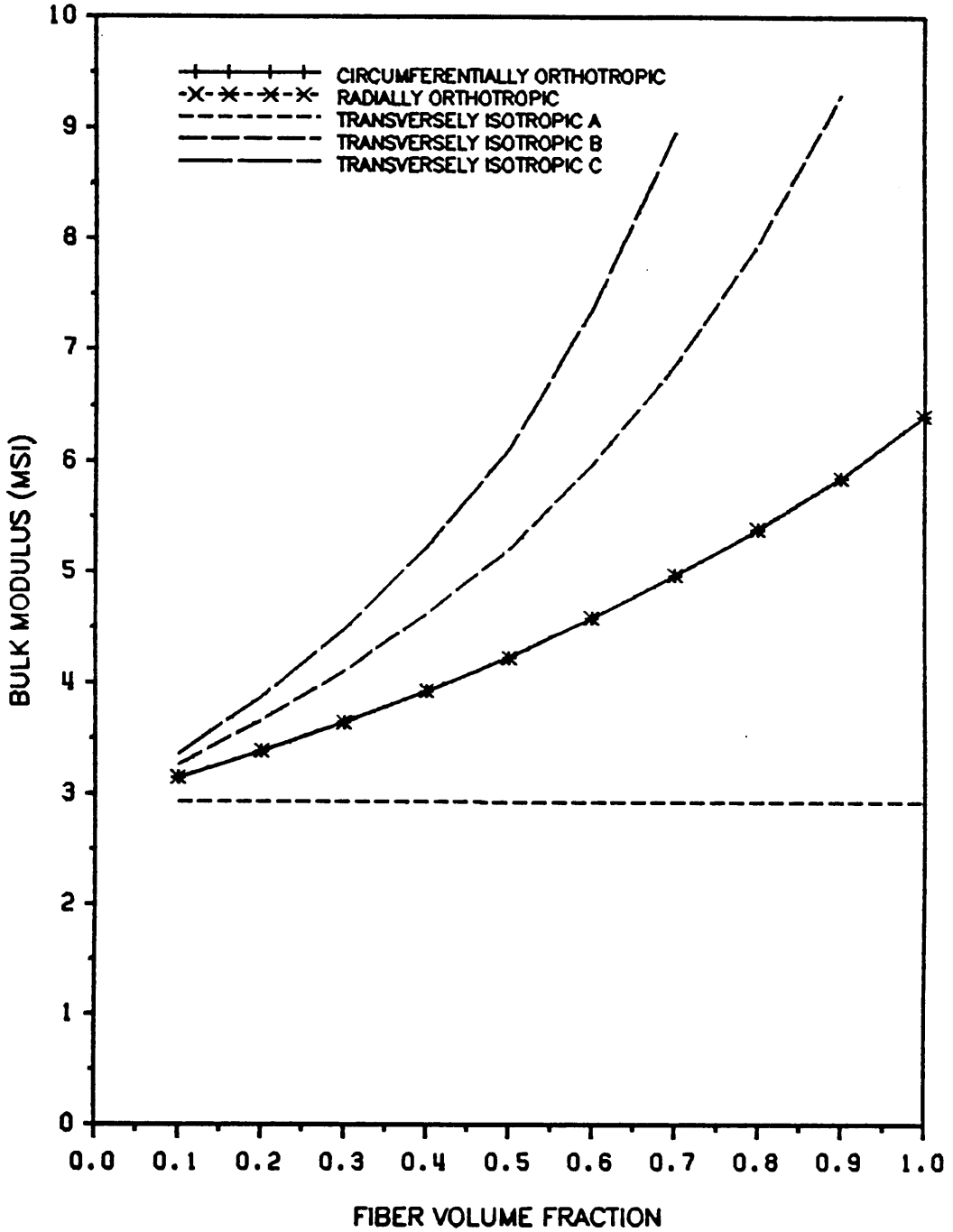

Figure 6. Effective Transverse Bulk Modulus vs. Fiber Volume Fraction

Figure 6 shows the variation of effective transverse bulk modulus for the ideal fiber types at various volume fractions. Again the graphs of the effective modulus for circumferentially and radially orthotropic fibers are identical. Examining the expression for k^*, since $(C^f_{\theta r} + C^f_{rr}\lambda)$ for a CO fiber is the same as $(C^f_{\theta r} + C^f_{rr}\lambda)$ for an RO fiber, we have exactly

$$k^*(CO) = k^*(RO). \tag{2.4.25}$$

It is noted that for the case of a composite with continuous fibers such as the one considered here, E^*_A and ν^*_A can be determined from k^* using the Hill [13] relations. This dependence of E^*_A and ν^*_A on k^* is purely geometrical though, and E^*_A, ν^*_A, and k^* are still independent material properties.

2.5 *Axial Shear Modulus*

The fourth modulus of the effectively transversely isotropic composite material to be determined is the axial shear modulus. This modulus is found by applying a shear displacement to the composite, and using the elasticity solution outlined in section 2.1.2.

The boundary conditions for the problem are

$$u_1(S) = \varepsilon^o_{12}x_2 + \varepsilon^o_{13}x_3 \tag{2.5.1a}$$

$$u_2(S) = \varepsilon^o_{12}x_1 \tag{2.5.1b}$$

$$u_3(S) = \varepsilon^o_{13}x_1. \tag{2.5.1c}$$

From section 2.1.2 the assumed form of the displacements are

$$u^m_1 = \phi^m - \varepsilon^m_{12}x_2 - \varepsilon^m_{13}x_3 \tag{2.5.2a}$$

$$u_2^m = \varepsilon_{12}^m x_1 \tag{2.5.2b}$$

$$u_3^m = \varepsilon_{13}^m x_1 \tag{2.5.2c}$$

and,

$$u_1^f = \phi^f - \varepsilon_{12}^f x_2 - \varepsilon_{13}^f x_3 \tag{2.5.3a}$$

$$u_2^f = \varepsilon_{12}^f x_1 \tag{2.5.3b}$$

$$u_3^f = \varepsilon_{12}^f x_1. \tag{2.5.3c}$$

The solution to the elasticity equation, as given previously, is

$$\phi^m(r, \theta) = a_o^m + \sum_{n=1}^{\infty} \left(A_n^m r^n + B_n^m r^{-n}\right)\left(C_n^m \sin(n\theta) + D_n^m \cos(n\theta)\right) \tag{2.5.4}$$

for the isotropic matrix, and,

$$\phi^f(r, \theta) = a_o^f + \sum_{n=1}^{\infty} \left(A_n^f r^{\gamma_n} + B_n^f r^{-\gamma_n}\right)\left(C_n^f \sin(n\theta) + D_n^f \cos(n\theta)\right) \tag{2.5.5a}$$

where

$$\gamma = \sqrt{\frac{G_{xr}^f}{G_{x\theta}^f}} \tag{2.5.5b}$$

for the orthotropic fiber.

The assumed displacements 2.5.2b and 2.5.2c satisfy the boundary conditions 2.5.1 for $\varepsilon_{12}^m = \varepsilon_{12}^o$ and $\varepsilon_{13}^m = \varepsilon_{13}^o$. Continuity of displacements at r=b then requires that $\varepsilon_{12}^f = \varepsilon_{12}^o$ and $\varepsilon_{12}^f = \varepsilon_{13}^o$. The assumed displacement 2.5.2a with the boundary condition 2.5.1a requires that

$$\phi^m(c) = 2\varepsilon_{12}^o x_2 + 2\varepsilon_{12}^o x_3 \tag{2.5.6}$$

In the analysis of the axial shear modulus only one shearing direction need be considered so ε_{13}^o can be taken to be 0. Thus 2.5.6 becomes

$$\begin{aligned} \phi^m(c) &= 2\varepsilon_{12}^o x_2 \\ &= 2c\varepsilon_{12}^o \cos\theta \end{aligned} \tag{2.5.7}$$

For 2.5.4 to satisfy this boundary condition $n = 1$, $C_1 = 0$, and $a_o = 0$. Therefore,

$$\phi^m(r, \theta) = \left(A_1^m r + \frac{B_1^m}{r} \right) \cos\theta. \tag{2.5.8}$$

Noting that the displacements at $r = 0$ must be finite in a solid fiber, and that for displacement continuity ϕ^f must be of the same form as ϕ^m, B_n^f must be zero and n must be 1 in Eqn 2.5.5, therefore

$$\phi^f(r, \theta) = A_1^f r^\gamma \cos\theta. \tag{2.5.9}$$

The expressions for ϕ^m and ϕ^f contain three unknowns. Therefore, two conditions in addition to the boundary condition 2.5.7 are needed to complete the problem. These conditions are the displacement and traction continuity at the fiber-matrix interface r = b . As already discussed, continuity of u_2 and u_3 are satisfied if $\varepsilon_{12}^m = \varepsilon_{12}^f = \varepsilon_{12}^o$ and $\varepsilon_{13}^m = \varepsilon_{13}^f = \varepsilon_{13}^o = 0$. Continuity of u_1 requires

$$\phi^m(b) = \phi^f(b) \tag{2.5.10}$$

or

$$\left(A_1^m b + \frac{B_1^m}{b}\right) = A_1^f b^\gamma. \tag{2.5.11}$$

The only traction surviving on r = b is

$$T_1 = \sigma_{12} n_2 + \sigma_{13} n_3. \tag{2.5.12}$$

In the matrix

$$T_1^m = G_m \frac{\partial \phi^m}{\partial n} \tag{2.5.13}$$

and in the fiber

$$T_1^f = C_{44} \frac{\partial \phi^f}{\partial x_2} n_2 + C_{46}\left(\frac{\partial \phi^f}{\partial x_3} n_2 + \frac{\partial \phi^f}{\partial x_2} n_3\right) + C_{66} \frac{\partial \phi^f}{\partial x_3} n_3 \tag{2.5.14}$$

Recalling that C_{44}, C_{46}, and C_{66} are not constant in the cartesian coordinate system, but functions of $G_{x\theta}$, G_{xr}, x_2, and x_3, 2.5.14 can be reduced to

$$T_1^f = G_{x\theta}^f \frac{\partial \phi^f}{\partial r} \tag{2.5.15}$$

in cylindrical coordinates. In cylindrical coordinates 2.5.13 becomes,

$$T_1^m = G_m \frac{\partial \phi^m}{\partial r} \tag{3.5.16}$$

The traction continuity condition at the fiber-matrix interface thus requires

$$G_{x\theta}^f \frac{\partial \phi^f}{\partial r} = G_m \frac{\partial \phi^m}{\partial r} \tag{2.5.17}$$

or

$$G^f_{x\theta}\left(\gamma A^f_1 b^{\gamma-1}\right) = G_m\left(A^m_1 - \frac{B^m_1}{b^2}\right) \tag{2.5.18}$$

Equations 2.5.7b, 2.5.11, and 2.5.18 are solved simultaneously to find

$$A^f_1 = \frac{4\varepsilon^o_{12} G_m}{b^{\gamma-1}\left(G_m + G^f_{x\theta\gamma}\right) + \frac{b^{\gamma+1}}{c^2}\left(G_m - G^f_{x\theta\gamma}\right)} \tag{2.5.19}$$

$$A^m_1 = \frac{2\varepsilon^o_{12}\left(G^f_{x\theta\gamma} + G_m\right)}{\left(G_m + G^f_{x\theta\gamma}\right) + v_f\left(G_m - G^f_{x\theta\gamma}\right)} \tag{2.5.20}$$

and

$$B^m_1 = \frac{-2\varepsilon^o_{12}\left(G^f_{x\theta\gamma} - G_m\right)b^2}{\left(G_m + G^f_{\theta x\gamma}\right) + v_f\left(G_m - G^f_{x\theta\gamma}\right)} \tag{2.5.21}$$

Using these values of A^f_1, A^m_1, and B^m_1

$$\phi^m(r,\theta) = \left[\frac{\left(G^f_{x\theta\gamma} + G_m\right)r + \left(G^f_{x\theta\gamma} - G_m\right)\frac{b^2}{r}}{\left(G_m + G_{\theta x\gamma}\right) + v_f\left(G_m - G^f_{x\theta\gamma}\right)}\right] 2\varepsilon^o_{12}\cos\theta \tag{2.5.22}$$

and

$$\phi^f(r,\theta) = \left[\frac{2G_m r^\gamma}{b^{\gamma-1}\left(G_m + G^f_{x\theta\gamma}\right) + \frac{b^{\gamma+1}}{c^2}\left(G_m - G^f_{x\theta\gamma}\right)}\right] 2\varepsilon^o_{12}\cos\theta. \tag{2.5.23}$$

Examining the tractions at $r = c$ it is again found that T_1 is the only surviving traction where

$$T_1(c) = G_m\frac{\partial\phi^m}{\partial r} \tag{2.5.24}$$

Substituting from 2.5.22

$$T_1(c) = 2G_A^* \varepsilon_{12}^o \cos\theta \tag{2.5.25}$$

where

$$G_A^* = G_m \left[\frac{\left(G_{x\theta\gamma}^f + G_m\right) + v_f\left(G_{x\theta\gamma}^f - G_m\right)}{\left(G_m + G_{x\theta\gamma}^f\right) + v_f\left(G_m - G_{x\theta\gamma}^f\right)} \right] \tag{2.5.26}$$

The argument used in sections 2.2 and 2.4 can also be used to show that G_A^*, the apparent axial shear modulus of the composite cylinder, as given in 2.5.26, is the effective axial shear modulus of a composite specimen. First a homogeneous transversely isotropic cylinder of radius c is subjected to the shear loading 2.5.1. The resulting boundary tractions are of the form 2.5.25. From the outside the composite cylinder is therefore indistinguishable from a homogeneous cylinder of modulus G_A^*.

Note that the boundary condition on the terminal end of the cylinder

$$\phi(x_2, x_3) = \varepsilon_{12}^o x_2 \tag{2.5.27}$$

is not satisfied by 2.5.22 and 2.5.23. However, for a long cylinder, the actual variation in ϕ at the terminal ends can be replaced by 2.5.27 with insignificant effects due to the St. Venant principle.

Now examining a homogeneous cylindrical body subjected to 2.5.1, any cylinder of radius $r = c$ within this body will have boundary conditions 2.5.1 and 2.5.25 when written in terms of a local coordinate system whose origin is at the center of the cylinder. Thus a cylinder in the homogeneous body can be replaced by a composite cylinder with volume fraction $\frac{b}{c}$ with no effect. This procedure can be continued until the body is filled with composite cylinders. Thus the effective modulus of the composite is G_A^*.

As is the case with the moduli discussed so far, Hashin's expression for the effective axial shear modulus of a composite cylinder with transversely isotropic fibers can be recovered from 2.5.26 if the fiber properties are taken to be transversely isotropic, i.e., for $G^f_{x\theta} = G^f_{xr} = G_f$

$$G^*_A = \frac{(G_f + G_m) + v_f(G_f - G_m)}{(G_f + G_m) + v_f(G_m - G_f)} \tag{2.5.28}$$

The variation of G^*_A with volume fraction is presented in Figure 7. Again it is noted that the circumferential and radial morphology seem to have the same effect on the effective modulus. Recalling the definition of γ (Eqn. 2.1.45b)

$$G^f_{x\theta\gamma} = \sqrt{G^f_{x\theta} G^f_{xr}} \tag{2.5.29}$$

thus using Eqn. 2.5.26

$$G^f_{x\theta\gamma}(RO) = G^f_{x\theta\gamma}(CO) \tag{2.5.30}$$

since

$$G^f_{x\theta}(RO) = G^f_{xr}(CO) \tag{2.5.31}$$

and

$$G^f_{xr}(RO) = G^f_{x\theta}(CO) \tag{2.5.32}$$

Radial and circumferential morphology in the fiber thus have the same effect on the effective axial shear modulus and

$$G^*_A(RO) = G^*_A(CO) \tag{2.5.33}$$

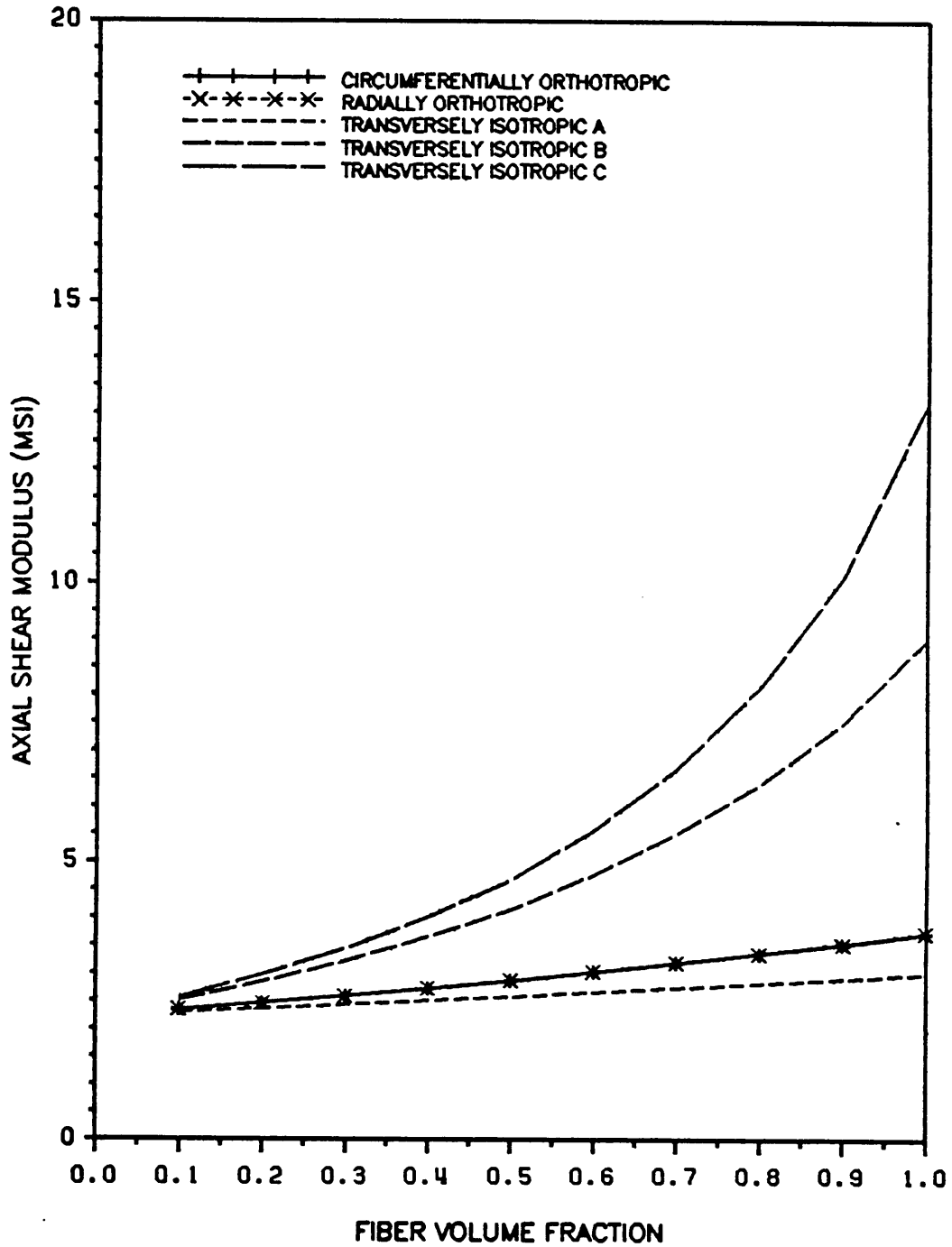

Figure 7. Effective Axial Shear Modulus vs. Fiber Volume Fraction

2.6 Torsional Modulus

The last section discussed the effective axial shear modulus of a composite. This shear modulus characterizes the response of the composite to either a pure shear loading or a torsional loading. As illustrated in Figure 8 the stress state in the composite cylinder within a composite subjected to either torsion or axial shear is pure shear. It also is of interest, however, to investigate the torsional modulus of the composite cylinder itself, i.e., the response of the composite cylinder subjected to the boundary condition

$$v(S) = \gamma^{o} rx, \quad u(S) = 0, \quad w(S) = 0. \tag{2.6.1}$$

This problem is axisymmetric so the solution from section 2.1.1 is applicable. Due to the fact that there is no shear extension coupling, since the x, θ, and r directions are material principal directions, all constants in the expressions 2.1.14, 2.1.18, and 2.1.19, for u and w, are identically zero. The only non-zero stress and strain in each layer is $\tau_{x\theta}$ and $\gamma_{x\theta}$.

From the displacement continuity conditions at r=b, $\gamma^{f} = \gamma^{m} = \gamma^{o}$, thus,

$$\gamma^{f}_{x\theta} = \gamma^{m}_{x\theta} = \gamma^{o}_{x\theta} \tag{2.6.2}$$

The shear stresses in the phases are then given by

$$\tau^{f}_{x\theta} = G^{f}_{x\theta} \gamma^{o} r \tag{2.6.3}$$

and

$$\tau^{m}_{x\theta} = G^{m}_{x\theta} \gamma^{o} r. \tag{2.6.4}$$

The average resultant moment or torque in the composite cylinder is

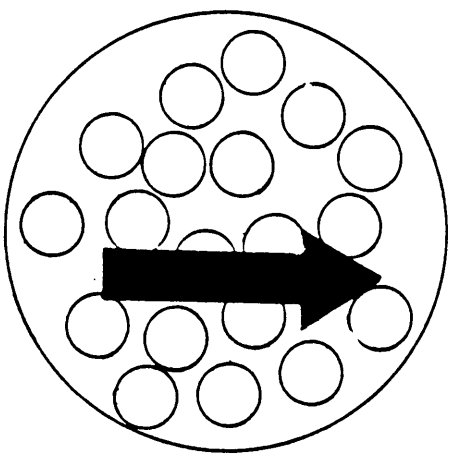

Axial Shear of a Composite Specimen

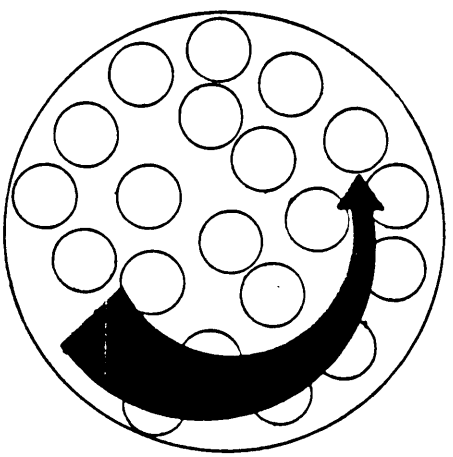

Torsion of a Composite Specimen

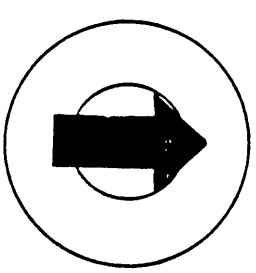

Effective Loading in a Single Composite Cylinder for Shear

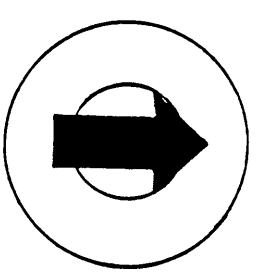

Effective Loading in a Single Composite Cylinder for Torsion

Figure 8. Schematic of torsion and shear in a composite material

$$T = \int_0^{2\pi}\int_0^{c} \tau_{\theta r} r dr d\theta \tag{2.6.5}$$

or

$$\begin{aligned} T &= 2\pi\left[\int_0^{b} \tau^{f}_{\theta r} r^2 dr + \int_b^{c} \tau^{m}_{\theta r} r^2 dr\right] \\ &= J\gamma^{o}G^{*} \end{aligned} \tag{2.6.6}$$

where G^* is the apparent torsional modulus of the composite cylinder given by

$$G^{*} = G^{f}_{x\theta} v_f^2 + G_m\left(1 - v_f^2\right) \tag{2.6.7}$$

In a homogeneous cylinder subjected to the boundary conditions 2.6.1 the resulting moment be

$$T = J\gamma^{o}G^{*} \tag{2.6.8}$$

which is of the same form as 2.6.6. Therefore, G^* can be taken as the apparent torsional modulus of the composite cylinder.

This torsional modulus of the composite cylinder is not an effective modulus of a composite material composed of composite cylinders. Note that the expression for the torsional modulus (2.6.7) is not a rule of mixtures, and it is not equivalent to the effective axial shear modulus of the cylinder. Figure 9 shows the variation of G^* with fiber volume fraction. It is noted that in pure torsion the morphology of the fiber does affect the response of the composite cylinder.

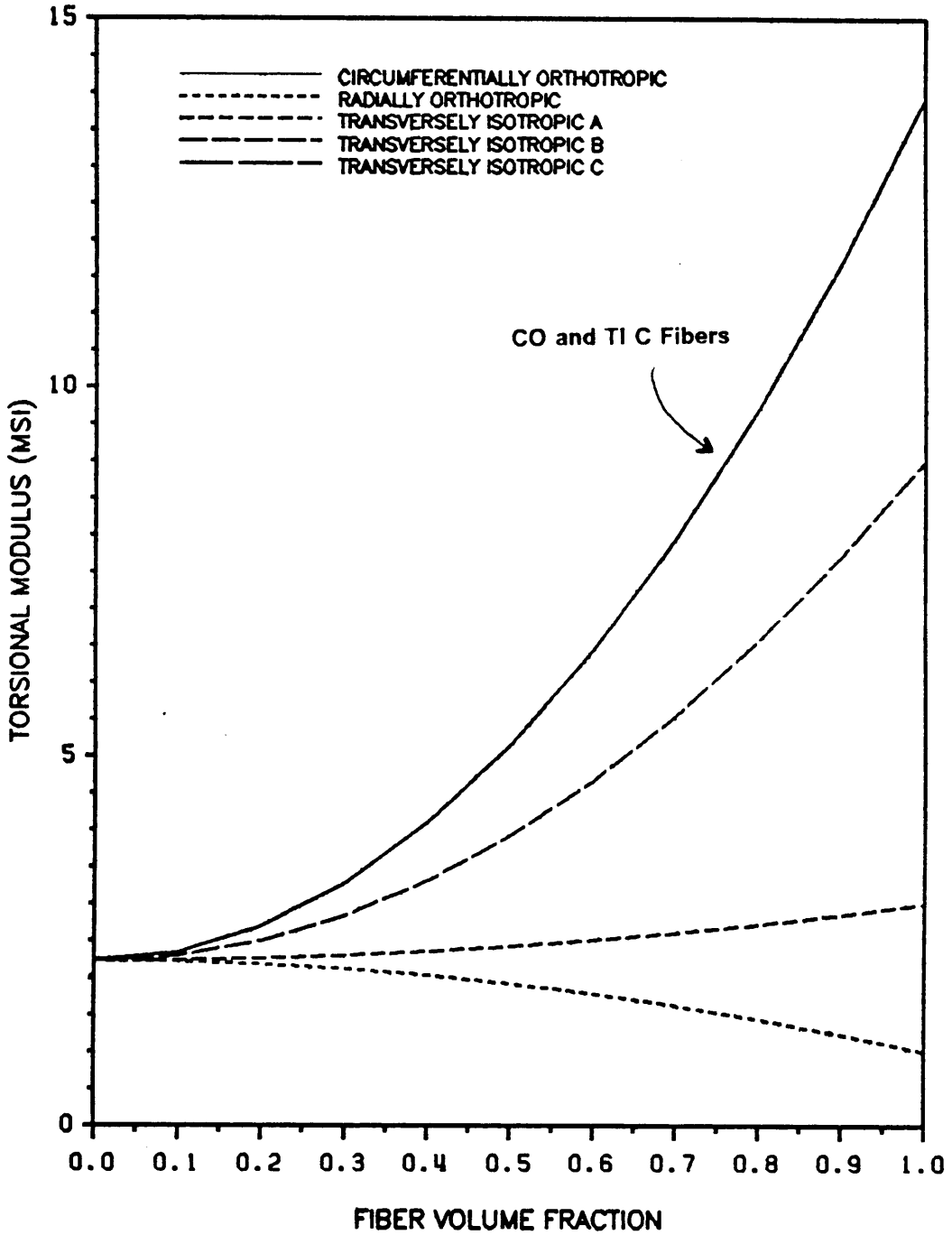

Figure 9. Torsional Modulus vs. Volume Fraction

2.7 Transverse Shear Modulus

Four of the five elastic moduli needed to completely characterize the effectively transversely isotropic composite material have been found. The remaining modulus to be found describes the behavior of the transverse plane, i.e., G_T, E_T, or ν_T. Unfortunately, this last property is not an easy one to determine. As Hashin[13] points out, the composite cylinder assemblage model fails to give a closed form expression for the transverse moduli when the phases are isotropic or transversely isotropic because in transverse loading a homogeneous traction field on the surface of the composite specimen does not yield the homogeneous displacement field. This is also the case when the fibers exhibit transverse orthotropy. Thus the composite cylinder assemblage could only be used to predict bounds on this modulus.

Christensen and Lo[16] use a three phase model to predict the effective transverse shear modulus of a composite specimen. Their model consists of a single composite cylinder imbedded in a cylinder whose properties are those of the effective composite material. They use the result obtained by Elsheby, that for a homogeneous medium containing an inclusion, the strain energy U under applied displacement conditions can be determined from the strain energy of the medium with no inclusion and the tractions and displacements in the medium with and without the inclusion, to arrive at an expression for the effective transverse shear modulus. For transversely isotropic fibers the solution to the equilibrium equations as given by Savin is used. In theory, the same method could be used when the fibers are transversely orthotropic. However, the equilibrium equations for an orthotropic material result in a general quartic relation which cannot be solved without knowing the specific relationship between the elastic constants of the phases. Since the goal of this study is to predict the modulus for a variety of morphologies, and therefore for a variety of relations between phase elastic constants no general solution could be found. For this reason it was decided that this study would not attempt to predict the effective transverse modulus needed to complete the characteriza-

tion of the effectively transversely isotropic composite material in terms of the properties of the constituent phases.

2.8 *Thermal Expansion Coefficients*

The effective thermal expansion coefficients of a composite cylinder are determined by applying a unit temperature change to the composite cylinder. This results in an axisymmetic stress state which can be analyzed using the solution found in section 2.1. As in the case of applied axial strain (section 2.2) since tractions on the surface of the cylinder must vanish, and due to continuity of tractions at $r=b$

$$F^f = F^m = E^f = E^m = 0. \tag{2.8.1}$$

Also,

$$\varepsilon^{om} = \varepsilon^{of} = \varepsilon^o \tag{2.8.2}$$

$$\gamma^{om} = \gamma^{of} = \gamma^o = 0. \tag{2.8.3}$$

Five constants A_1^f, A_2^f, A_1^m, A_2^m , and ε^o remain to be determined. The five conditions remaining to be satisfied are

1) Finite displacement at $r=0$.

$$A_1^f r^\lambda + H_1^f \varepsilon^o r + H_2^f \Delta T r \quad \text{is finite.} \tag{2.8.4}$$

2) Continuity of radial displacement at $r=b$.

$$A_1^m b + A_2^m \frac{1}{b} = A_1^f b^\lambda + H_1^f \varepsilon^o b + H_2^f \Delta T b \tag{2.8.5}$$

3) Continuity of radial stress at r=b.

$$A_1^m(C_{\theta r}^m + C_{rr}^m) + A_2^m(C_{\theta r}^m - C_{rr}^m)\frac{1}{b^2} - C_{rj}^m\alpha_j^m\Delta T + C_{xr}^m\varepsilon^o = A_1^f(C_{\theta r}^f + C_{rr}^f\lambda)b^{\lambda-1} + L_r^f\varepsilon^o + N_j^f\Delta T \tag{2.8 6}$$

4) Stress free boundary at r=c.

$$A_1^m(C_{\theta r}^m + C_{rr}^m) + A_2^m\frac{1}{c_2}(C_{\theta r}^m - C_{rr}^m) + C_{xr}^m\varepsilon^o - C_{rj}^m\alpha_j^m\Delta T = 0 \tag{2.8.7}$$

and

5) Zero net axial force, which is mathematically expressed

$$P = 2\pi\int_0^c \sigma_x r dr = 0 \tag{2.8.8}$$

and for the composite cylinder with orthotropic fibers results in the expression

$$A_1^f(C_{x\theta}^f + C_{xr}^f\lambda)\frac{b^{\lambda+1}}{\lambda+1} + L_x^f\varepsilon^o\frac{b_2}{2} + N_x^f\Delta T\frac{b^2}{2} + A_1^m(C_{x\theta}^m + C_{xr}^m)\frac{(c^2-b^2)}{2} + A_2^m(C_{x\theta}^m - C_{xr}^m)[\ln c - \ln b] + C_{xx}^m\varepsilon^o\frac{(c^2-b^2)}{2} - C_{xj}^m\alpha_j^m\Delta T\frac{(c^2-b^2)}{2} = 0 \tag{2.8.9}$$

From condition 1, $A_2^f = 0$. The system of equations resulting from the remaining conditions can be solved simultaneously to find

$$
\begin{aligned}
A_1^f = \frac{1}{\mathrm{DET}} \times \Bigg\{ & - H_2 \Delta T b \Bigg\{ (C_{r\theta}^m + C_{rr}^m) \Bigg[(C_{r\theta}^m - C_{rr}^m) \frac{1}{c^2} \left(L_x^f \frac{b^2}{2} + C_{xx}^m \frac{c^2 - b^2}{2} \right) \Bigg] \\
& + (C_{r\theta}^m - C_{rr}^m) \Bigg[(C_{r\theta}^m + C_{rr}^m) \left(L_x^f \frac{b^2}{2} + C_{xx}^m \frac{c^2 - b^2}{2} \right) \Bigg] \\
& + \left(L_r^f - C_{rx}^m \right) \Bigg[- (C_{x\theta}^m + C_{xr}^m) \frac{c^2 - b^2}{2} (C_{r\theta}^m - C_{rr}^m) \frac{1}{c^2} \Bigg] \Bigg\} \\
& + b \Bigg\{ \left(- N_r^f - C_{rj}^m \alpha_j^m \right) \Delta T \Bigg[(C_{r\theta}^m - C_{rr}^m) \frac{1}{c^2} \left(L_x^f \frac{b^2}{2} + C_{xx}^m \frac{c^2 - b^2}{2} \right) \Bigg] \\
& + (C_{r\theta}^m - C_{rr}^m) \frac{1}{b^2} \Bigg[C_{rj}^m \alpha_j^m \Delta T \left(L_x^f \frac{b^2}{2} + C_{xx}^m \frac{c^2 - b^2}{2} \right) - \left(- N_x^f \Delta T \frac{b^2}{2} + C_{xj}^m \alpha_j^m \Delta T \frac{c^2 - b^2}{2} \right) L_r^m \Bigg] \\
& + \left(L_r^f - C_{rx}^m \right) \Bigg[- \left(- N_x^f \Delta T \frac{b^2}{2} + C_{xj}^m \alpha_j^m \Delta T \frac{c^2 - b^2}{2} \right) \left(L_r^f - C_{rx}^m \right) \Bigg] \Bigg\} \\
& - \frac{1}{b} \Bigg\{ \left(- N_r^f + C_{ij}^m \alpha_j^m \right) \Delta T \Bigg[(C_{r\theta}^m + C_{rr}^m) \left(L_x^f \frac{b^2}{2} + C_{xx}^m \frac{c^2 - b^2}{2} \right) - (C_{x\theta}^m + C_{xr}^m) \frac{c^2 - b^2}{2} (C_{rx}^m) \Bigg] \\
& + (C_{r\theta}^m + C_{rr}^m) \Bigg[C_{rj}^m \alpha_j^m \Delta T \left(L_x^f \frac{b^2}{2} + C_{xx}^m \frac{c^2 - b^2}{2} \right) - \left(- N_x^f \frac{b^2}{2} + C_{xj}^m \alpha_j^m \frac{c^2 - b^2}{2} \right) C_{rx}^m \Delta T \Bigg] \\
& + \left(L_r^f - C_{rx}^m \right) \Bigg[C_{rj}^m \alpha_j^m \Delta T (C_{x\theta}^m + C_{xr}^m) \frac{c^2 - b^2}{2} - \left(- N_x^f \frac{b^2}{2} + C_{xj}^m \alpha_j^m \frac{c^2 - b^2}{2} \right) \Delta T (C_{r\theta}^m + C_{rr}^m) \Bigg] \Bigg\} \\
& - H_1^f b \Bigg\{ \left(- N_r^f - C_{rj}^m \alpha_j^m \right) \Delta T \Bigg[- (C_{x\theta}^m + C_{xr}^m) \frac{c^2 - b^2}{2} (C_{r\theta}^m - C_{rr}^m) \frac{1}{c^2} \Bigg] \\
& + (C_{r\theta}^m + C_{rr}^m) \Bigg[- \left(- N_x^f \frac{b^2}{2} + C_{xj}^m \alpha_j^m \frac{c^2 - b^2}{2} \right) \Delta T (C_{r\theta}^m - C_{rr}^m) \frac{1}{c^2} \Bigg] \\
& - (C_{r\theta}^m - C_{rr}^m) \Bigg[(C_{rj}^m \alpha_j^m \Delta T)(C_{x\theta}^m + C_{xr}^m) \frac{c^2 - b^2}{2} \\
& - \left(- N_x^f \frac{b^2}{2} + C_{xj}^m \alpha_j^m \frac{c^2 - b^2}{2} \right) \Delta T (C_{r\theta}^m + C_{rr}^m) \Bigg] \Bigg\} \Bigg\}
\end{aligned}
$$

(2.8.10)

$$
\begin{aligned}
A_1^m = \frac{1}{\mathrm{DET}} \times \Bigg\{ & b^{\lambda} \Bigg\{ \left(-N_r^f - C_{rj}^m \alpha_j^m \right) \Delta T \left[\left(C_{r\theta}^m - C_{rr}^m \right) \frac{1}{c^2} \left(L_x^f \frac{b^2}{2} + C_{xx}^m \frac{c^2 - b^2}{2} \right) \right] \\
& + \left(C_{r\theta}^m - C_{rr}^m \right) \frac{1}{b^2} \left[C_{rj}^m \alpha_j^m \Delta T \left(L_x^f \frac{b^2}{2} + C_{xx}^m \frac{c^2 - b^2}{2} \right) - \left(-N_x^f \Delta T \frac{b^2}{2} + C_{xx}^m \Delta T \frac{c^2 - b^2}{2} \right) C_{rx}^m \right] \\
& + \left(L_r^f - C_{rx}^m \right) \left[-\left(-N_x^f \frac{b^2}{2} + C_{xj}^m \alpha_j^m \frac{c^2 - b^2}{2} \right) \Delta T \left(C_{r\theta}^m - C_{rr}^m \right) \frac{1}{c^2} \right] \Bigg\} \\
& + H_2^f \Delta T b \Bigg\{ \left(C_{r\theta}^f + C_{rr}^f \lambda \right) b^{\lambda - 1} \left[\left(C_{r\theta}^m - C_{rr}^m \right) \frac{1}{c^2} \left(L_x^f \frac{b^2}{2} + C_{xx}^m \frac{c^2 - b^2}{2} \right) \right] \\
& + \left(C_{r\theta}^m - C_{rr}^m \right) \frac{1}{b^2} \left[-\left(C_{x\theta}^f + C_{xr}^f \lambda \right) \frac{b^{\lambda+1}}{\lambda + 1} \left(C_{rx}^m \right) \right] \\
& + \left(L_r^f - C_{rx}^m \right) \left[-\left(C_{x\theta}^f + C_{xr}^f \lambda \right) \frac{b^{\lambda+1}}{\lambda + 1} \left(C_{r\theta}^m - C_{rr}^m \right) \right] \Bigg\} \\
& - \frac{1}{b} \Bigg\{ \left(C_{r\theta}^f + C_{rr}^f \lambda \right) b^{\lambda - 1} \left[C_{rj}^m \alpha_j^m \Delta T \left(L_x^f \frac{b^2}{2} + C_{xx}^m \frac{c^2 - b^2}{2} \right) - \left(-N_x^f \frac{b^2}{2} + C_{xj}^m \alpha_j^m \Delta T \right) \Delta T C_{rx}^m \right] \\
& - \left(-N_r^f - C_{rj}^m \alpha_j^m \right) \Delta T \left[-\left(C_{x\theta}^f + C_{xr}^f \lambda \right) \frac{b^{\lambda+1}}{\lambda + 1} \left(C_{rx}^m \right) \right] \\
& + \left(L_r^f - C_{rx}^m \right) \left[-\left(C_{x\theta}^f + C_{xr}^f \lambda \right) \frac{b^{\lambda+1}}{\lambda + 1} \left(C_{rj}^m \alpha_j^m \Delta T \right) \right] \Bigg\} \\
& - H_1^f b \Bigg\{ \left(C_{r\theta}^f + C_{rr}^f \lambda \right) \left[-\left(-N_x^f \frac{b^2}{2} + C_{xj}^m \alpha_j^m \frac{c^2 - b^2}{2} \right) \Delta T \left(C_{r\theta}^m - C_{rr}^m \right) \frac{1}{c^2} \right] \\
& - \left(-N_r^f - C_{rj}^m \alpha_j^m \right) \Delta T \left[-\left(C_{x\theta}^f + C_{xr}^f \lambda \right) \frac{b^{\lambda+1}}{\lambda + 1} \left(C_{r\theta}^m - C_{rr}^m \right) \frac{1}{c^2} \right] \\
& - \left(C_{r\theta}^m - C_{rr}^m \right) \frac{1}{b^2} \left[-\left(C_{x\theta}^f + C_{xr}^f \lambda \right) \frac{b^{\lambda+1}}{\lambda + 1} \left(C_{rj}^m \alpha_j^m \Delta T \right) \right] \Bigg\} \Bigg\}
\end{aligned}
\tag{2.8.11}
$$

$$
\begin{aligned}
A_2^m = \frac{1}{\mathrm{DET}} x\Bigg\{ & b^{\lambda}\Bigg\{ -(C_{r\theta}^m + C_{rr}^m)\Bigg[C_{rj}^m \alpha_j^m \Delta T\left(L_x^f \frac{b^2}{2} + C_{xx}^m \frac{c^2-b^2}{2} \right) \\
& - \left(N_x^f \frac{b^2}{2} + C_{xj}^m \alpha_j^m \frac{c^2-b^2}{2} \right) \Delta T C_{rr}^m \Bigg] \\
& - \left(-N_r^f - C_{rj}^m \alpha_j^m \right) \Delta T \Bigg[(C_{r\theta}^m + C_{rr}^m)\left(L_x^f \frac{b^2}{2} + C_{xx}^m \frac{c^2-b^2}{2} \right) \\
& - (C_{x\theta}^m + C_{xr}^m) \frac{c^2-b^2}{2} C_{rx}^m \Bigg] \\
& + \left(L_r^f - C_{rx}^m \right) \Bigg[(C_{r\theta}^m + C_{rr}^m)\left(-N_x^f \frac{b^2}{2} + C_{xj}^m \alpha_j^m \frac{c^2-b^2}{2} \right) \Delta T \\
& - (C_{x\theta}^m + C_{xr}^m) \frac{c^2-b^2}{2} C_{xj}^m \alpha_j^m \Delta T \Bigg] \Bigg\} \\
& + b\Bigg\{ (C_{r\theta}^f + C_{rr}^f \lambda) b^{\lambda-1} \Bigg[C_{rj}^m \alpha_j^m \Delta T\left(L_x^f \frac{b^2}{2} + C_{xx}^m \frac{c^2-b^2}{2} \right) \\
& - \left(-N_x^f \frac{b^2}{2} + C_{xj}^m \alpha_j^m \frac{c^2-b^2}{2} \right) \Delta T C_{rx}^m \Bigg] \\
& - \left(-N_r^f - C_{rj}^m \alpha_j^m \right) \Delta T \Bigg[-(C_{x\theta}^f + C_{xr}^f \lambda) \frac{b^{\lambda+1}}{\lambda+1} C_{rx}^m \Bigg] \\
& + \left(L_r^f - C_{rx}^m \right) \Bigg[-(C_{x\theta}^f + C_{xr}^f \lambda) \frac{b^{\lambda+1}}{\lambda+1} (C_{rj}^m \alpha_j^m \Delta T) \Bigg] \Bigg\} \\
& - H_2 \Delta T b \Bigg\{ (C_{r\theta}^f + C_{rr}^f \lambda) b^{\lambda-1} \Bigg[(C_{r\theta}^m + C_{rr}^m)\left(L_x^f \frac{b^2}{2} + C_{xx}^m \frac{c^2-b^2}{2} \right) - (C_{x\theta}^m + C_{xr}^m) \frac{c^2-b^2}{2} C_{rx}^m \Bigg] \\
& + (C_{r\theta}^m + C_{rr}^m) \Bigg[-(C_{x\theta}^f + C_{xr}^f \lambda) \frac{b^{\lambda+1}}{\lambda+1} C_{rx}^m \Bigg] \\
& + \left(L_r^f + C_{rx}^m \right) \Bigg[-(C_{x\theta}^f + C_{xr}^f \lambda) \frac{b^{\lambda+1}}{\lambda+1} (C_{r\theta}^m + C_{rr}^m) \Bigg] \Bigg\} \\
& - H_1^f b \Bigg\{ (C_{r\theta}^f + C_{rr}^f \lambda) b^{\lambda-1} \Bigg[(C_{r\theta}^m + C_{rr}^m)\left(-N_x^f \frac{b^2}{2} + C_{xj}^m \alpha_j^m \frac{c^2-b^2}{2} \right) \Delta T \\
& - (C_{x\theta}^m + C_{xr}^m) \frac{c^2-b^2}{2} (C_{rj}^m \alpha_j^m \Delta T) \Bigg] \\
& + (C_{r\theta}^m + C_{rr}^m) \Bigg[-(C_{x\theta}^f + C_{xr}^f \lambda) \frac{b^{\lambda+1}}{\lambda+1} (C_{rj}^m \alpha_j^m \Delta T) \Bigg] \\
& + \left(-N_r^f - C_{rj}^m \alpha_j^m \right) \Delta T \Bigg[-(C_{x\theta}^f + C_{xr}^f \lambda) \frac{b^{\lambda+1}}{\lambda+1} (C_{r\theta}^m + C_{rr}^m) \Bigg] \Bigg\} \Bigg\}
\end{aligned}
\tag{2.8.12}
$$

$$
\begin{aligned}
\varepsilon^{o} = \frac{1}{\mathrm{DET}} x \Bigg\{ & b^{\lambda} \Bigg\{ - (C_{r\theta}^{m} + C_{rr}^{m}) \Bigg[(C_{r\theta}^{m} - C_{rr}^{m}) \frac{1}{c^2} \left(- N_x^f \frac{b^2}{2} + C_{xj}^{m} \alpha_j^{m} \frac{c^2 - b^2}{2} \right) \Delta T \Bigg] \\
& + (C_{r\theta}^{m} - C_{rr}^{m}) \frac{1}{b^2} \Bigg[(C_{r\theta}^{m} + C_{rr}^{m}) \left(- N_x^f \frac{b^2}{2} + C_{xj}^{m} \alpha_j^{m} \frac{c^2 - b^2}{2} \right) \Delta T - (C_{x\theta}^{m} + C_{xr}^{m}) \frac{c^2 - b^2}{2} (C_{rj}^{m} \alpha_j^{m} \Delta T) \Bigg] \\
& + \left(- N_r^f - C_{rj}^{m} \alpha_j^{m} \right) \Delta T \Bigg[- (C_{x\theta}^{m} + C_{xr}^{m}) \frac{c^2 - b^2}{2} (C_{r\theta}^{m} - C_{rr}^{m}) \frac{1}{c^2} \Bigg] \Bigg\} \\
& + b \Bigg\{ (C_{r\theta}^{f} + C_{rr}^{f} \lambda) b^{\lambda - 1} \Bigg[(C_{r\theta}^{m} - C_{rr}^{m}) \frac{1}{c^2} \left(- N_x^f \frac{b^2}{2} + C_{xj}^{m} \alpha_j^{m} \frac{c^2 - b^2}{2} \right) \Delta T \Bigg] \\
& + (C_{r\theta}^{m} - C_{rr}^{m}) \frac{1}{b^2} \Bigg[- (C_{x\theta}^{f} + C_{xr}^{f} \lambda) \frac{b^{\lambda + 1}}{\lambda + 1} (C_{rj}^{m} \alpha_j^{m} \Delta T) \Bigg] \\
& + \left(- N_r^f - C_{rj}^{m} \alpha_j^{m} \right) \Delta T \Bigg[- (C_{x\theta}^{f} + C_{xr}^{f} \lambda) \frac{b^{\lambda + 1}}{\lambda + 1} (C_{r\theta}^{m} - C_{rr}^{m}) \frac{1}{c^2} \Bigg] \Bigg\} \\
& - \frac{1}{b} \Bigg\{ (C_{r\theta}^{f} + C_{rr}^{f} \lambda) b^{\lambda - 1} \Bigg[(C_{r\theta}^{m} + C_{rr}^{m}) \left(- N_x^f \frac{b^2}{2} + C_{xj}^{m} \alpha_j^{m} \frac{c^2 - b^2}{2} \right) \Delta T \\
& - (C_{x\theta}^{m} + C_{xr}^{m}) \frac{c^2 - b^2}{2} (C_{rj}^{m} \alpha_j^{m}) \Delta T \Bigg] \\
& + (C_{r\theta}^{m} + C_{rr}^{m}) \Bigg[(C_{x\theta}^{f} + C_{xr}^{f} \lambda) \frac{b^{\lambda + 1}}{\lambda + 1} C_{rj}^{m} \alpha_j^{m} \Delta T \Bigg] \\
& + \left(N_r^f - C_{rj}^{m} \alpha_j^{m} \right) \Delta T \Bigg[- (C_{x\theta}^{f} + C_{xr}^{f} \lambda) \frac{b^{\lambda + 1}}{\lambda + 1} (C_{r\theta}^{m} + C_{rr}^{m}) \Bigg] \Bigg\} \\
& + H_2 \Delta T b \Bigg\{ (C_{r\theta}^{f} + C_{rr}^{f} \lambda) b^{\lambda - 1} \Bigg[- (C_{x\theta}^{m} + C_{xr}^{m}) \frac{c^2 - b^2}{2} (C_{r\theta}^{m} - C_{rr}^{m}) \frac{1}{c^2} \Bigg] \\
& + (C_{r\theta}^{m} + C_{rr}^{m}) \Bigg[- (C_{x\theta}^{f} + C_{xr}^{f} \lambda) \frac{b^{\lambda + 1}}{\lambda + 1} (C_{r\theta}^{m} + C_{rr}^{m}) \frac{1}{c^2} \Bigg] \\
& - (C_{r\theta}^{m} - C_{rr}^{m}) \frac{1}{b^2} \Bigg[- (C_{x\theta}^{f} + C_{xr}^{f} \lambda) \frac{b^{\lambda + 1}}{\lambda + 1} (C_{r\theta}^{m} + C_{rr}^{m}) \Bigg] \Bigg\} \Bigg\}
\end{aligned}
\tag{2.8.13}
$$

and,

$$
\begin{aligned}
\mathrm{DET} = b^{\lambda}\Bigg\{ & -(C^m_{r\theta}-C^m_{rr})\left[(C^m_{r\theta}-C^m_{rr})\frac{1}{c^2}\left(L^f_x\frac{b^2}{2}+C^m_{xx}\frac{c^2-b^2}{2}\right)\right] \\
& +(C^m_{r\theta}-C^m_{rr})\frac{1}{b^2}\left[(C^m_{r\theta}+C^m_{rr})\left(L^f_x\frac{b^2}{2}+C^m_{xx}\frac{c^2-b^2}{2}\right)-C^m_{rx}(C^m_{r\theta}+C^m_{xr})\frac{c^2-b^2}{2}\right] \\
& +(L^f_r-C^m_{rx})\left[-(C^m_{x\theta}+C^m_{xr})\frac{c^2-b^2}{2}(C^m_{r\theta}-C^m_{rr})\frac{1}{c^2}\right]\Bigg\} \\
& +b\Bigg\{(C^m_{r\theta}+C^m_{rr})b^{\lambda-1}\left[(C^m_{r\theta}-C^m_{rr})\frac{1}{c^2}\left(L^f_x\frac{b^2}{2}+C^m_{xx}\frac{c^2-b^2}{2}\right)\right] \\
& +(C^m_{r\theta}-C^m_{rr})\frac{1}{b^2}\left[-(C^f_{x\theta}+C^f_{xr}\lambda)\frac{b^{\lambda+1}}{\lambda+1}(C^m_{rx})\right] \\
& +(L^f_r-C^m_{rx})\left[-(C^f_{x\theta}+C^f_{xr}\lambda)\frac{b^{\lambda+1}}{\lambda+1}(C^m_{r\theta}+C^m_{rr})\frac{1}{c^2}\right]\Bigg\} \\
& -\frac{1}{b}\Bigg\{(C^f_{r\theta}+C^f_{rr}\lambda)b^{\lambda-1}\left[(C^m_{r\theta}+C^m_{rr})\left(L^f_x\frac{b^2}{2}+C^m_{xx}\frac{c^2-b^2}{2}\right)-(C^m_{x\theta}+C^m_{rr})\frac{c^2-b^2}{2}C^m_{rx}\right) \\
& +(C^m_{r\theta}+C^m_{rr})\left[-(C^f_{x\theta}+C^f_{xr}\lambda)\frac{b^{\lambda+1}}{\lambda+1}C^m_{rx}\right] \\
& +(L^f_r-C^m_{rx})\left[-(C^f_{x\theta}+C^f_{xr}\lambda)\frac{b^{\lambda+1}}{\lambda+1}(C^m_{r\theta}+C^m_{rr})\right]\Bigg\} \\
& -H_1 b\Bigg\{(C^f_{r\theta}+C^f_{rr}\lambda)b^{\lambda-1}\left[-(C^m_{x\theta}+C^m_{xr})\frac{c^2-b^2}{2}(C^m_{r\theta}-C^m_{rr})\frac{1}{c^2}\right] \\
& +(C^m_{r\theta}+C^m_{rr})\left[-(C^f_{x\theta}+C^f_{xr}\lambda)\frac{b^{\lambda+1}}{\lambda+1}(C^m_{r\theta}-C^m_{rr})\frac{1}{c^2}\right] \\
& -(C^m_{r\theta}-C^m_{rr})\frac{1}{b^2}\left[-(C^f_{x\theta}-C^f_{xr}\lambda)\frac{b^{\lambda+1}}{\lambda+1}(C^m_{r\theta}+C^m_{rr})\right]\Bigg\}\Bigg\}
\end{aligned}
\tag{2.8.14}
$$

ε^o in Equation 2.8.13 can be written in the form

$$
\varepsilon^o = \alpha^*_x \Delta T \tag{2.8.15}
$$

where α^*_x is the apparent axial coefficient of thermal expansion of the composite cylinder.

The radial displacement on the surface of the cylinder is given by

$$u_r(c) = A_1^m c + A_2^m \frac{1}{c}. \tag{2.8.16}$$

Substituting from Eqns. 2.8.11, 2.8.12, and 2.8.14 this expression can be written in the form

$$u_r(c) = \alpha_t^* r \Delta T. \tag{2.8.17}$$

α_t^* in this expression is the apparent transverse coefficient of thermal expansion of the composite cylinder.

Using an argument similar to that used in previous sections it can be shown that the boundary tractions and displacements resulting in the composite cylinder are of the same form as those resulting in a homogeneous cylinder subjected to the same temperature change. Therefore it is possible to show that cylinders within a homogeneous body can be repeatedly replaced with composite cylinders with no effect on the stress or strain state within the body. Thus α_x^* and α_t^* are the effective thermal moduli of the composite cylinder.

As with the elastic moduli circumferential and radial morphology have the same effect on the effective thermal moduli of a composite. In Figure 10 and Figure 11 the curves for the effective properties of the CO and RO fiber composite cylinders coincide. Hashin[13] determined the effective coefficients of thermal expansion in a different manner, and due to the complexity of his method only determined an expression for the effective CTE's of composites with isotropic phases. The result of this study has therefore not been reduced further. Numerically the results for the effective thermal coefficients of thermal expansion of composites with transversely isotropic fibers have been compared with results obtained by Bowles[28] and found to agree closely. Bowles uses a method similar to that used by Hashin to calculate the coefficients of thermal expansion for a composite.

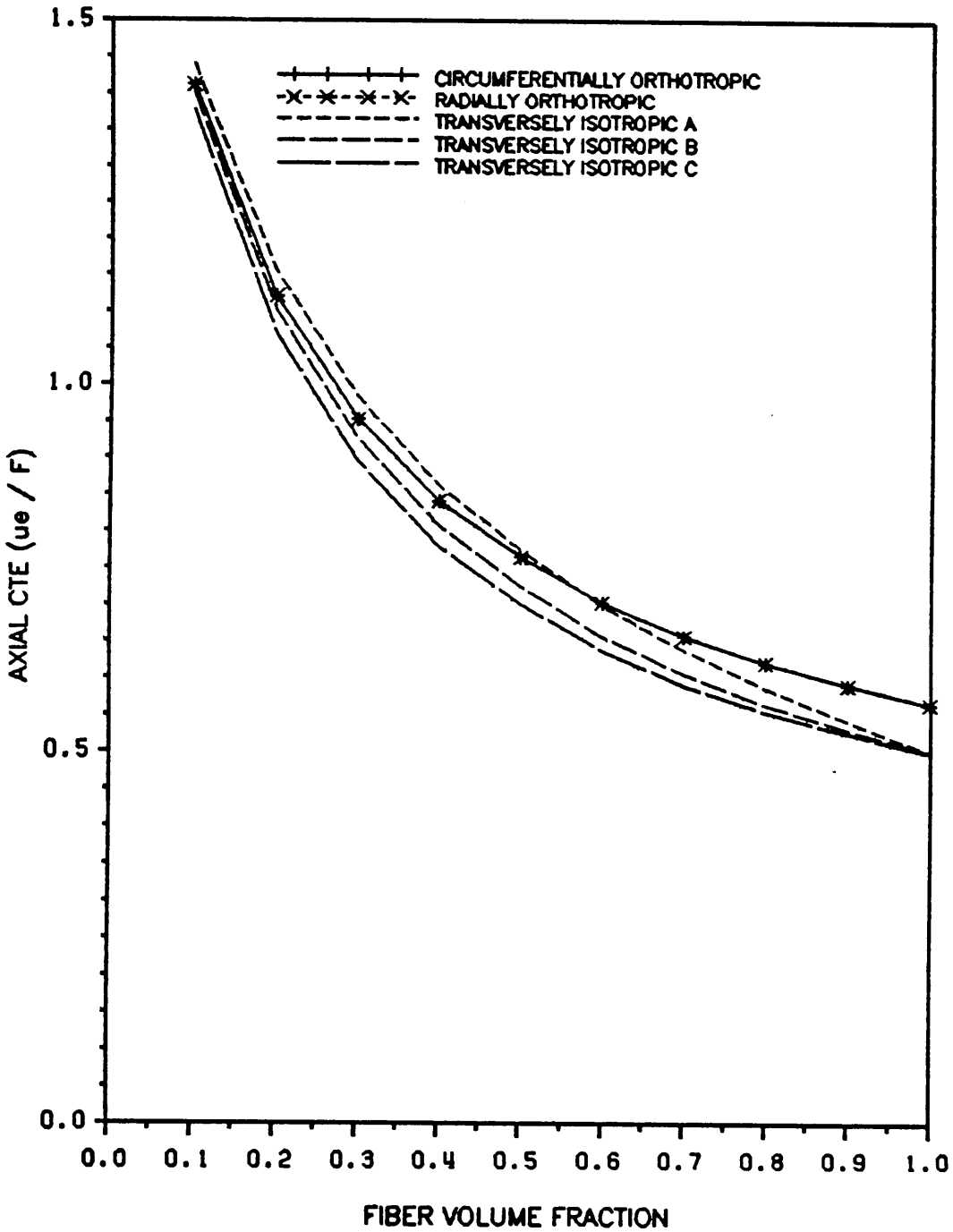

Figure 10. Effective Axial CTE vs. Fiber Volume Fraction

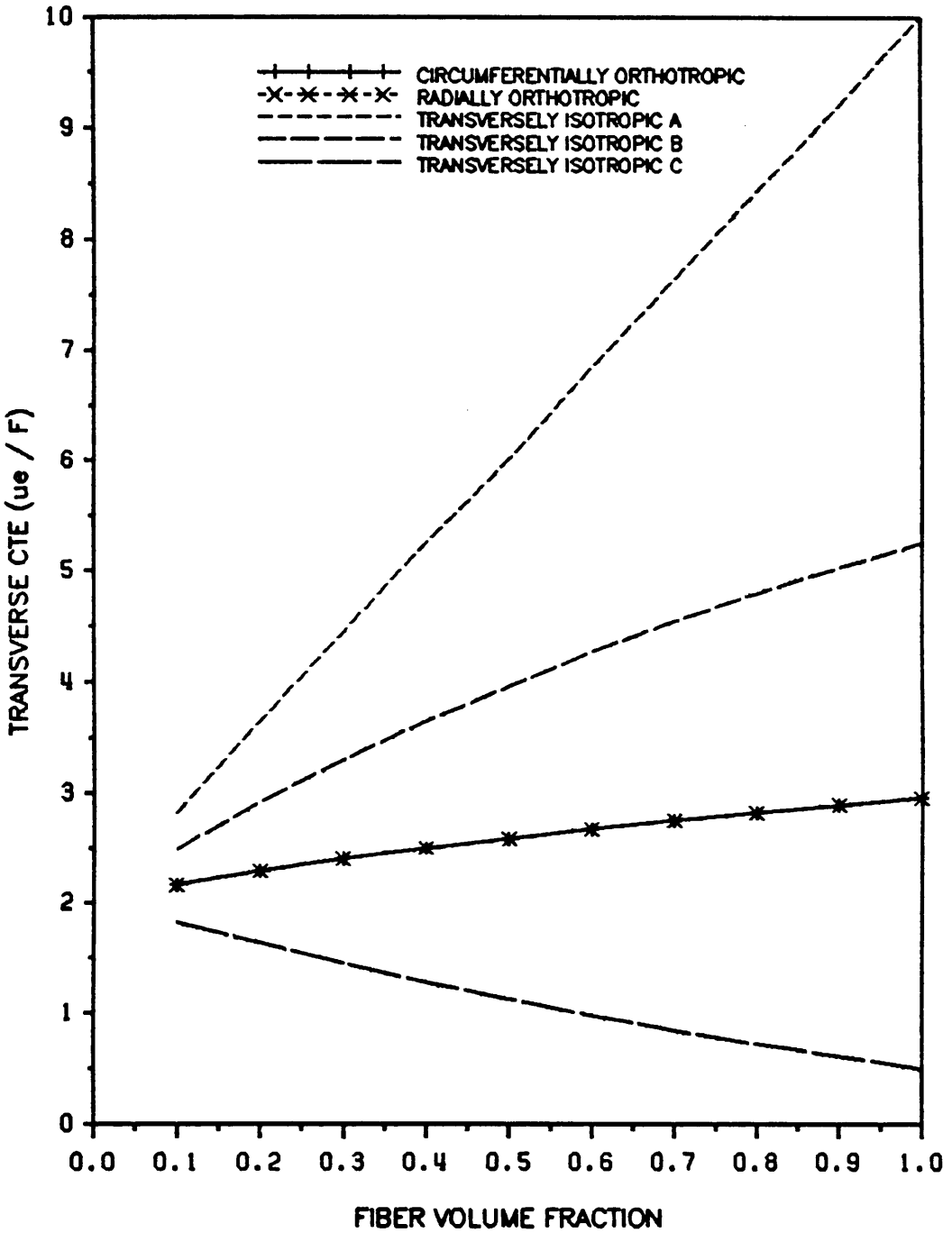

Figure 11. Effective Transverse CTE vs. Fiber Volume Fraction

3.0 Stress Distributions

The stress distributions that result in a single composite cylinder under the applied loadings considered in the previous chapter are discussed in this chapter. Results for a fiber volume fraction of 0.602 are presented. The morphology of the fiber is shown to have a significant influence on the stress distribution in the composite cylinder.

3.1 Axial Loading

An applied axial strain (ε^o) of 1% is considered. Recalling from Section 2.2 that for solid fibers $A_2^f = 0$, the expressions (2.1.25 and 2.1.26) for the stresses simplify to

1) in an orthotropic fiber

$$\sigma_i^f = A_1^f\left(C_{i\theta}^f + C_{ir}^f\lambda\right)r^{\lambda-1} + \left[C_{ix}^f + H_1^f\left(C_{i\theta}^f + C_{ir}^f\right)\right]\varepsilon^o \tag{3.1.1}$$

2) in a transversely isotropic fiber

$$\sigma_i^f = A_1^f\left(C_{i\theta}^f + C_{ir}^f\right) + C_{ix}^f\varepsilon^o \tag{3.1.2}$$

and 3) in the isotropic matrix

$$\sigma_i^m = A_1^m(C_{i\theta}^m + C_{ir}^m) + A_2^m(C_{i\theta}^m - C_{ir}^m)\frac{1}{r^2} + C_{ix}^m\varepsilon^o. \tag{3.1.3}$$

In all phases the shear stresses vanish;

$$\tau_{\theta r} = \tau_{xr} = \tau_{x\theta} = 0. \tag{3.1.4}$$

Circumferentially Orthotropic Fibers

In a circumferentially orthotropic fiber the basal planes are oriented in the x and theta directions. Thus $C_{\theta\theta} > C_{rr}$ and $\lambda = \sqrt{\frac{C_{\theta\theta}}{C_{rr}}} > 1$. Due to the term $A_1^f(C_{i\theta}^f + C_{ir}^f\lambda)r^{\lambda-1}$ in eqn 3.1.1 the stresses in the fiber have a power law dependence on radius. As shown in Figure 12, the dependence of axial stress in the fiber on r is negligible due to the relative strength of the ε^o term. In the axial stress this term is especially significant since C_{xx}^f is much larger that C_{xr}^f and $C_{x\theta}^f$. The radial and circumferential stresses in the fiber are two orders of magnitude lower than the axial stress. The radial stress remains tensile throughout the fiber. The circumferential stress is tensile at the center of the fiber, but becomes compressive near the fiber matrix interface. It is interesting to note that the radial and circumferential stresses have the same value at the center of the fiber. This has physical significance since at the center of the fiber the radial and circumferential directions are the same. In general the stresses in the matrix have an inverse relationship with radius. The axial stress however is constant since the term $A_2^m(C_{x\theta}^m - C_{xr}^m)\frac{1}{r^2}$ is zero because for the isotropic matrix $C_{x\theta}^m = C_{xr}^m$. The circumferential stress is compressive in the matrix, while the radial stress is tensile. At the interface between the fiber and the matrix, the radial stress is tensile.

Radially Orthotropic Fibers

The stresses in a composite cylinder with a radially orthotropic fiber are shown in Figure 13. In the radially orthotropic fiber $C_{rr} > C_{\theta\theta}$ and $\lambda < 1$. The term $A_1^f(C_{i\theta}^f + C_{ir}^f)r^{\lambda-1}$ is thus singular

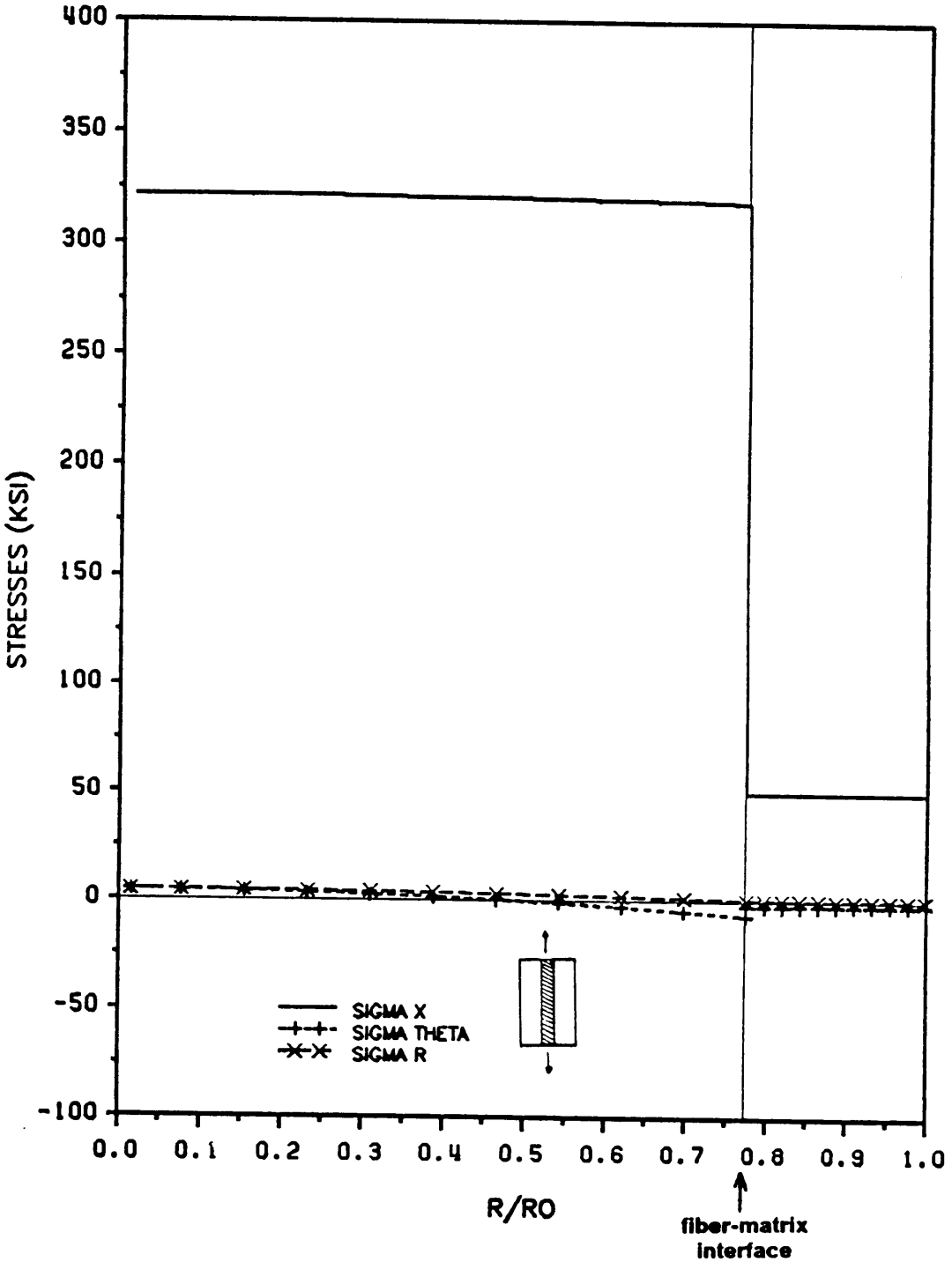

Figure 12. Stress distributions in a composite cylinder with a circumferentially orthotropic fiber subjected to axial loading

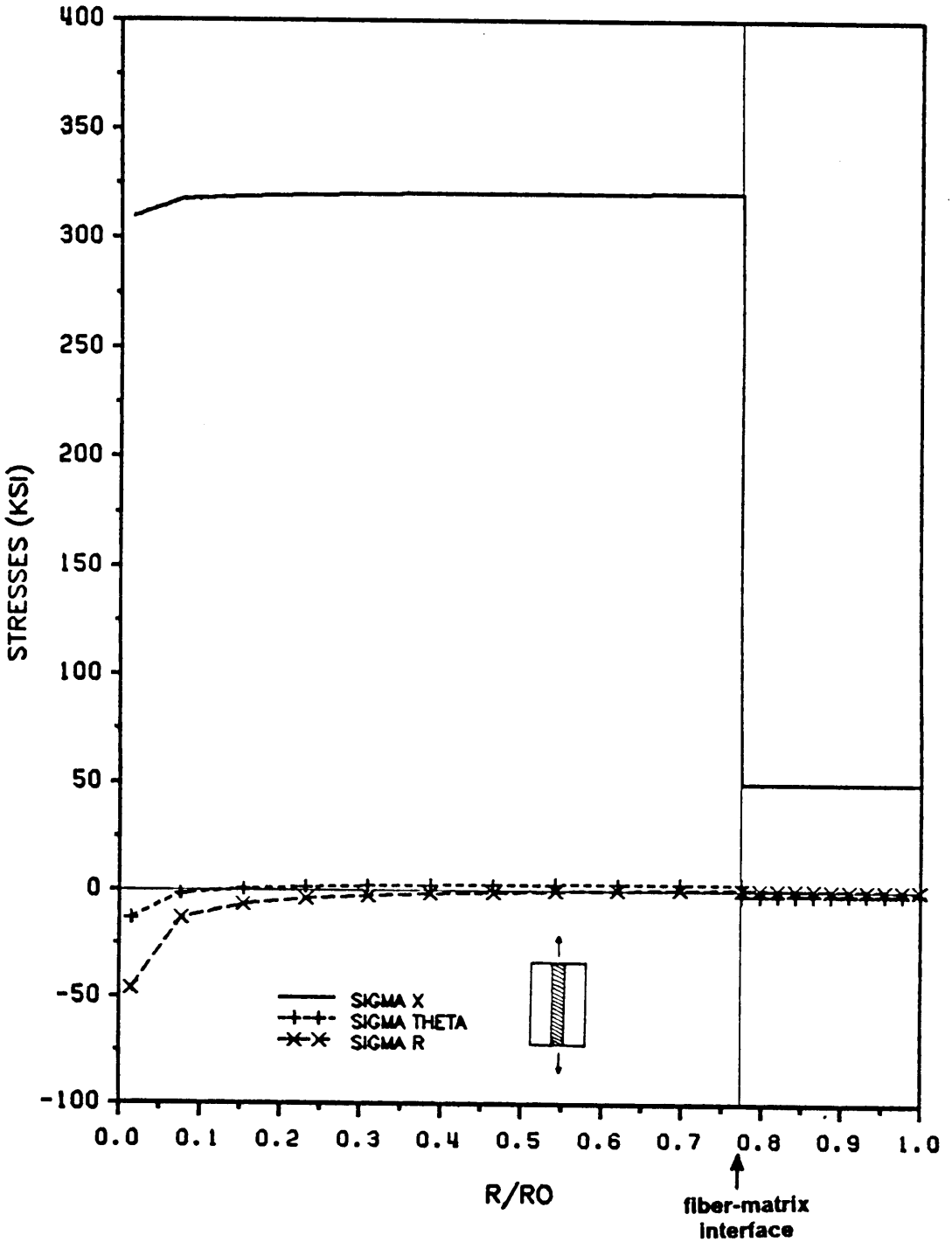

Figure 13. Stress distributions in a composite cylinder with a radially orthotropic fiber subjected to axial loading.

of order $\lambda - 1$. For the fibers examined in this study the order of the singularity, which depends only on material constants, is 0.649. The strength of the singularity, S, for each component of stress under an applied axial strain of 1% is

$$S_x = A_1^f\left(C_{x\theta}^f + C_{xr}^f\lambda\right) = -3.288 \tag{3.1.5}$$

$$S_r = A_1^f\left(C_{r\theta}^f + C_{rr}^f\lambda\right) = -13.831 \tag{3.1.6}$$

and

$$S_\theta = A_1^f\left(C_{\theta\theta}^f + C_{\theta r}^f\lambda\right) = -4.854. \tag{3.1.7}$$

The radial stress therefore has the most singular nature. Due to the relative strength of the term multiplying ε_x^o the axial stress is essentially constant throughout the fiber. However near the center of the fiber, as r approaches zero, the singular term begins to over power the ε_x^o term and the stress decreases. Both the radial and circumferential stresses in the fiber are compressively singular at r=0, and become tensile at the fiber matrix interface. In the matrix the axial stress is constant since the term involving radial dependence is zero. The radial stress in the matrix is again tensile, decreasing with radius, and the circumferential stress is compressive, becoming less compressive with increasing radius.

Transversely Isotropic Fibers

The stress distributions in the three transversely isotropic fibers studied have the same character although the magnitudes vary due to the different fiber properties. As illustrated in Figure 14, Figure 15, and Figure 16, the axial stress in the transversely isotropic fiber is constant. This is expected as in equation 3.1.2 the term involving radial dependence is zero for a transversely isotropic fiber since $C_{xr}^f = C_{x\theta}^f$. The radial and circumferential stresses in each fiber are the same, as expected from equation 3.1.2. In the matrix the circumferential

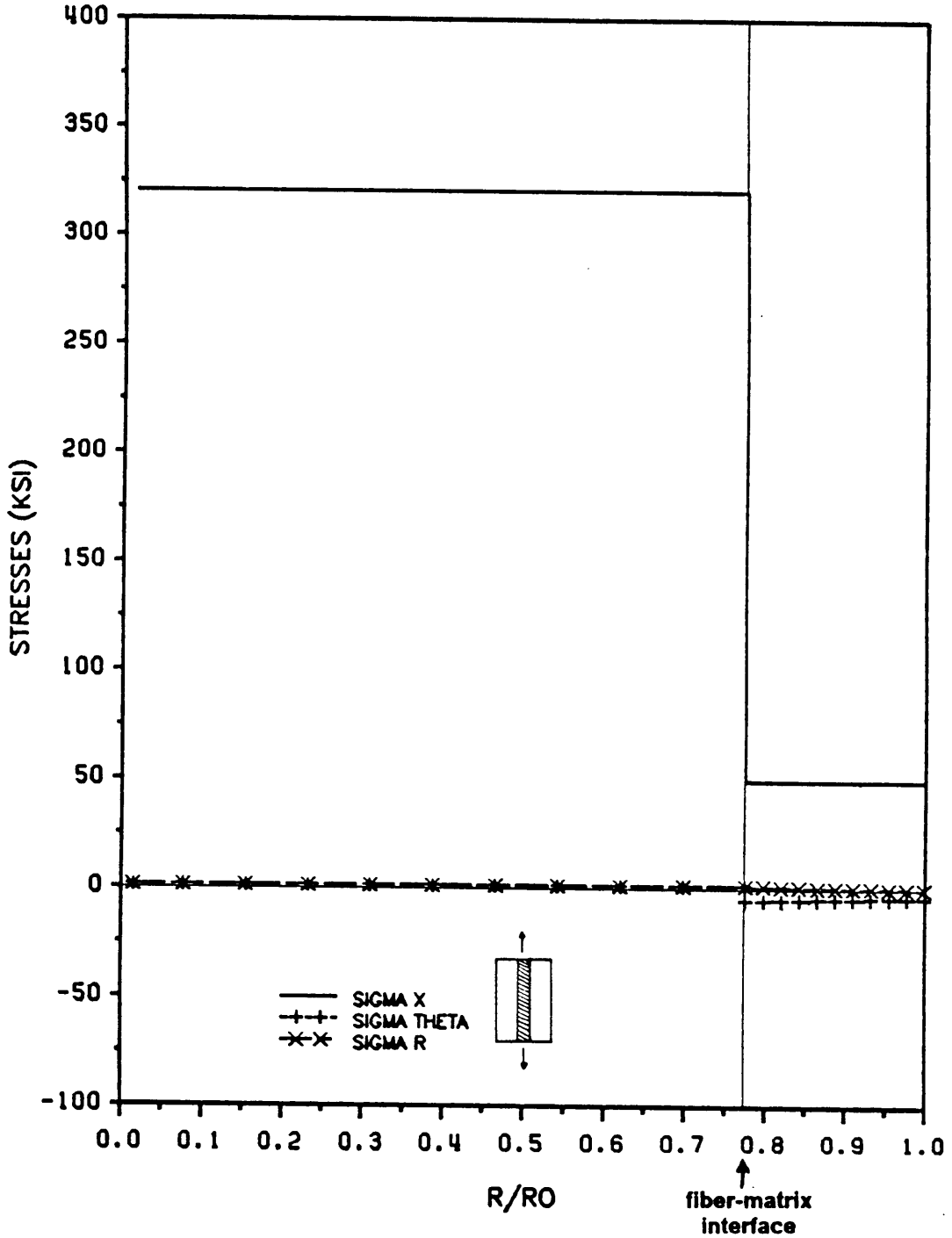

Figure 14. Stress distributions in a composite cylinder with transversely istotropic (A) fiber subjected to axial loading

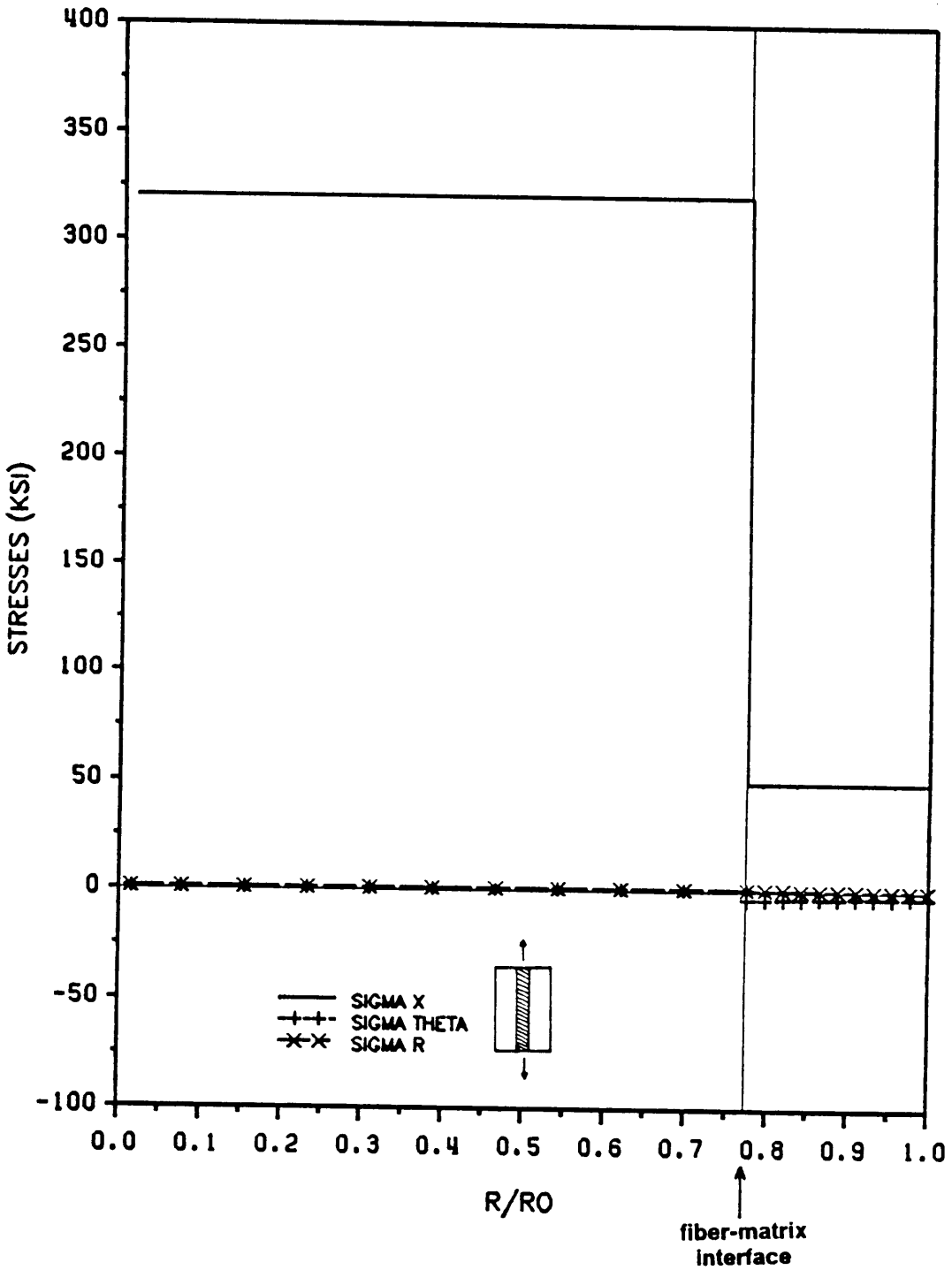

Figure 15. **Stress distributions in a composite cylinder with transversely istotropic (B) fiber subjected to axial loading.**

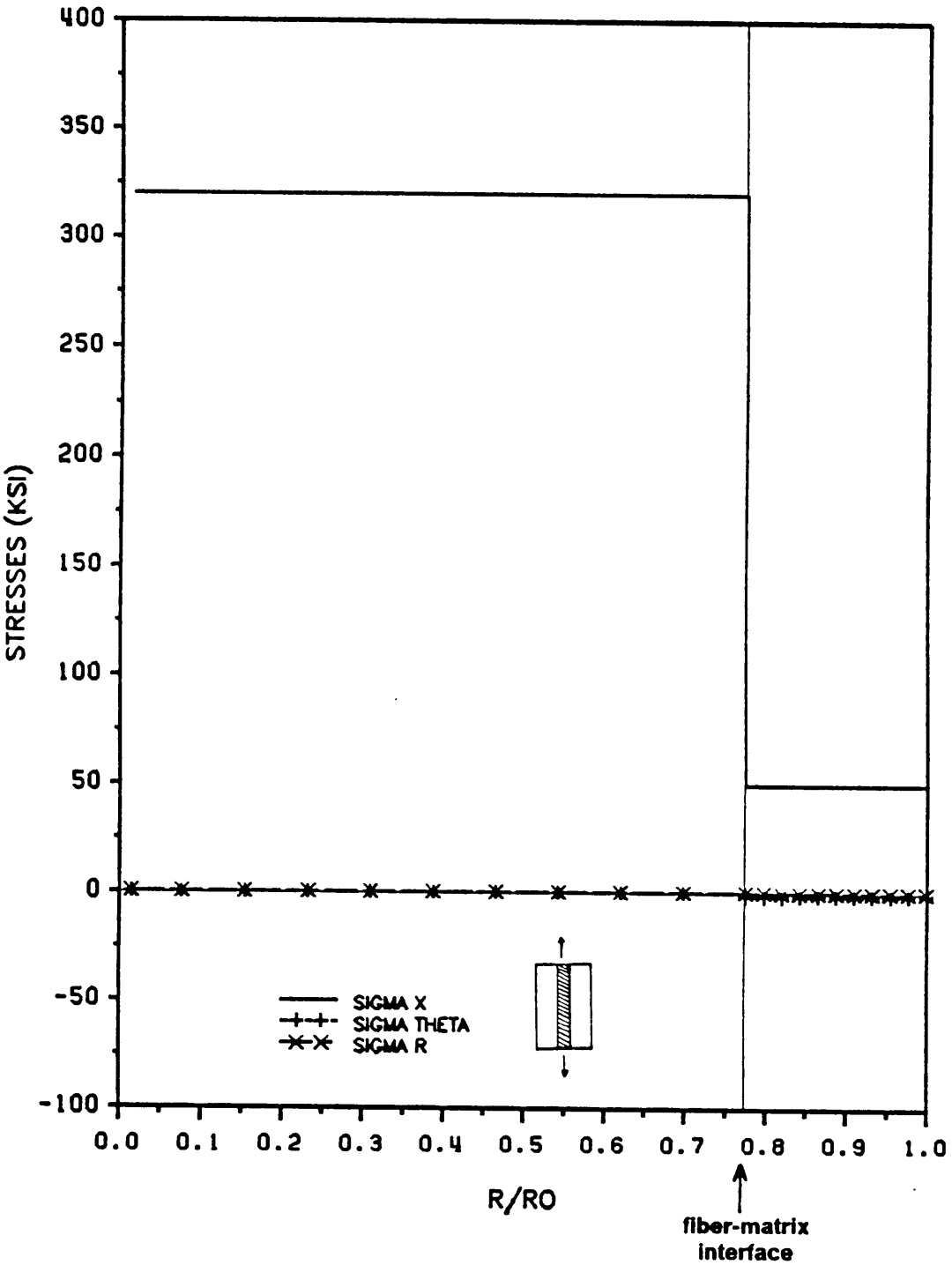

Figure 16. Stress distributions in a composite cylinder with transversely istotropic (C) fiber subjected to axial loading.

stresses are again compressive, decreasing with increasing radius. The radial stresses are tensile, approaching zero at the surface of the composite cylinder.

3.2 Radial Loading

To determine the effective transverse bulk modulus of a composite material a radial displacement $w = \varepsilon_r^o b$ is applied to the surface of the composite cylinder. The stresses resulting when $\varepsilon_r^o = 1\%$ are presented in Figures 13-17. The stresses are given by

1) in an orthotropic fiber

$$\sigma_i^f = A_1^f\left(C_{i\theta}^f + C_{ir}^f\lambda\right)r^{\lambda-1} \tag{3.2.1}$$

2) in a transversely isotropic fiber

$$\sigma_i^f = A_1^f\left(C_{i\theta}^f + C_{ir}^f\right) \tag{3.2.2}$$

and 3) in the isotropic matrix

$$\sigma_i^m = A_1^m\left(C_{i\theta}^{m+}C_{ir}^m\right) + A_2^m\left(C_{i\theta}^m - C_{ir}^m\right)\frac{1}{r^2} \tag{3.2.3}$$

Again in all layers

$$\tau_{xr} = \tau_{x\theta} = \tau_{\theta r} = 0. \tag{3.2.4}$$

Circumferentially Orthotropic Fibers

In the circumferentially orthotropic fiber $\lambda > 1$ and all components of stress have a power law distribution with radius. The maximum stress is in the circumferential direction. The axial

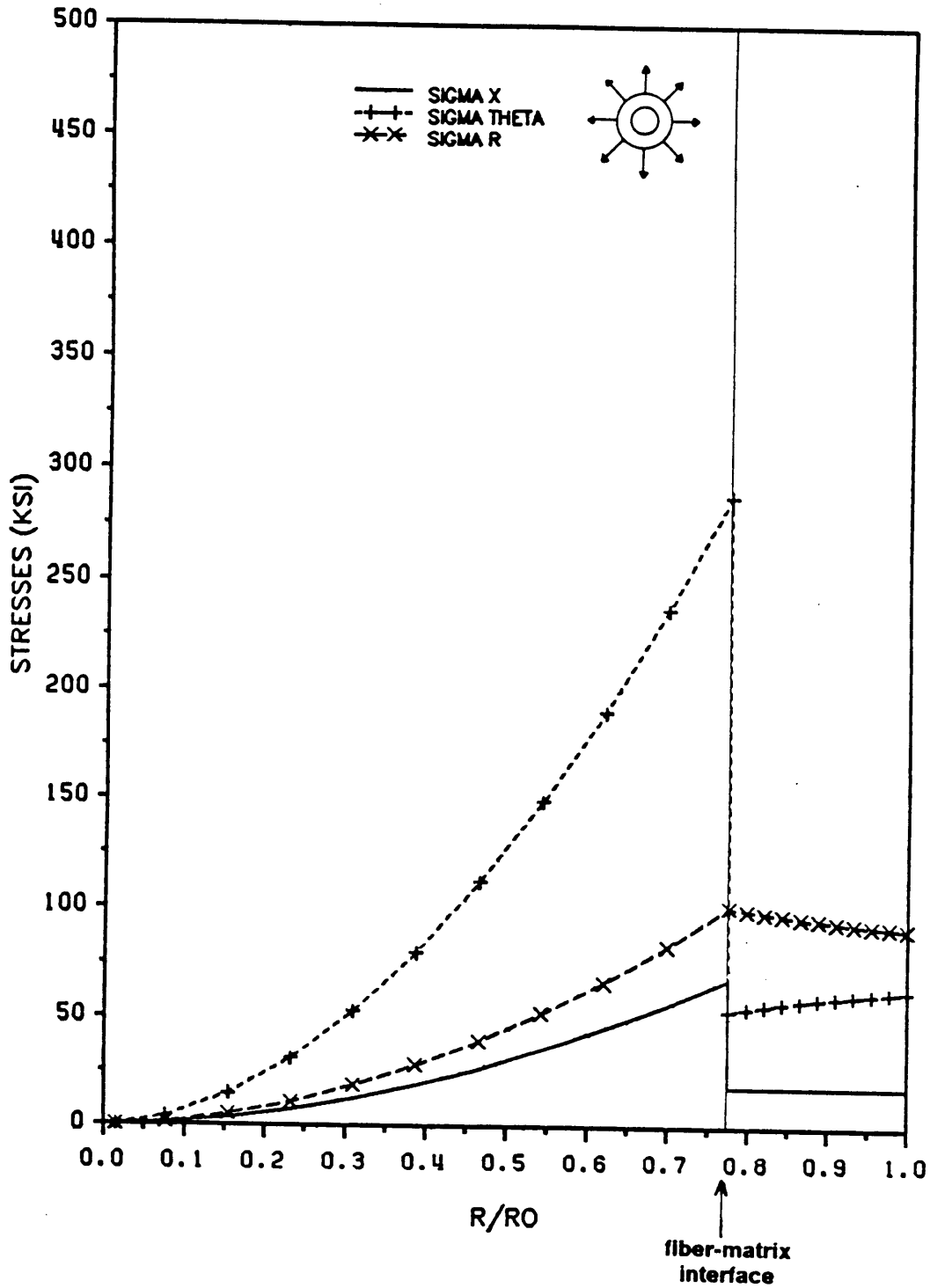

Figure 17. Stress distributions in a composite cylinder with a circumferentially orthotropic fiber subjected to radial loading.

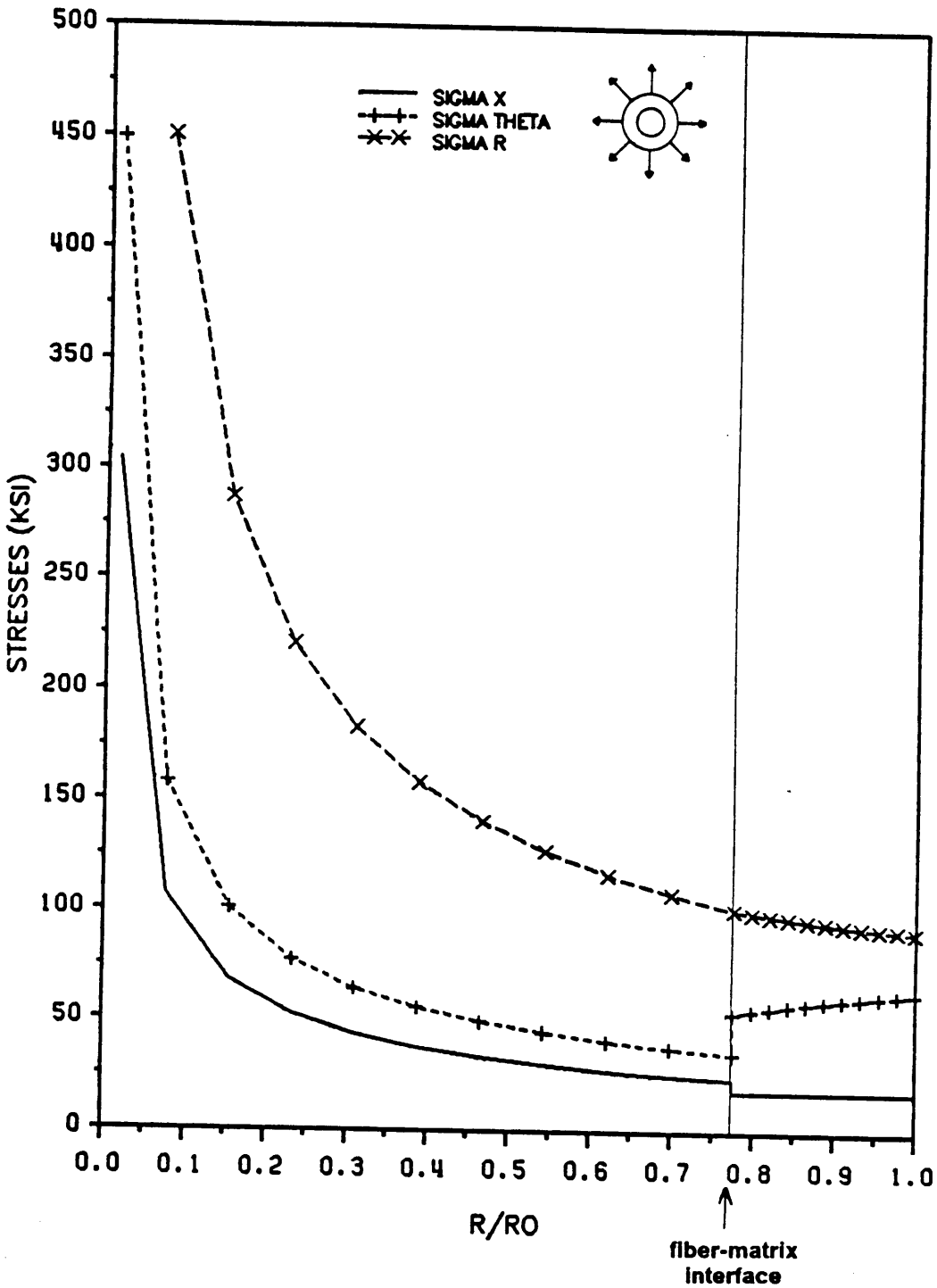

Figure 18. Stress distributions in a composite cylinder with a radially orthotropic fiber subjected to radial loading.

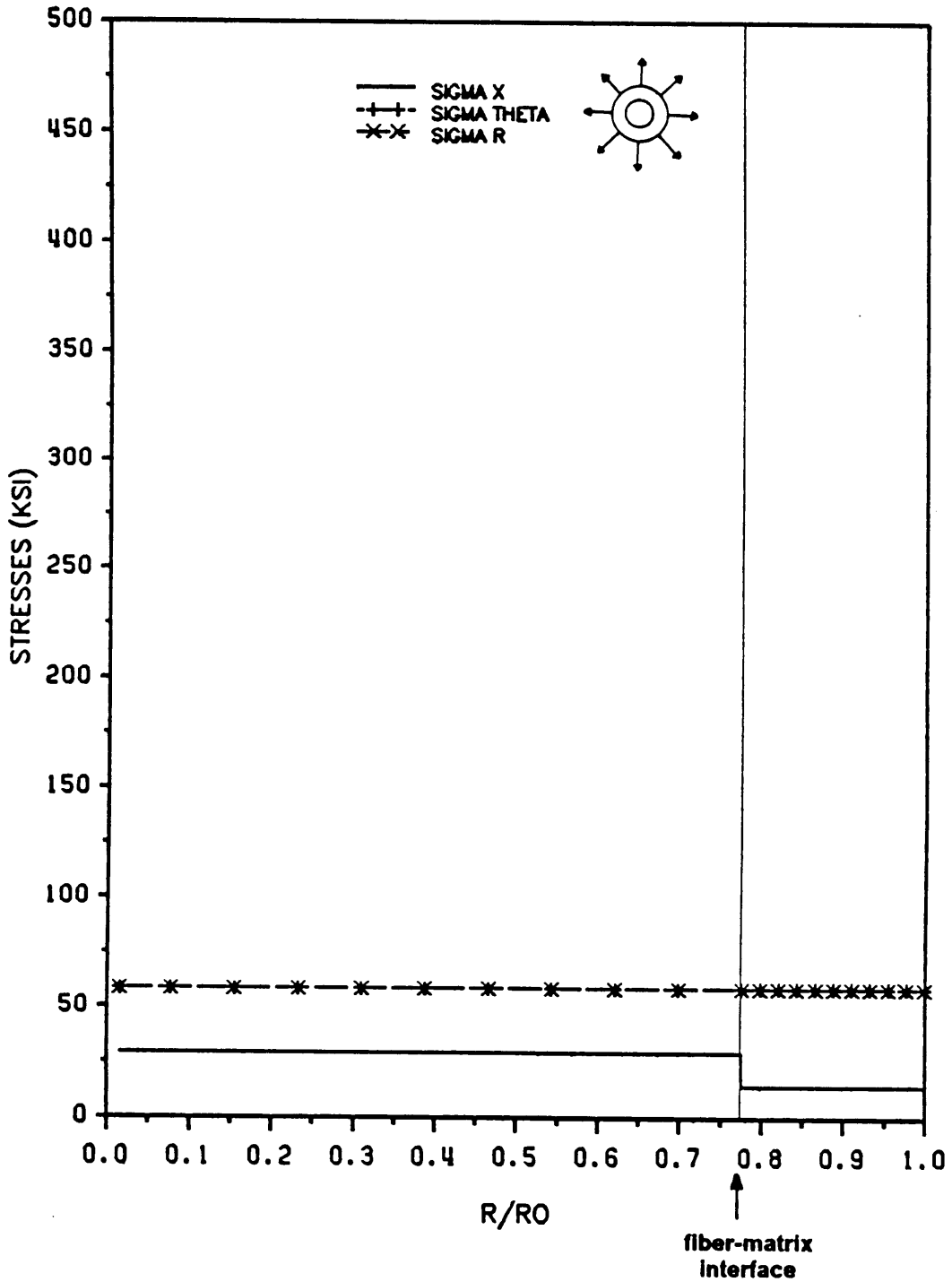

Figure 19. Stress distributions in a composite cylinder with transversely istotropic (A) fiber subjected to radial loading.

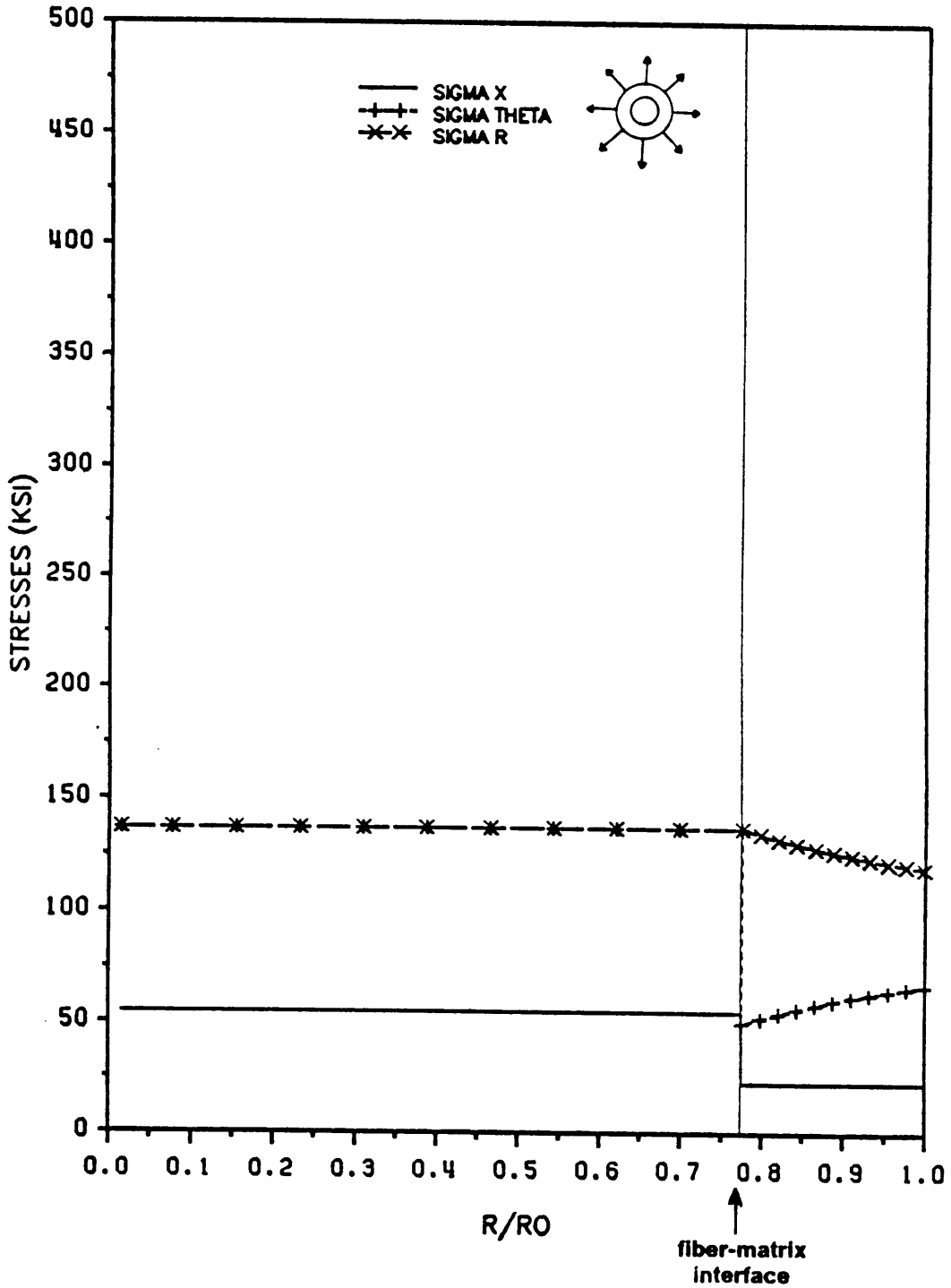

Figure 20. Stress distributions in a composite cylinder with transversely istotropic (B) fiber subjected to radial loading.

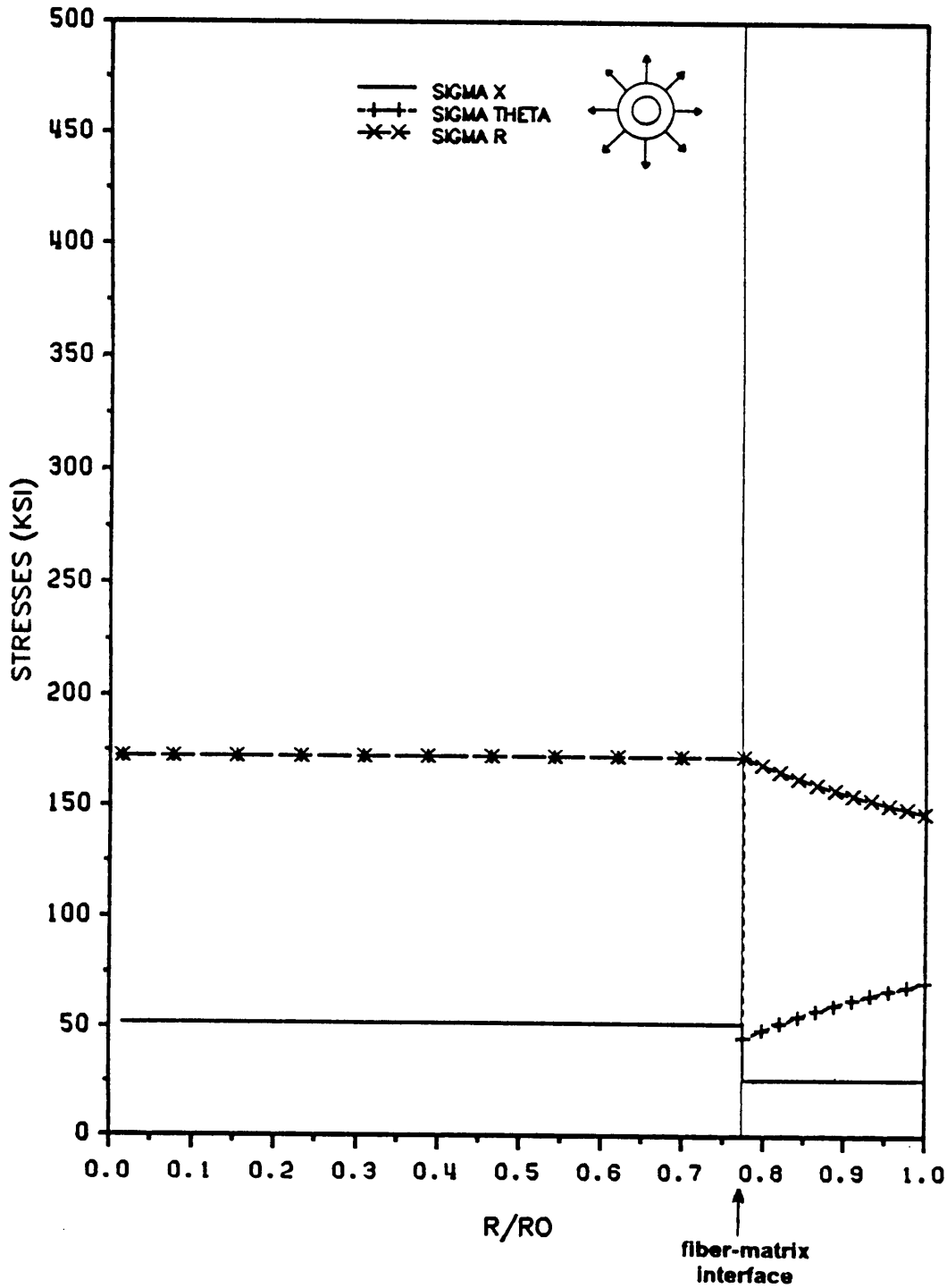

Figure 21. Stress distributions in a composite cylinder with transversely istotropic (C) fiber subjected to radial loading

stress is the smallest. All stresses increase in tension from zero at the center of the fiber to a maximum at the fiber matrix interface. In the matrix all stresses are tensile. While the axial stress in the matrix is constant since $C^m_{x\theta} = C^m_{xr}$, the radial and circumferential stresses vary with radius due to the term $A^m_2(C^m_{i\theta} - C^m_{ir})\frac{1}{r^2}$. The radial stress increases with increasing radius while the circumferential stress decreases with increasing radius.

Radially Orthotropic Fiber

The stresses in the radially orthotropic fiber are again singular since $\lambda < 1$. As for the axial loading the order of the singularity is 0.649 since the order of the singularity depends only on material constants. The strength of the singularity, S, for each stress component is again given by 3.1.5,6, and 7, but the values for $\varepsilon^o_r = 1\%$ are

$$S_x = 83.65 \tag{3.2.5}$$

$$S_r = 351.83 \tag{3.2.6}$$

$$S_\theta = 123.47. \tag{3.2.7}$$

Again the strength of the singularity for the radial stress is highest. All stresses in the fiber are tensile, decreasing as they approach the fiber matrix interface. In the matrix the stresses are also tensile, and inversely proportional to radius. The matrix stresses are in fact practically the same as in the matrix of a composite cylinder with a cylindrically orthotropic fiber.

Transversely Isotropic Fibers

The stresses in a transversely isotropic fiber subjected to $\varepsilon^o_r = 1\%$ are independent of radius. The radial and hoop stresses have the same value as expected from equation 3.2.2. The axial stress is less that the other stresses, and all components are tensile. The stresses in the matrix are also tensile. The axial stress in the matrix is constant since $C^m_{x\theta} - C^m_{xr} = 0$. The radial stress and the circumferential stress vary with radius. Note that in Figure 19, although

on the scale of the graph they appear the same, the radial stress and circumferential stress are slightly different, as expected from Eqn 3.2.3

3.3 Axial Shear Loading

Displacement boundary conditions of the form

$$u_1(S) = \varepsilon^o_{12} x_2 \tag{3.3.1a}$$

$$u_2(S) = \varepsilon^o_{12} x_1 \tag{3.3.1b}$$

$$u_3 = 0 \tag{3.3.1c}$$

are applied to determine the effective axial shear modulus of a composite. The stresses resulting in the composite cylinder, in the x, θ, r coordinate system are

1) for orthotropic fibers

$$\tau^f_{xr} = A^f_1 r^{\gamma-1} \gamma G^f_{\theta x} \cos\theta \tag{3.3.2a}$$

$$\tau^f_{x\theta} = -A^f_1 r^{\gamma-1} G^f_{xr} \sin\theta \tag{3.3.2b}$$

2) in a transversely isotropic fiber

$$\tau^f_{xr} = A^f_1 G^f_{\theta x} \cos\theta \tag{3.3.3a}$$

$$\tau^f_{x\theta} = A^f_1 G^f_{xr} \sin\theta \tag{3.3.3b}$$

3) in the isotropic matrix

$$\tau_{xr}^{m} = \left(A_1^m - \frac{B_1^m}{r^2} \right) G^m \cos\theta \tag{3.3.4a}$$

$$\tau_{x\theta}^{m} = -\left(A_1^m + \frac{B_1^m}{r^2} \right) G^m \sin\theta \tag{3.3.4b}$$

and in all phases

$$\sigma_r = \sigma_\theta = \sigma_x = \tau_{\theta r} = 0. \tag{3.3.5}$$

The applied displacement in the x_1, x_2, x_3 coordinate system causes the stresses in the orthotropic fiber in both the x_1, x_2, x_3 system and the x, θ, r system to vary with position, since the material properties of the fiber vary with position. Stresses in the x, θ, r coordinate system depend on position regardless of whether the fiber is orthotropic or transversely isotropic due to the coordinate transformation.

Circumferentially Orthotropic Fiber

In the circumferentially orthotropic fiber $\gamma = \sqrt{\frac{G_{xr}}{G_{x\theta}}} < 1$. Thus the shear stresses $\tau_{x\theta}$ and τ_{xr} are singular of order 0.732. Figure 22 shows the variation of τ_{xr} and $\tau_{x\theta}$ with radius and angle. τ_{xr} is positive throughout the fiber and decreases with increasing radius and angle. $\tau_{x\theta}$ is negative throughout the fiber, more negative with increasing angle from 0° to 90°, but less negative with increasing radius. In the matrix τ_{xr} is positive and $\tau_{x\theta}$ is negative. Both stresses in the matrix show radial dependence as evident in Eqn. 3.3.4.

Radially Orthotropic Fiber

Figure 23 shows the radial variation of τ_{xr} and $\tau_{x\theta}$ for a composite cylinder with a radially orthotropic fiber. In the radially orthotropic fiber $\gamma > 1$ and the stresses have a power law dependence on radius. τ_{xr} within the fiber increases from zero at the center to a maximum

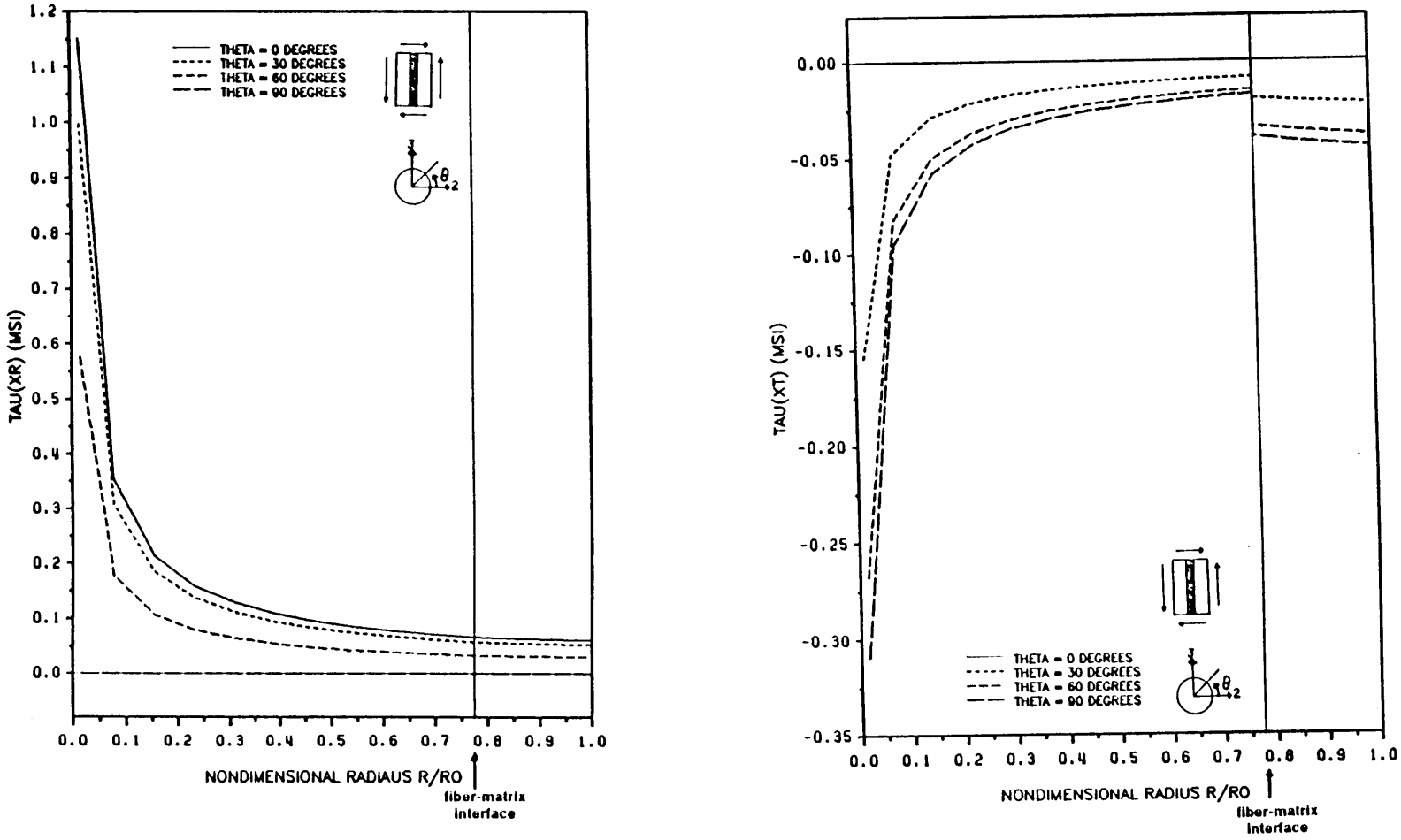

Figure 22. Shear stresses in a composite cylinder with a circumferentially orthotropic fiber subjected to axial shear displacement.

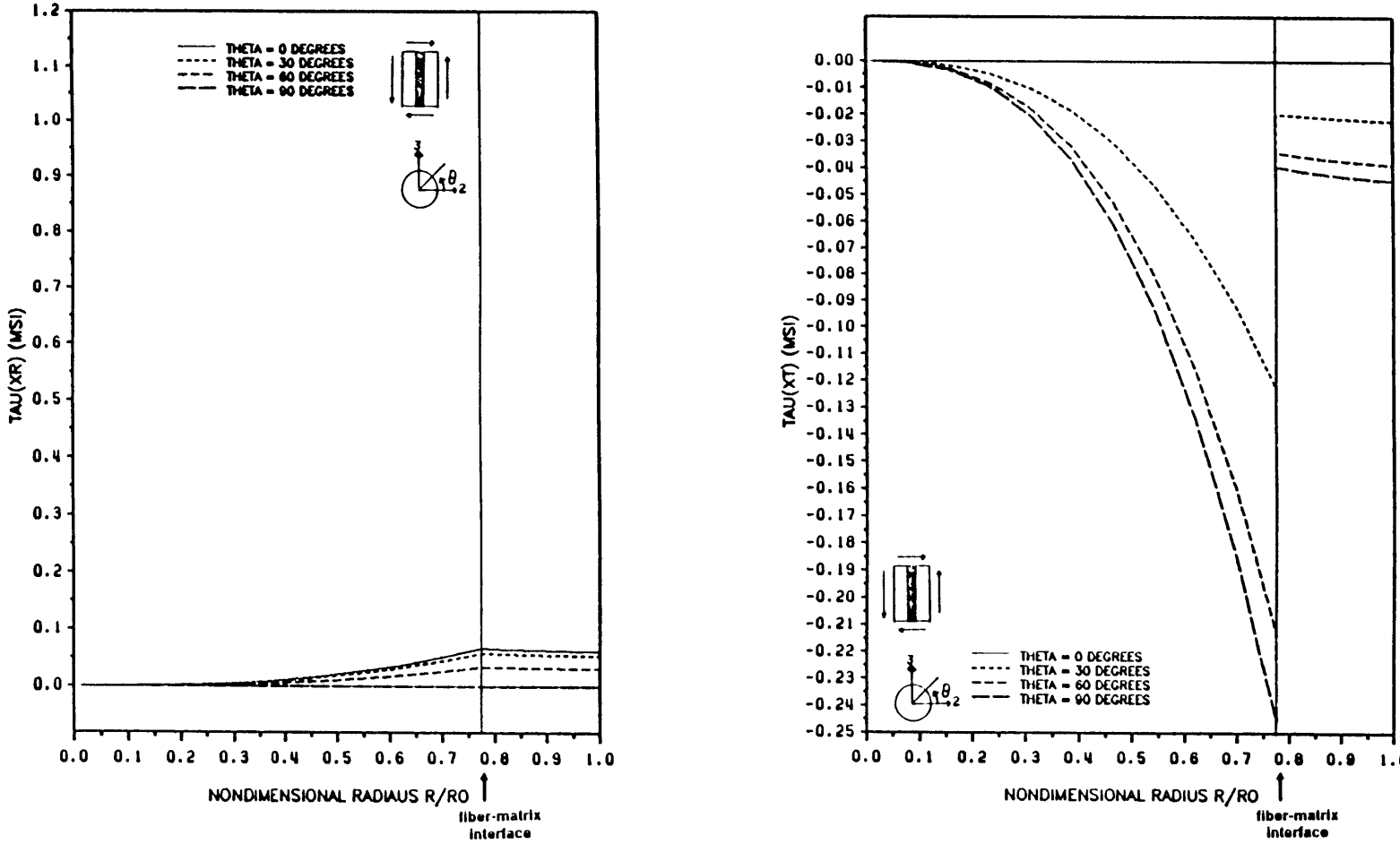

Figure 23. Shear stresses in a composite cylinder with a radially orthotropic fiber subjected to axial shear displacement.

value at the fiber matrix interface. $\tau_{x\theta}$ is negative increasing from zero to a maximum value at the interface. Stresses in the matrix again show a radial dependence. τ_{xr} is positive, decreasing with increasing radius, and $\tau_{x\theta}$ is negative, increasing with increasing radius.

Transversely Isotropic Fiber

The shear stresses in a transversely isotropic fiber are constant within the fiber for a given value of θ. The stiffer the transverse properties, the higher the stresses. τ_{xr} is positive and $\tau_{x\theta}$ is negative. In the matrix also, τ_{xr} is positive and $\tau_{x\theta}$ is negative. As in the other composite cylinders the stresses in the matrix vary with $\frac{1}{r^2}$ The stress distributions are illustrated in Figures 22-24, as a function of r and θ.

3.4 Thermal Loading

The stresses resulting in a composite cylinder from an applied temperature change ΔT are given by

1) in an orthotropic fiber

$$\sigma_i^f = A_1^f\left(C_{i\theta}^f + C_{ir}^f\lambda\right)r^{\lambda-1} + L_i^f\varepsilon^o + N_i^f\Delta T \tag{3.4.1}$$

where, L_i^f and N_i^f are given by 2.1.25b and c.

2) in a transversely isotropic fiber

$$\sigma_i^f = A_1^f\left(C_{i\theta}^f + C_{ir}^f\right) + C_{ix}^f\varepsilon^o + C_{ij}^f\alpha_j^f\Delta T \tag{3.4.2}$$

3) in the isotropic matrix

$$\sigma_i^m = A_1^m(C_{i\theta}^m + C_{ir}^m) + A_2^m(C_{i\theta}^m - C_{ir}^m)\frac{1}{r^2} + C_{ix}^m\varepsilon^o + C_{ij}^m\alpha^m\Delta T \tag{3.4.3}$$

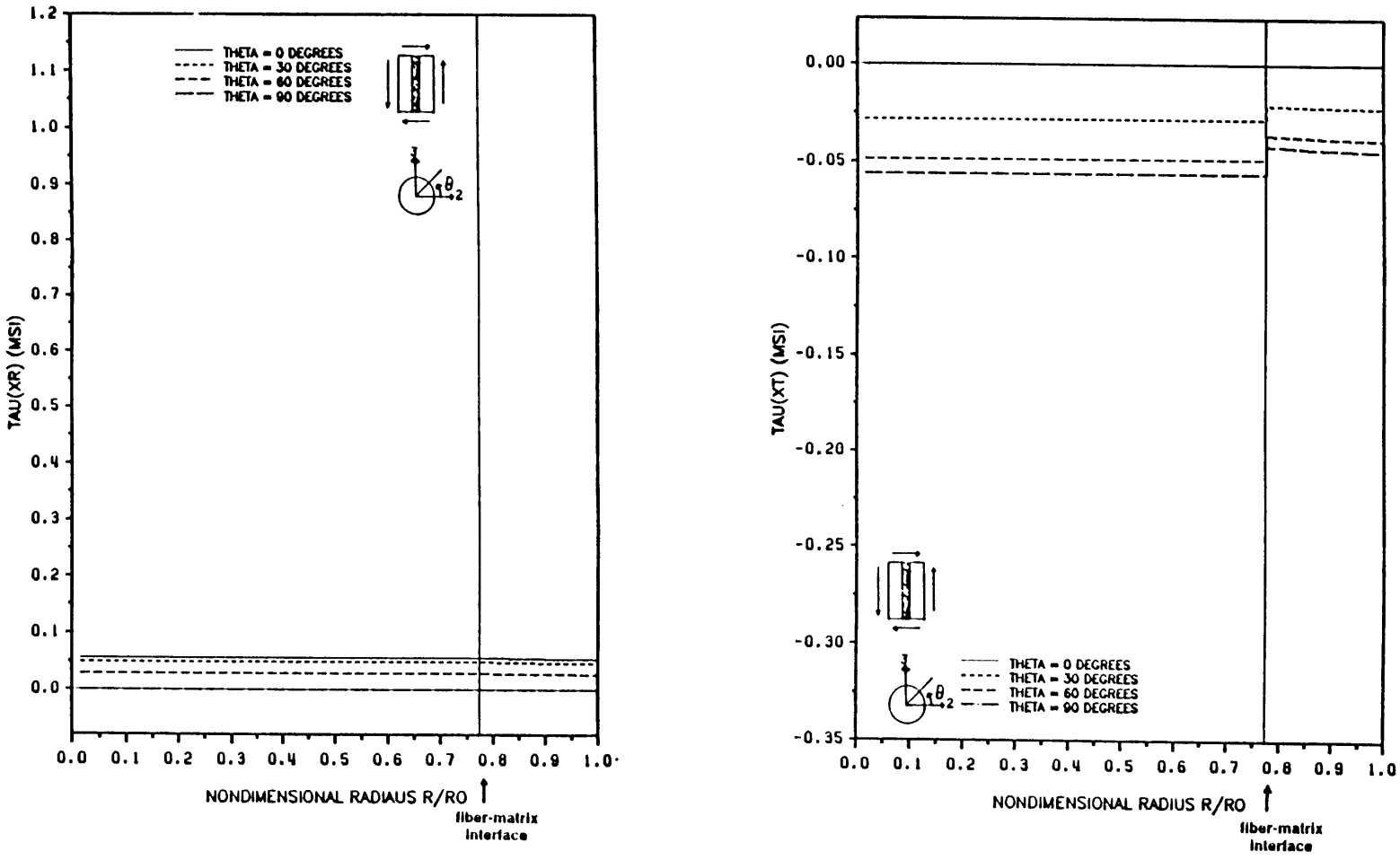

Figure 24. Shear stresses in a composite cylinder with transversely isotropic fiber (A) subjected to axial shear displacement.

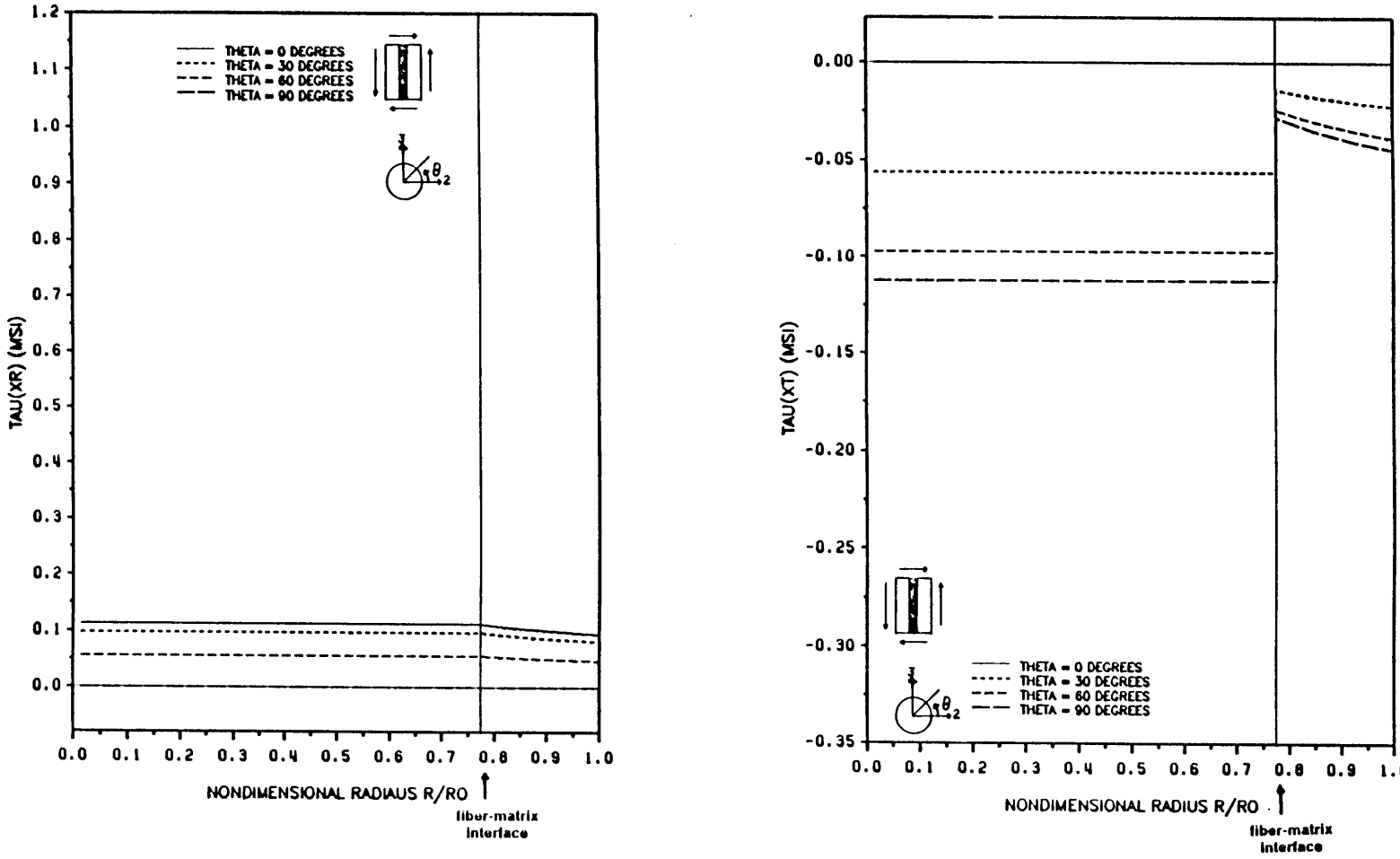

Figure 25. Shear stresses in a composite cylinder with transversely isotropic fiber (B) subjected to axial shear displacement.

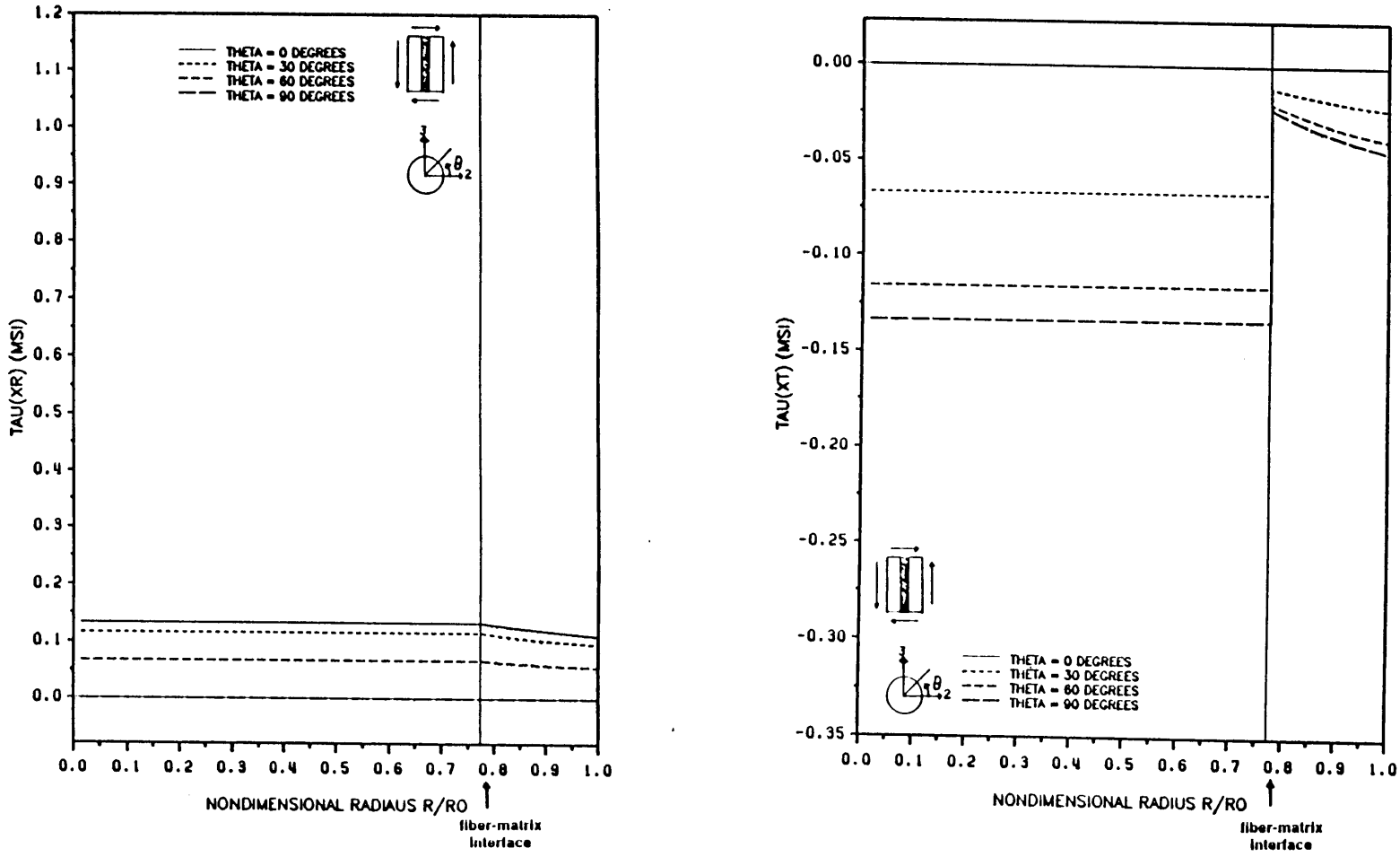

Figure 26. Shear stresses in a composite cylinder with transversely isotropic fiber (C) subjected to axial shear displacement.

and in all phases

$$\tau_{\theta r} = \tau_{xr} = \tau_{x\theta} = 0. \tag{3.4.4}$$

The stresses resulting from an applied temperature change of 1° F are shown in Figures 25-29.

Circumferentially Orthotropic Fibers

In the circumferentially orthotropic fiber $\lambda > 1$ and the stresses have a power series law distribution with radius. All stress components are compressive at the center of the fiber. The radial and hoop stresses have the same value at the center of the fiber as is physically expected. The axial and hoop stresses become tensile at the fiber matrix interface, while although the radial stress becomes less compressive with increasing radius it remains compressive throughout the fiber. The stresses in the matrix have a slight radial dependence due to the $A_2^m(C_{i\theta}^m - C_{ir}^m)\frac{1}{r^2}$ term. All components of stress in the matrix are small in magnitude. The radial and hoop stresses are tensile decreasing with radius. The axial stress is compressive and constant.

Radially Orthotropic Fibers

In the radial orthotropic fiber $\lambda > 1$ and the stresses in the fiber are singular of order 0.649. The strength of the singularity, S, in each component is again given by Eqns 3.1.5, 6, and 7 with values

$$S_x = 0.035 \tag{3.4.5}$$

$$S_r = 0.149 \tag{3.4.6}$$

$$S_\theta = 0.052. \tag{3.4.7}$$

All stresses are tensile at the center of the fiber and decrease with increasing radius. The axial and radial stresses are tensile at the fiber-matrix interface while the hoop stress is

compressive. In the matrix the radial and hoop stresses are tensile and again vary with $\frac{1}{r^2}$. The axial stress is constant in compression. The stress distribution in the matrix is approximately the same as it is in the composite cylinder with a circumferentially orthotropic fiber subjected to the same loading.

Transversely Isotropic Fiber

In the transversely isotropic fibers the stresses are constant. The radial and hoop stresses are equal and slightly compressive. The axial stress is slightly tensile. The stresses in the matrix again vary with $\frac{1}{r^2}$. The hoop stress is tensile in the matrix of all transversely isotropic composite cylinders considered. The axial and radial stresses are compressive. The axial stress is again constant while the radial stress decreases with increasing radius.

3.5 Thermal-Mechanical Loading

A case of practical interest is an axial loading $u_x = \varepsilon^o x$ superimposed on a temperature change of $\Delta T = -280°F$. This represents a 1% axial strain applied to a composite cured at 350° F. The solution for the thermal and mechanical problem is the same, and is discussed in Chapter 2. In the linear problem superposition can be used to find the resulting stresses for the thermal mechanical loading. The stresses in the composite cylinders are given by Equations 3.4.1-3.4.4 where ε^o is now the applied axial strain of 1% and ΔT is the difference between cure and room temperature, namely -280°F. Figures 30-34 illustrate the effect of this thermal-mechanical loading on the five composite cylinders studied. In all cases the axial stress in the fiber is larger under combined loading than under either thermal or mechanical loading applied separately. In addition the radial variation of σ_x in the CO and RO fibers under thermal load is apparent in thermal-mechanical loading. The radial and hoop stresses are also

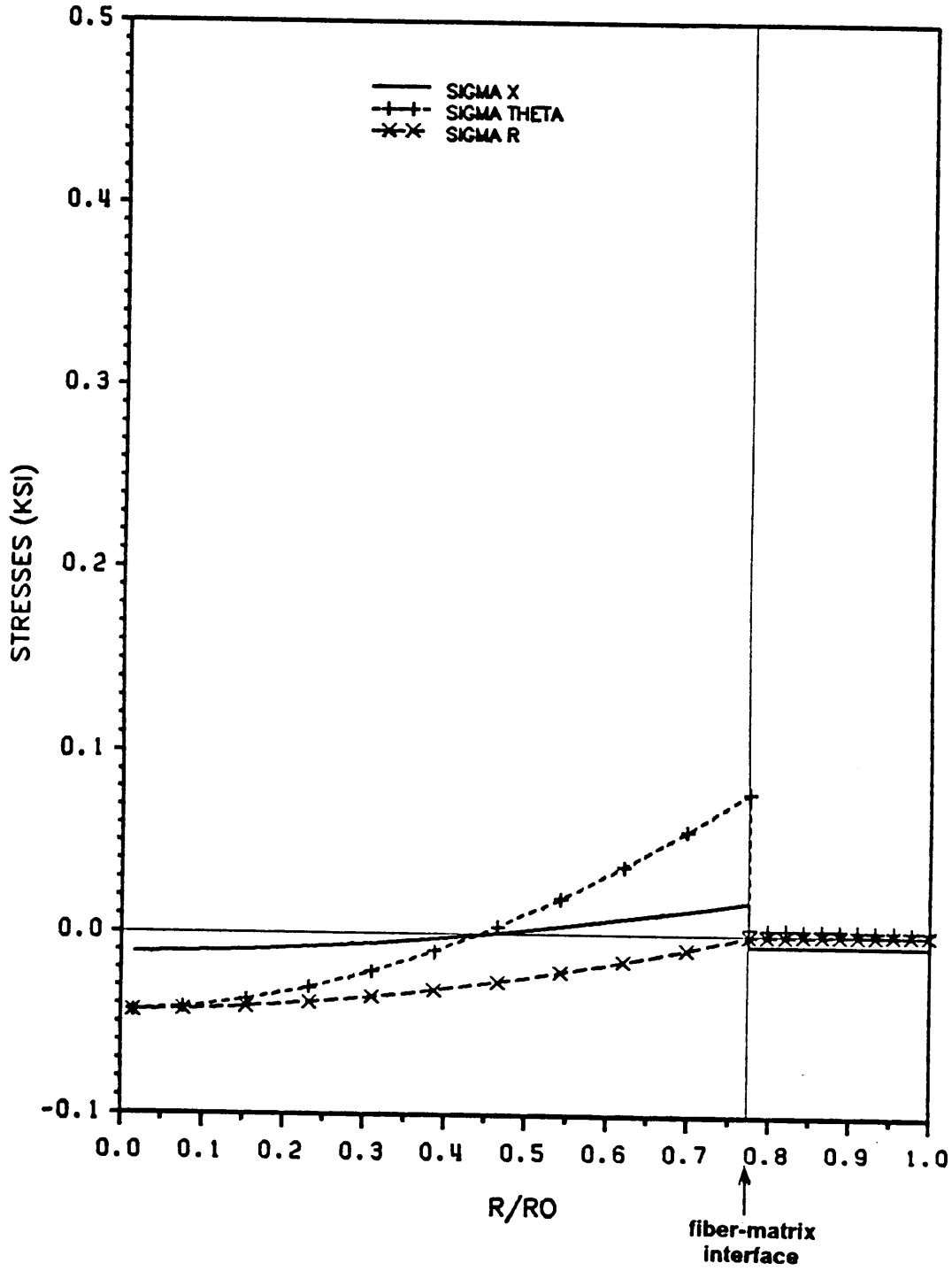

Figure 27. Stress distributions in a composite cylinder with a circumferentially orthotropic fiber subjected to thermal loading.

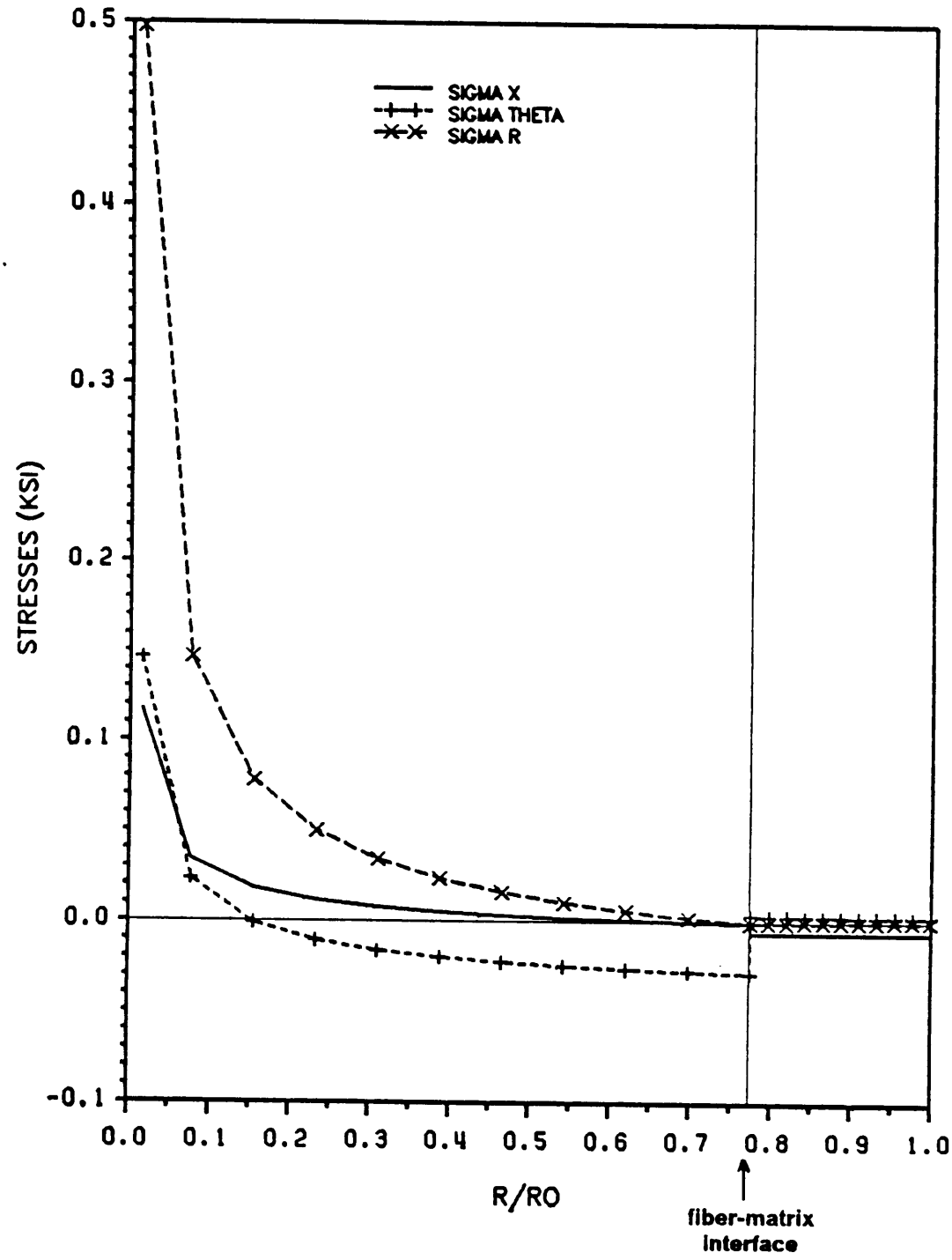

Figure 28. Stress distributions in a composite cylinder with a radially orthotropic fiber subjected to thermal loading.

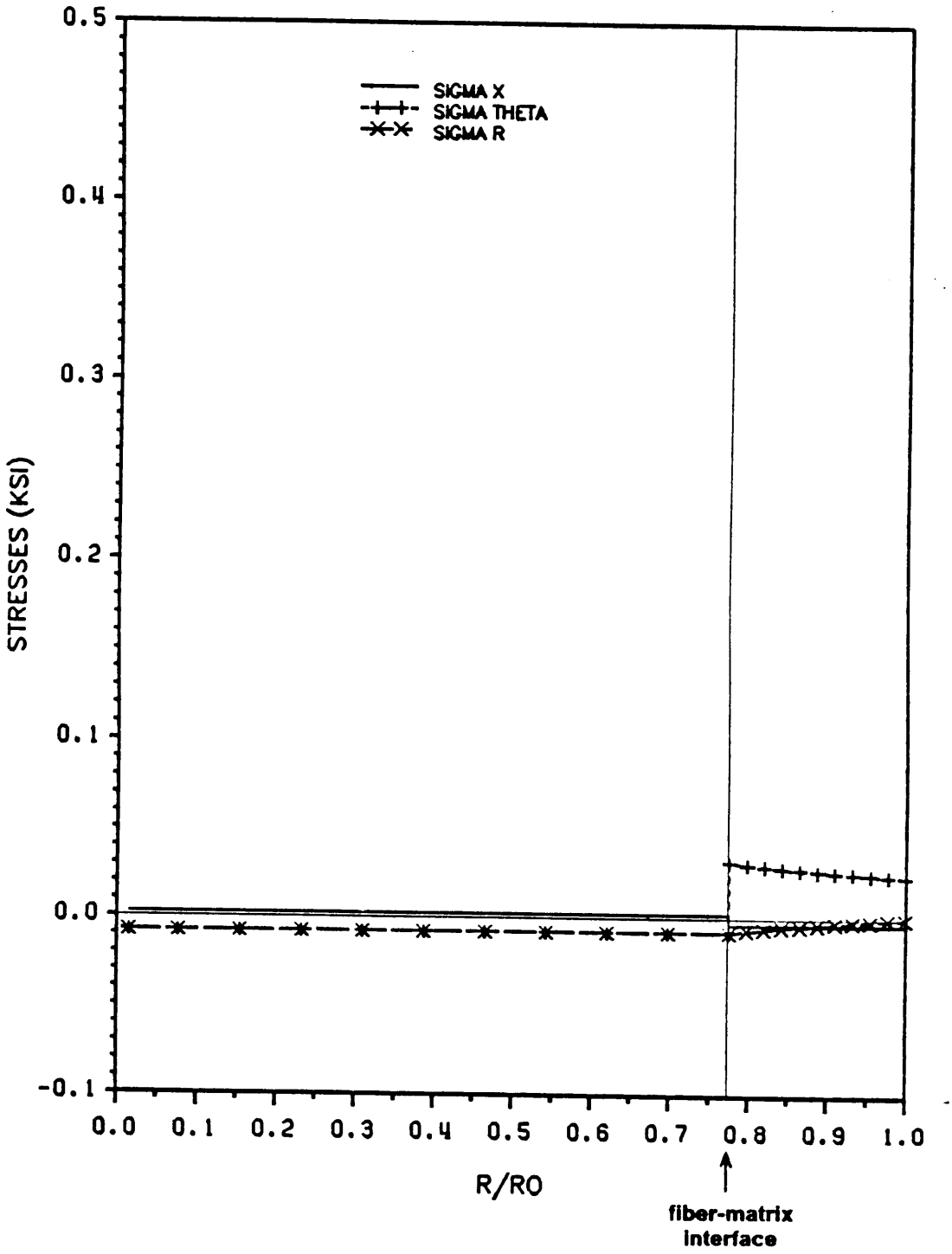

Figure 29. Stress distributions in a composite cylinder with transversely istotropic (A) fiber subjected to thermal loading.

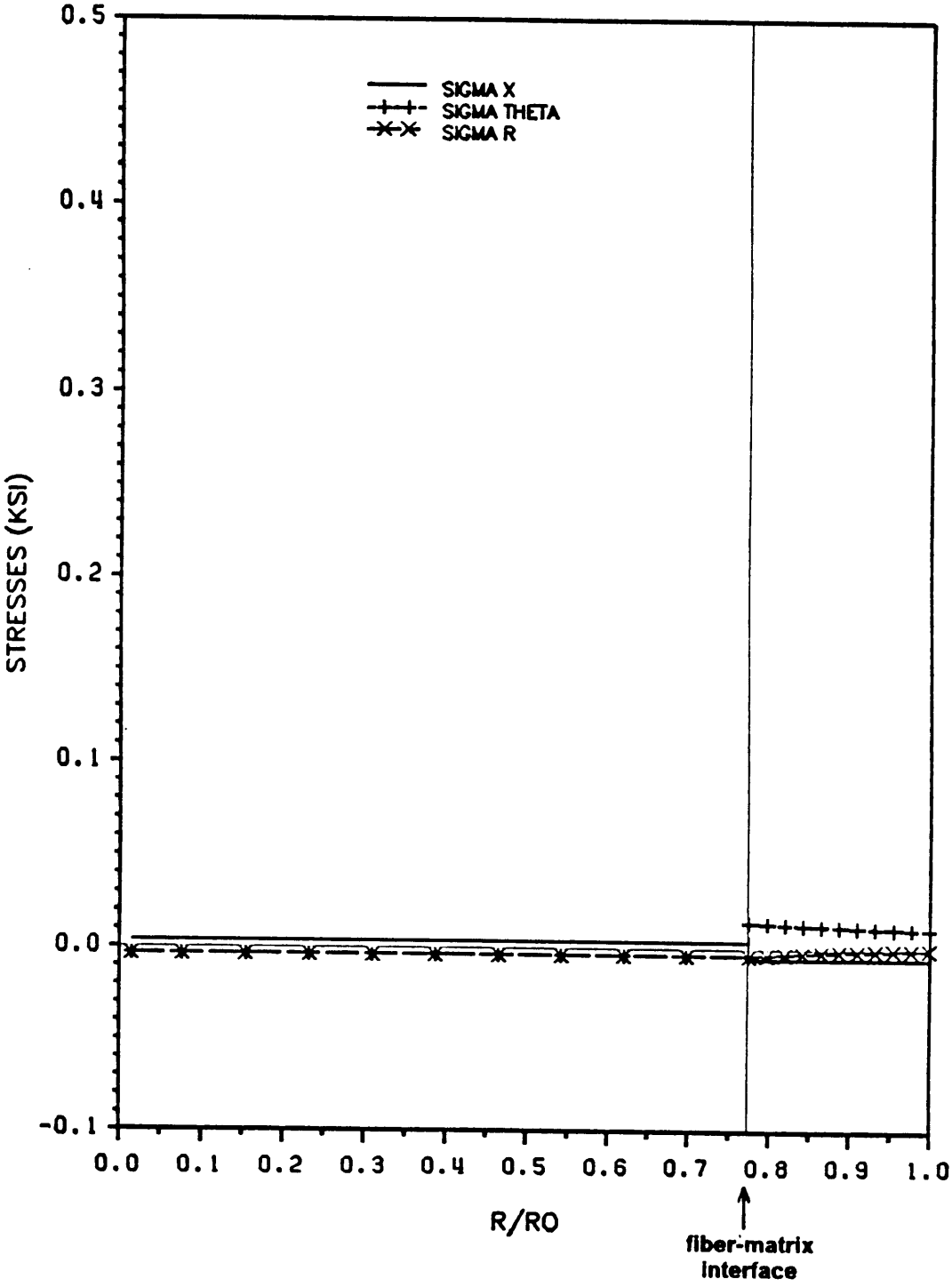

Figure 30. Stress distributions in a composite cylinder with transversely istotropic (B) fiber subjected to thermal loading.

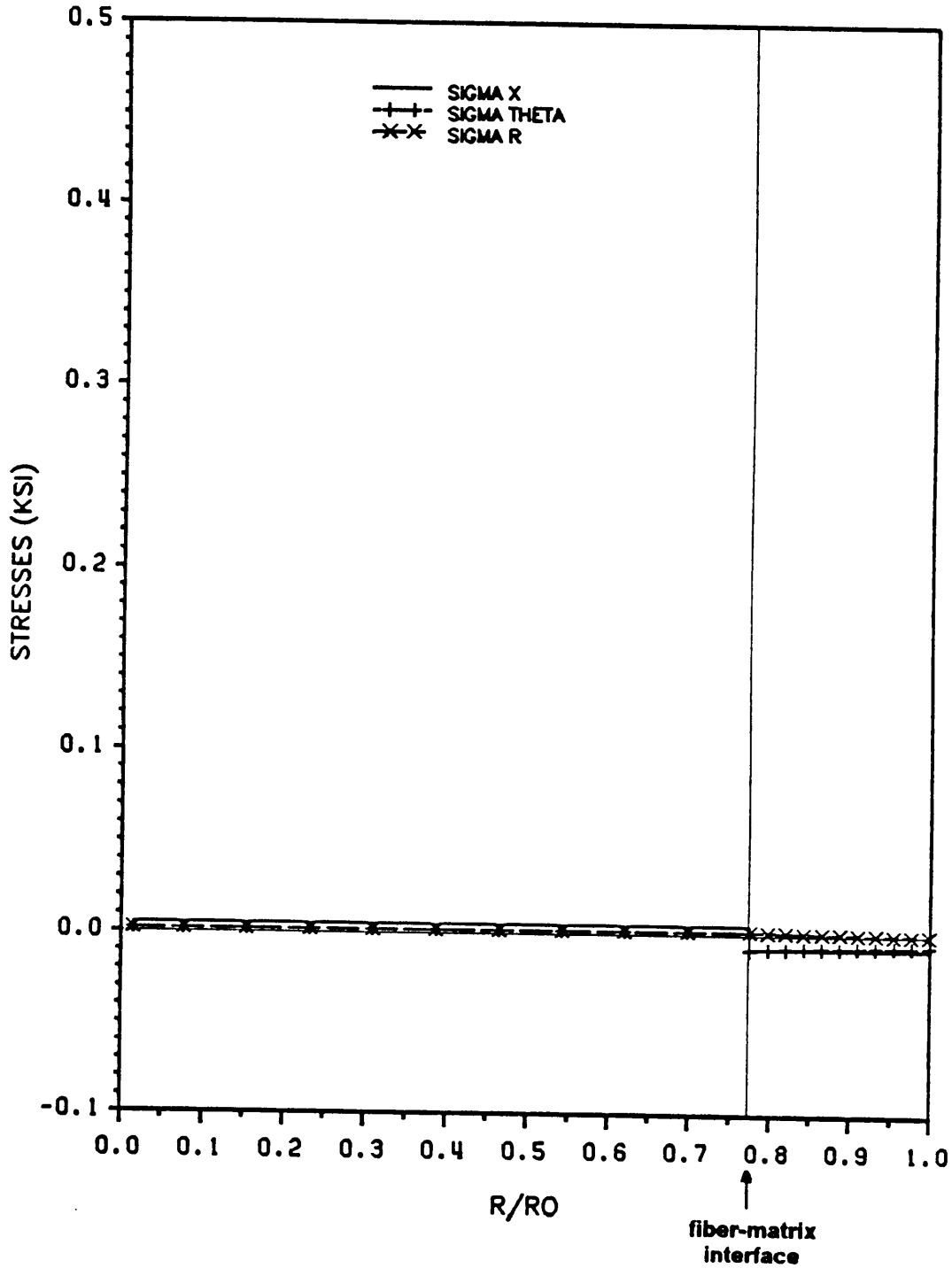

Figure 31. **Stress distributions in a composite cylinder with transversely istotropic (C) fiber subjected to thermal loading.**

slightly larger under combined loading than when the cylinder is subjected to the loadings separately. In all types of composite cylinder the negative temperature change reinforces the trends in the stresses under axial loading. In particular, the stresses in the composite cylinder with a radially orthotropic fiber are still singular at the center of the fiber, and the strength of the singularity is greater than when either an axial or thermal load is applied separately. The strength, S, of the singularity for each component of stress in the RO fiber is

$$\begin{aligned} S_x &= -13.25 \\ S_\theta &= -19.55 \\ S_r &= -55.72 \end{aligned} \tag{3.5.1}$$

3.6 Summary

The transverse morphology of the graphite fibers greatly influences the stress state resulting in the composite cylinder. Axial, radial, and thermal loading lead to singular stresses in the radially orthotropic fiber, but not in the circumferentially orthotropic or transversely isotropic fiber. Shear loading produces singular stresses in the circumferentially orthotropic fibers. The order and strength of the singularity in the stresses is summarized in Table 2 and Table 3. Although the morphology of the fiber affects the stresses in the fiber of the composite cylinder, the stresses in the matrix are the same in the composite cylinder with radially and circumferentially orthotropic fibers.

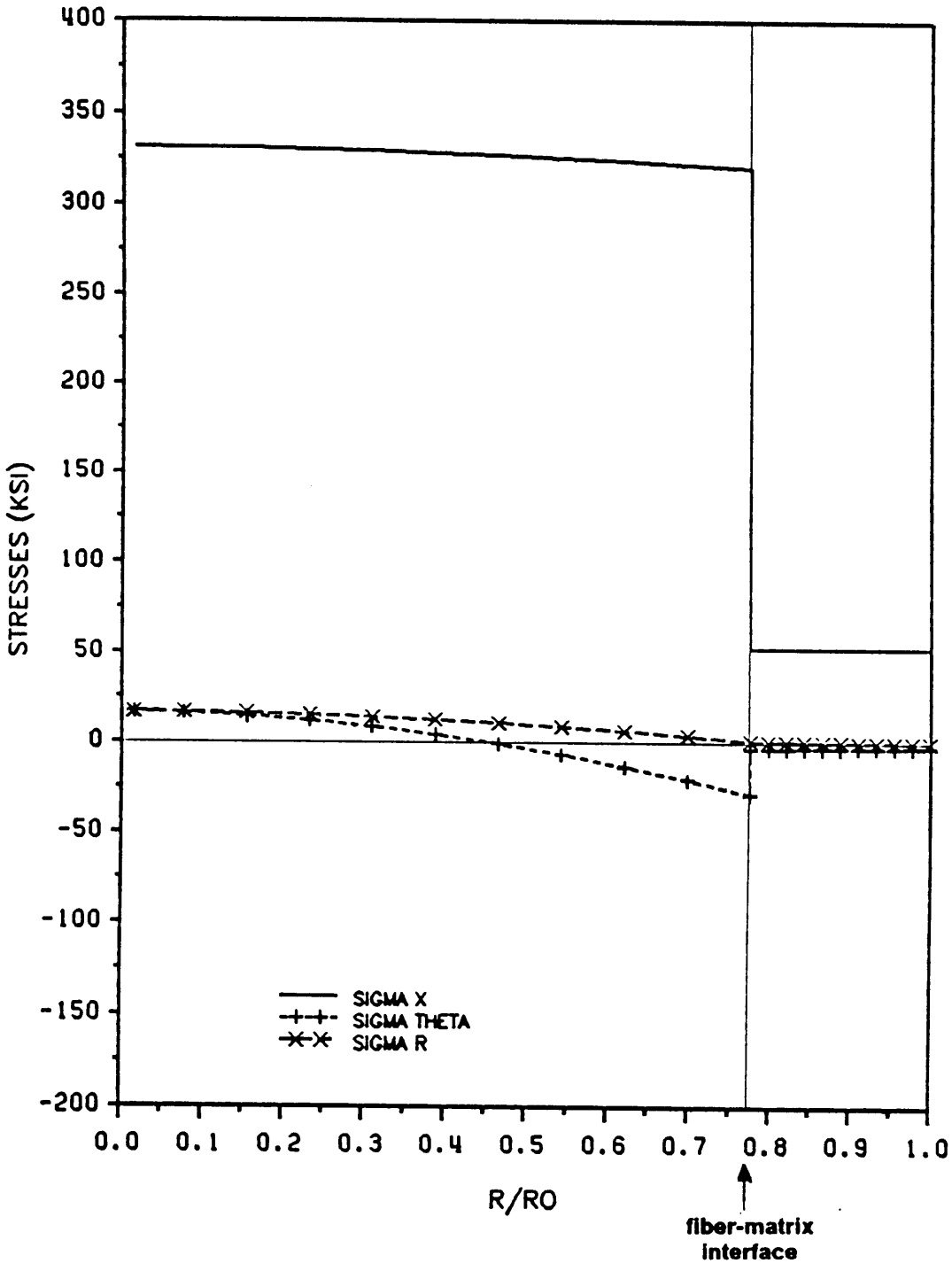

Figure 32. **Stress distributions in a composite cylinder with a circumferentially orthotropic fiber subjected to thermal-mechanical loading.**

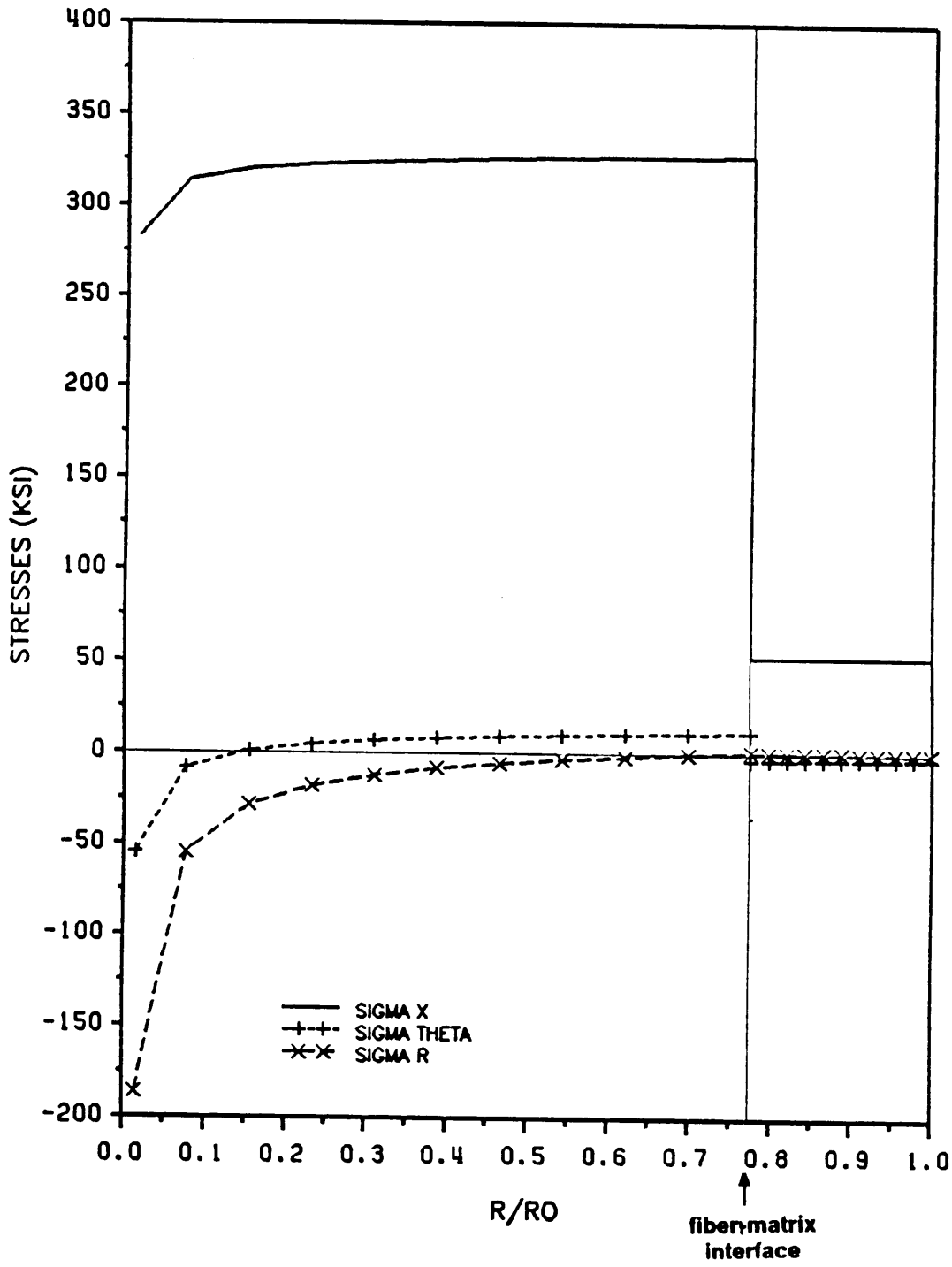

Figure 33. Stress distributions in a composite cylinder with a radially orthotropic fiber subjected to thermal-mechanical loading.

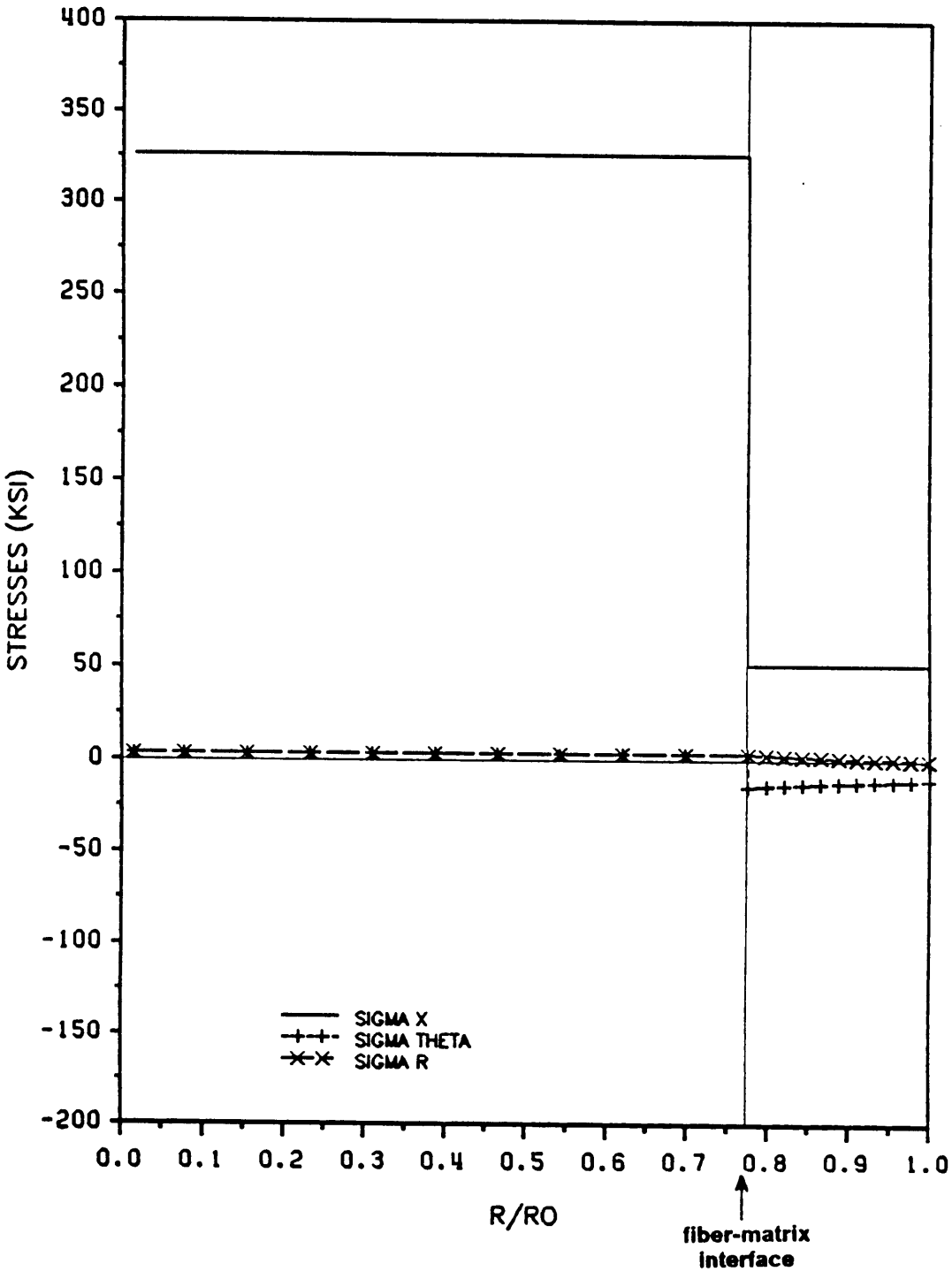

Figure 34. Stress distributions in a composite cylinder with transversely istotropic (A) fiber subjected to thermal-mechanical loading.

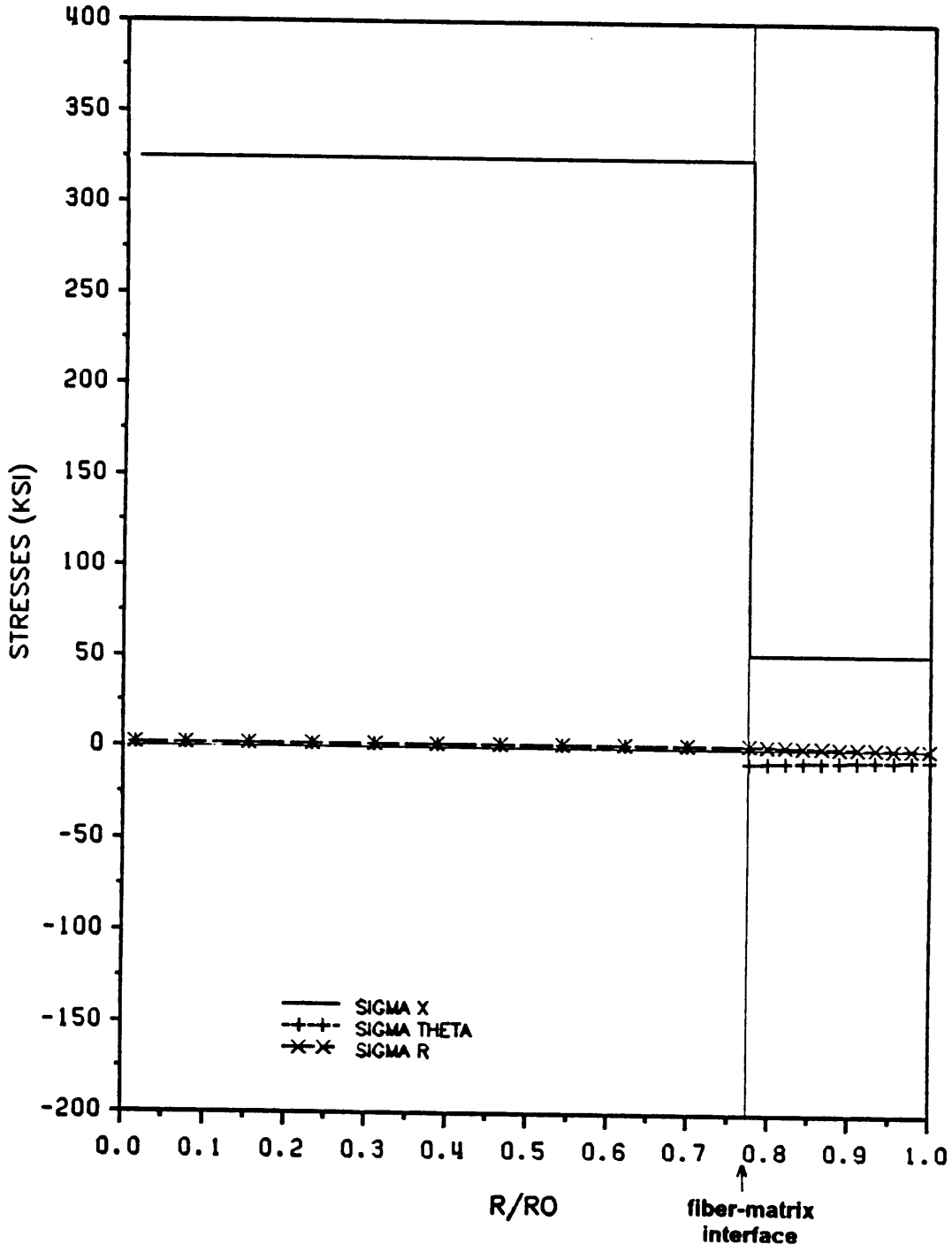

Figure 35. Stress distributions in a composite cylinder with transversely istotropic (B) fiber subjected to thermal-mechanical loading.

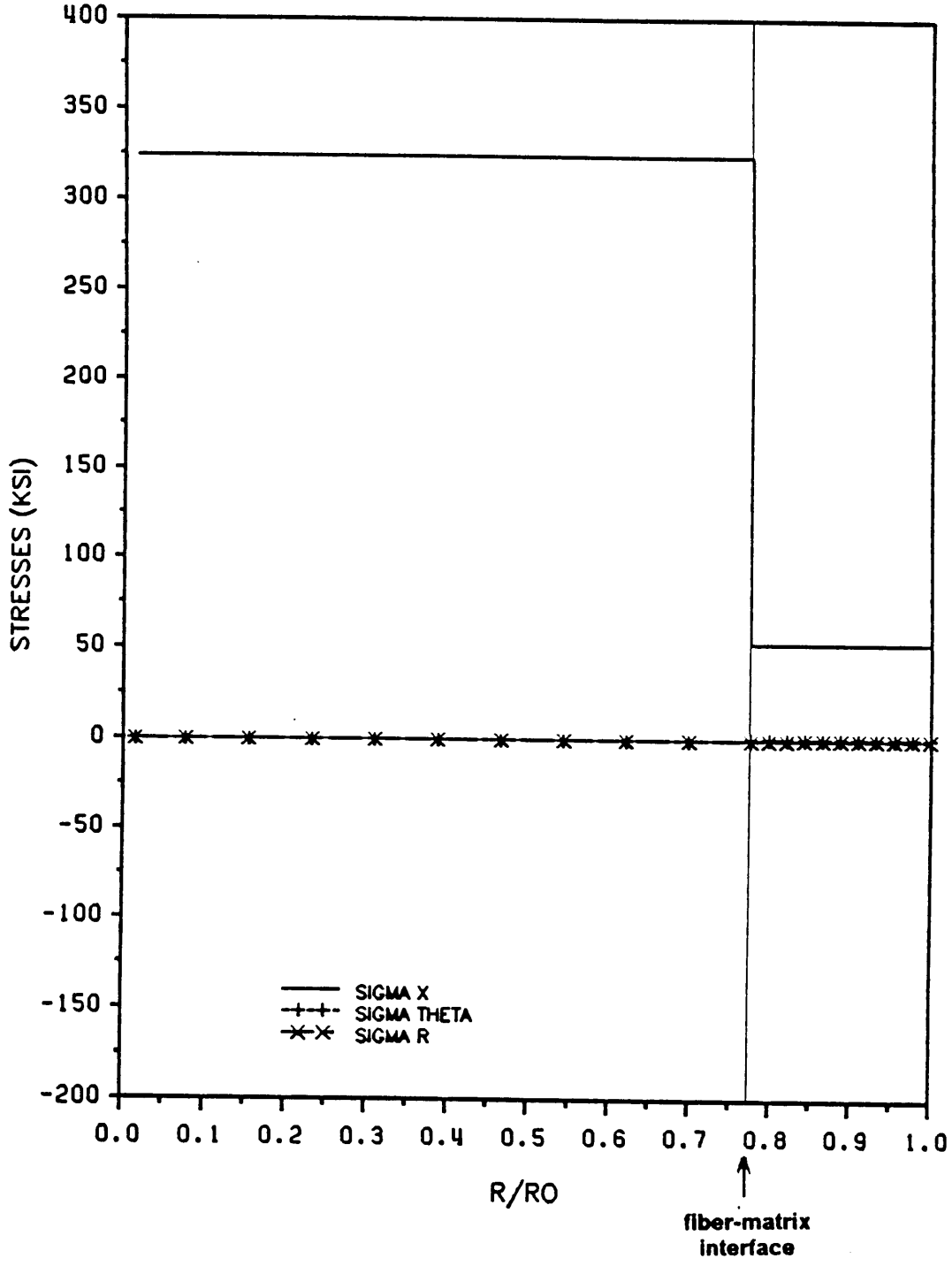

Figure 36. Stress distributions in a composite cylinder with transversely istotropic (C) fiber subjected to thermal-mechanical loading.

Table 2. Order and Strength of Stress Singularities in Radially Orthotropic Fibers.

Strength and Order of Singularity in
the Stresses of a Radially Orthotropic Fiber

Loading	Order	S_r	S_θ	S_x
$\varepsilon_x = 1\%$	0.649	-13.831	-4.8535	-3.288
$\varepsilon_r = 1\%$	0.649	351.83	123.47	83.65
$\Delta T = 1°F$	0.649	0.1486	0.052	0.035
$\Delta T = -280°F$	0.649	-41.617	-14.605	-9.895
$\varepsilon = 1\%$, $\Delta T = -280°F$	0.649	-55.719	-19.554	13.248

Table 3. Order and Strength of Stress Singularities in Circumferentially Orthotropic Fibers.

Strength and Order of Singularity in
the Stresses of a Circumferentially Orthotropic Fiber

Loading	Order	S_{xr}	$S_{x\theta}$
$\varepsilon_{12} = 1\%$	0.7319	105.43	-29.81

4.0 Hybrid Fibers

In the preceding chapters we have considered composite cylinders with fibers that have the ideal morphologies depicted in Figures 1a, 1b, and 1c. As mentioned previously the purely radially orthotropic and purely circumferentially orthotropic fiber are not physically possible. This is because the properties at the center of the fiber cannot have directional dependence since at the center the θ direction is also the r direction. For this reason a core of transversely isotropic material must exist in an orthotropic fiber. This chapter examines the effect of the size of the transversely isotropic core on the effective composite material properties and on the stress distributions within the composite cylinder. The fiber volume for computing the fiber volume fraction of the composite cylinder includes both the volume of the transversely isotropic core and the orthotropic sheath.

The results to follow were determined for a fiber volume fraction of 0.602. The radius a (see Figure 3) of the transversely isotropic core is varied to result in a core volume fraction of 0.01% to 50%. The properties of the transversely isotropic core in this discussion are those of TI fiber A in Table 1. The response of the composite cylinder if the core has the properties of either TI fiber B or TI fiber C is characteristically the same as for a core composed of TI fiber A although the magnitudes of the effective properties and the stresses are slightly different.

4.1 Effective Moduli

The addition of a transversely isotropic core to an orthotropic fiber has little effect on the effective axial Youngs modulus of a composite. The axial modulus of the composite with radially orthotropic fibers decreases more with increasing transversely isotropic core size than the modulus of the composite with circumferentially orthotropic fibers. A higher modulus transversely isotropic core has less effect on the effective axial modulus. Figure 37 and Figure 38 show the variation of normalized effective moduli of the hybrid fibers with size of the transversely isotropic core. The effective moduli have been normalized with the value of the effective modulus for the ideal orthotropic fiber.

The effective axial Poisson's ratio increases with transversely isotropic core size. The increase in Poisson's ratio is greater in the radially orthotropic fiber than in the circumferentially orthotropic fiber. A stiffer transversely isotropic core has less effect on the effective Poisson's ratio of the composite cylinder.

The effective transverse bulk modulus is decreased by the addition of a transversely isotropic core to the center of an orthotropic fiber in a composite. As seen in Figure 37 and Figure 38 the effect of the size of the transversely isotropic core on the effective bulk modulus of the composite with radially orthotropic fiber is greater than on the modulus of the composite with circumferentially orthotropic fibers.

The axial shear modulus is only slightly effected by the size of the transversely isotropic core. In the composite with radially orthotropic fibers there is almost no change in axial shear modulus with increasing core size while in the composite cylinder with circumferentially orthotropic fiber there is a slight decrease in G_A^* with increasing core size.

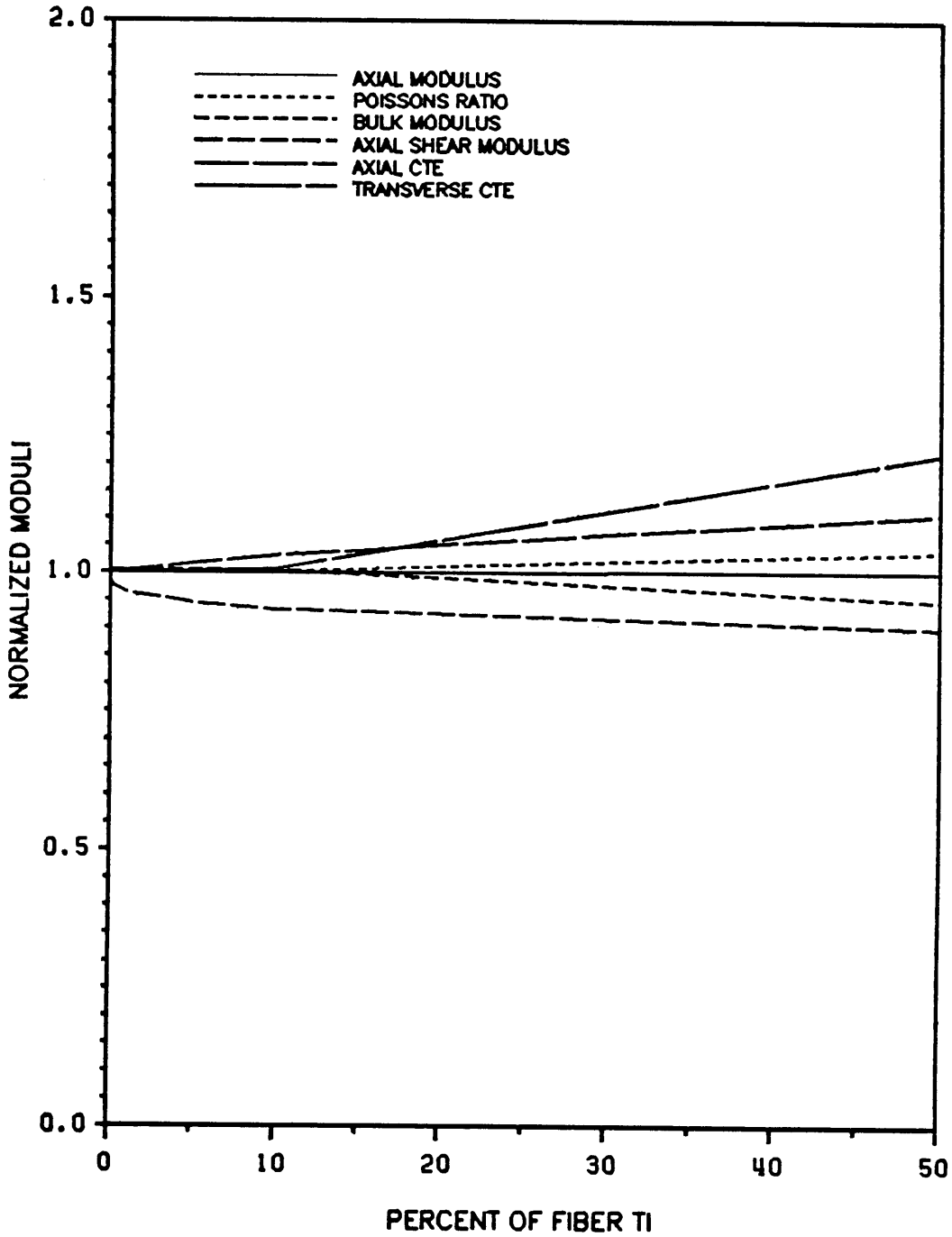

Figure 37. Normalized Effective Moduli of a Composite Cylinder with Circumferentially Orthotropic Fiber with TI Core.

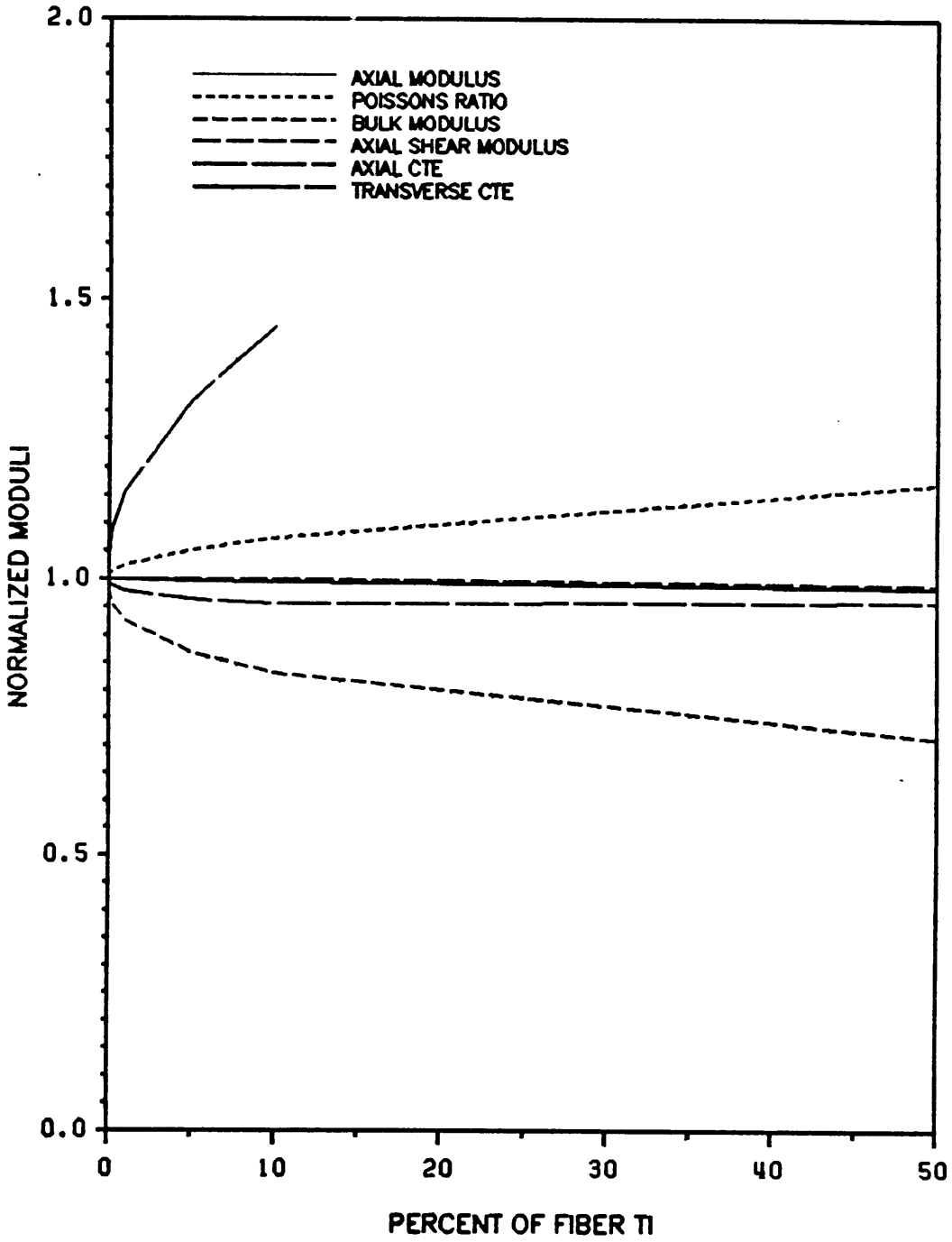

Figure 38. Normalized Effective Moduli of a Composite Cylinder with Radially Orthotropic Fiber with TI Core.

The axial coefficient of thermal expansion is increased by increasing the percentage of the fiber that is in the transversely isotropic core. The effect of the core on the axial CTE is the same in both orthotropic fiber composites.

The transverse coefficient of thermal expansion is also increased by the addition of a transversely isotropic core. In the composite with circumferentially orthotropic fibers increasing the core size increases the transverse CTE slightly. The effect of core size in the radially orthotropic fibers on the transverse CTE is more pronounced, an increase in core size increasing the transverse CTE.

The existence of a transversely isotropic core in the orthotropic fibers is slightly detrimental to the effective elastic properties of the composite material. In general, the larger the core the more detrimental the effect. The effect of the size of the core on E_A^*, ν_A^*, k^*, α_A^*, and α_T^* is more pronounced in the composite with radially orthotropic fibers than the composite with circumferentially orthotropic fibers. The effect of core size on G_A^* is greater in composites with circumferentially orthotropic fibers than in those with radially orthotropic fibers.

4.2 Stress Distributions

The expressions for the stresses in a composite cylinder were developed in Chapter 2. Recalling Equations 2.1.25 and 2.1.26 the stresses resulting when an axisymmetric load is applied to the cylinder are given by

$$\sigma_i = A_i^{ti}\left(C_{i\theta}^{ti} + C_{ir}^{ti}\right) + C_{ix}^{ti}\varepsilon^o - C_{ij}^{ti}\alpha_j^{ti}\Delta T \tag{4.1}$$

in the transversely isotropic core,

$$\sigma_i = A_1^f\left(C_{i\theta}^f + C_{ir}^f\lambda\right)r^{\lambda-1} + A_2^f\left(C_{i\theta}^f - C_{ir}^f\lambda\right)r^{-\lambda-1} + L_i^f\varepsilon^o - N_i^f\Delta T \tag{4.2}$$

where L_i^f and N_i^f are given by (2.1.25b,c) in the orthotropic fiber, and

$$\sigma_i = A_1^m(C_{i\theta}^m + C_{ir}^m) + A_2^m(C_{i\theta}^m - C_{ir}^m)\frac{1}{r^2} + C_{ix}^m\varepsilon^o - C_{ij}^m\alpha_j^m\Delta T \tag{4.3}$$

in the isotropic matrix. The constants A_1^k and A_2^k are solved for using the boundary and continuity conditions outlined in Chapter 2.

For shear loading, recalling Equations 3.3.2-3.3.4 the stresses are given by

$$\tau_{xr}^{tl} = A_1^{tl}G_{\theta x}^{tl}\cos\theta \tag{4.4a}$$

$$\tau_{x\theta}^{tl} = -A_1^{tl}G_{xr}^{tl}\sin\theta \tag{4.4b}$$

in the transversely isotropic core,

$$\tau_{xr}^f = \left(A_1^f r^{\gamma-1} - A_2^f r^{-(\gamma+1)}\right)\gamma G_{\theta x}^f\cos\theta \tag{4.5a}$$

$$\tau_{x\theta}^f = -\left(A_1^f r^{\gamma-1} + A_2^f r^{-(\gamma+1)}\right)G_{xr}^f\cos\theta \tag{4.5b}$$

in the orthotropic fiber, and

$$\tau_{xr}^m = \left(A_1^m - \frac{A_2^m}{r^2}\right)G_m\cos\theta \tag{4.6a}$$

$$\tau_{r\theta}^m = \left(A_1^m - \frac{A_2^m}{r^2}\right)G_m\cos\theta \tag{4.6b}$$

in the isotropic matrix. Again the constants A_1^k and A_2^k are solved for using the boundary and continuity conditions outlined in Chapter 2. Stress distributions for transversely isotropic core sizes of 0.01% of the fiber and 50% of the fiber are presented in the figures in this chapter.

4.2.1 Axial Loading

The stress distributions in all ideal composite cylinders for axial loading $\varepsilon^o = 1\%$ are very similar as was seen in Figure 12- Figure 16 in the previous chapter. The addition of a transversely isotropic core to an orthotropic fiber does little to affect the stress state under axial loading(Figure 39-Figure 40). For small transversely isotropic cores the stresses in the fiber are essentially the same as those in the ideal orthotropic fibers. However, an important difference is that while the stresses in the ideal radially orthotropic fiber are singular at $r=0$, inserting a transversely isotropic core into the radially orthotropic fiber removes the singularity. For small transversely isotropic cores the gradient of the stresses within the radially orthotropic sheath, near the core, is large. Also for small core size the stresses in the transversely isotropic core are not the same as in the simple transversely isotropic fiber. As the core size increases the stresses in the core become more like those in the pure transversely isotropic fiber, and the gradient of the stresses in the sheath near the core decreases. Stresses in the orthotropic fiber near the fiber matrix interface and in the matrix are unaffected by the transversely isotropic core.

4.2.2 Radial Loading

The stresses caused by an applied displacement $u_r = \varepsilon^o c$ where $\varepsilon^o = 1\%$, in an orthotropic fiber with a small transversely isotropic core (Figure 41 and Figure 42) are approximately the same as in the purely orthotropic fiber (Figure 17and Figure 18). In the radially orthotropic fiber the singularity in the stresses at $r=0$ is removed by the presence of a transversely isotropic core. In the circumferentially orthotropic fiber the stresses within the orthotropic sheath of the fiber are basically undisturbed by the presence of the transversely isotropic

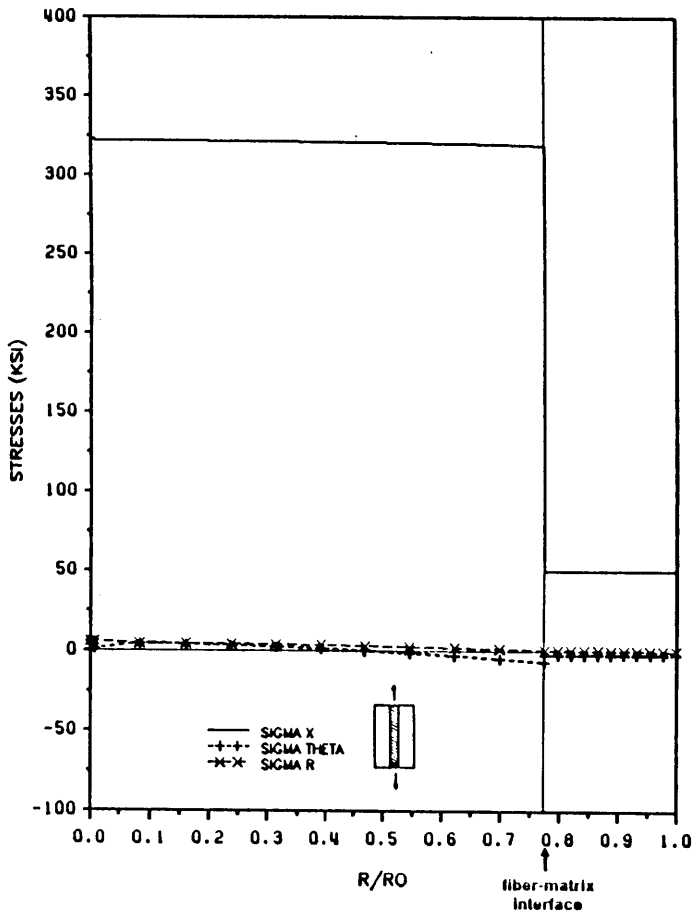

a) 0.01% transversely isotropic core

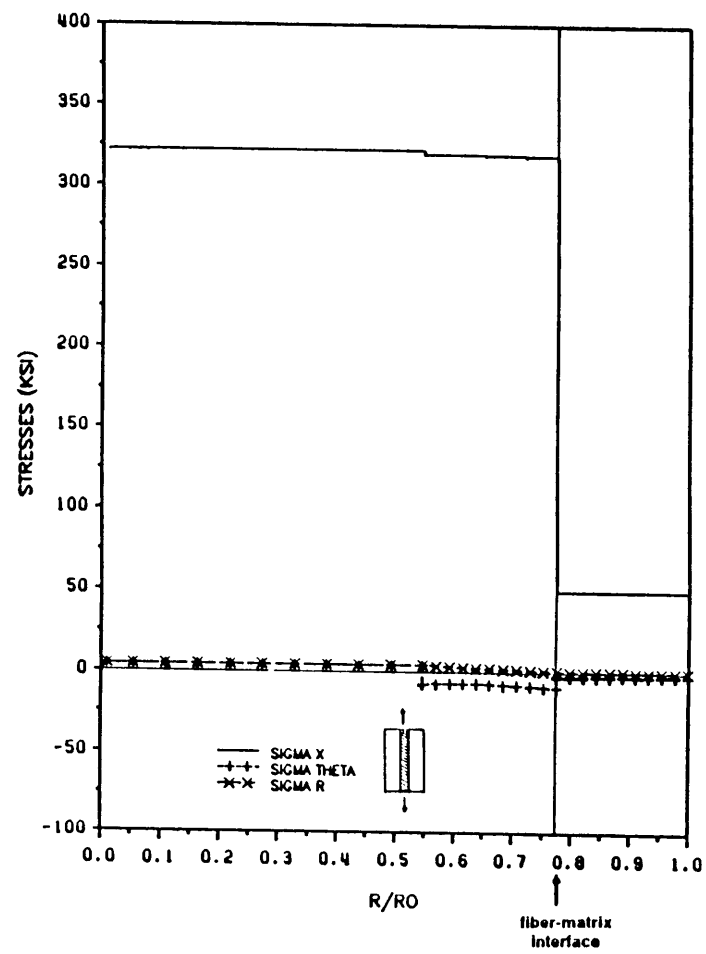

b) 50% transversely isotropic core

Figure 39. Stresses in a composite cylinder with a circumferentially orthotropic hybrid fiber for axial load.

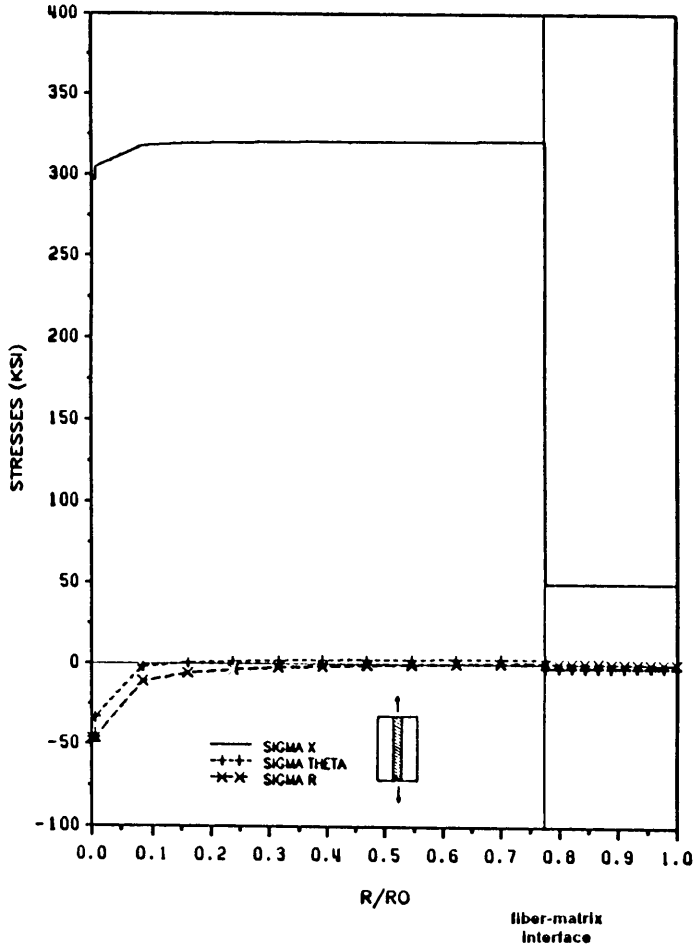

a) 0.01% transversely isotropic core

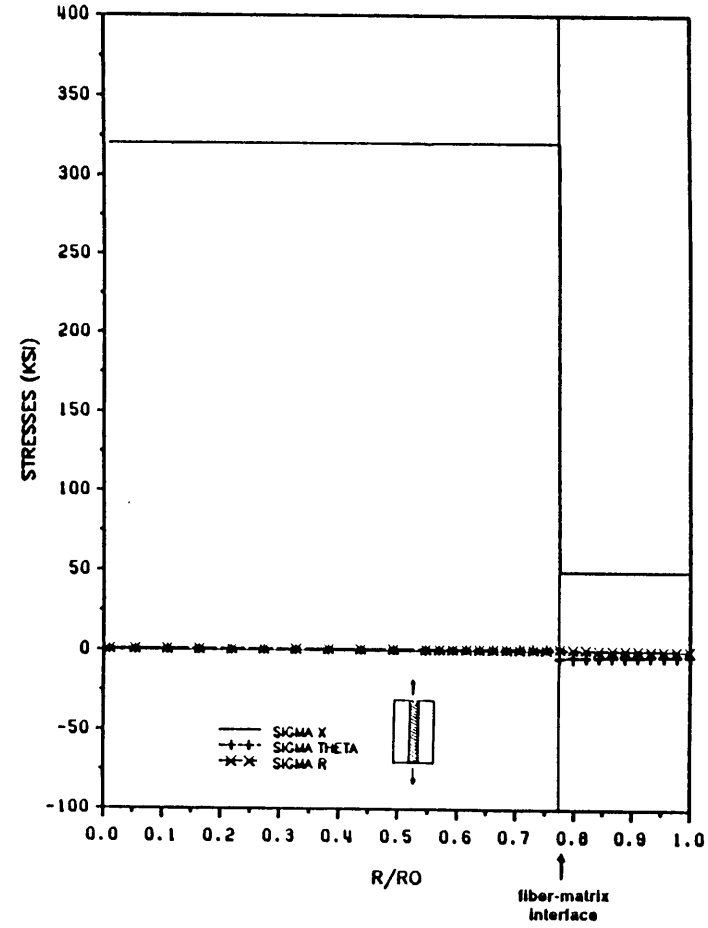

b) 50% transversely isotropic core

Figure 40. Stresses in a composite cylinder with a radially orthotropic hybrid fiber for axial load.

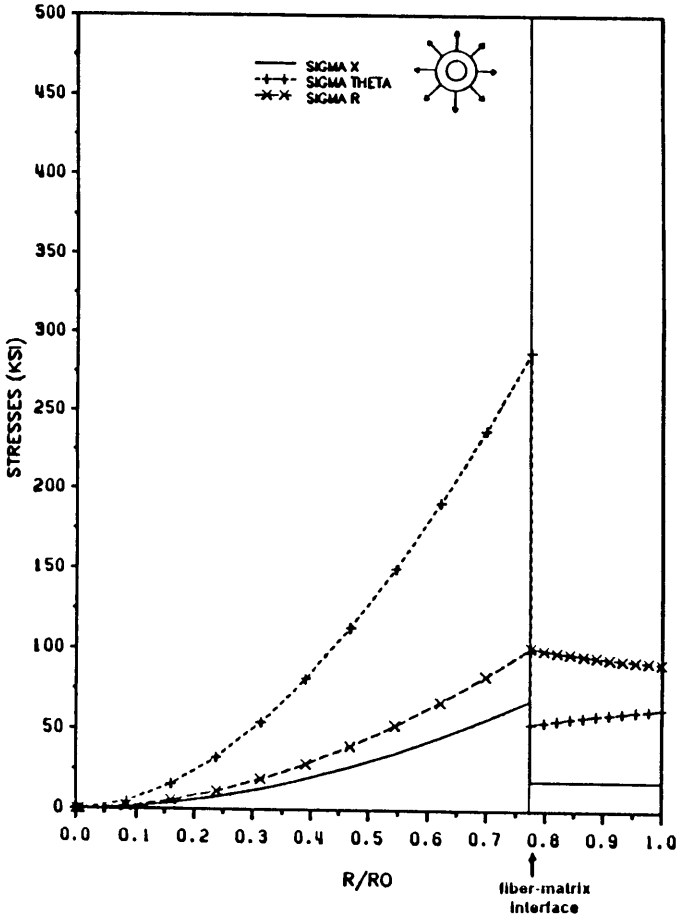

a) 0.01% transversely isotropic core

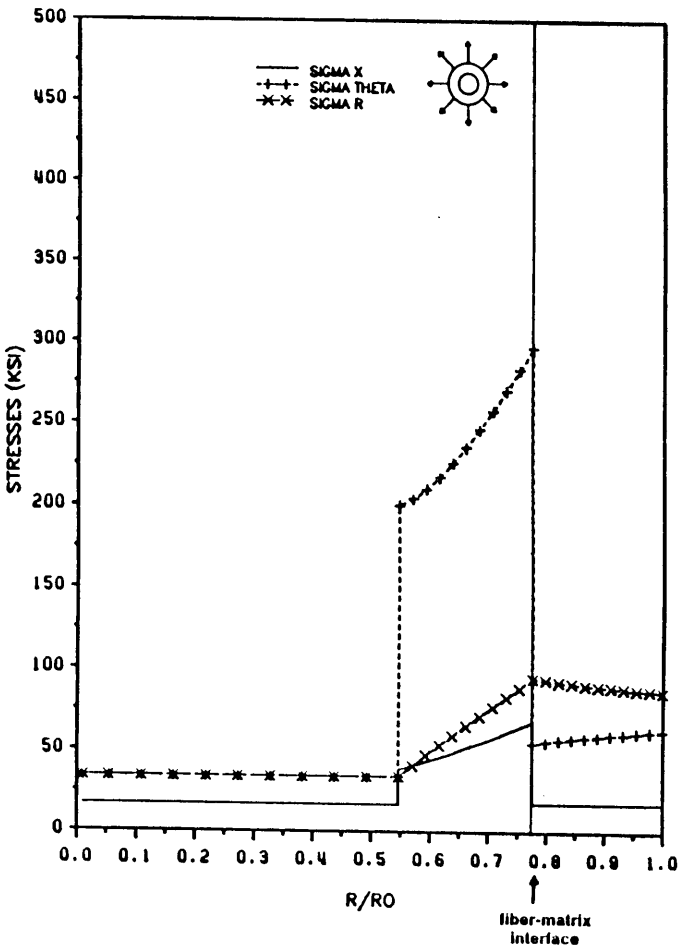

b) 50% transversely isotropic core

Figure 41. Stresses in a composite cylinder with a circumferentially orthotropic hybrid fiber for radial load.

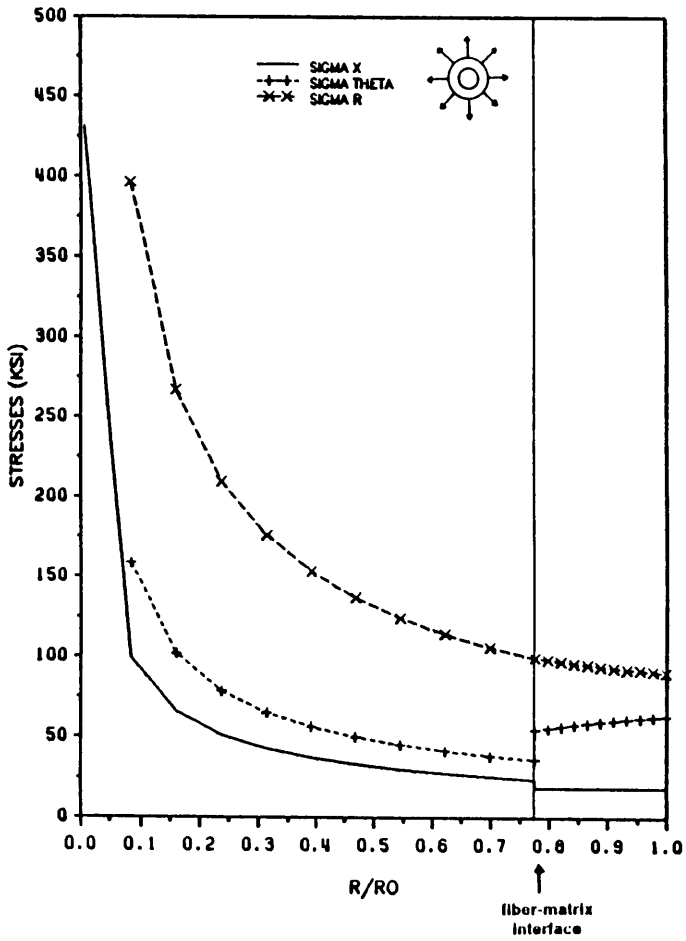

a) 0.01% transversely isotropic core

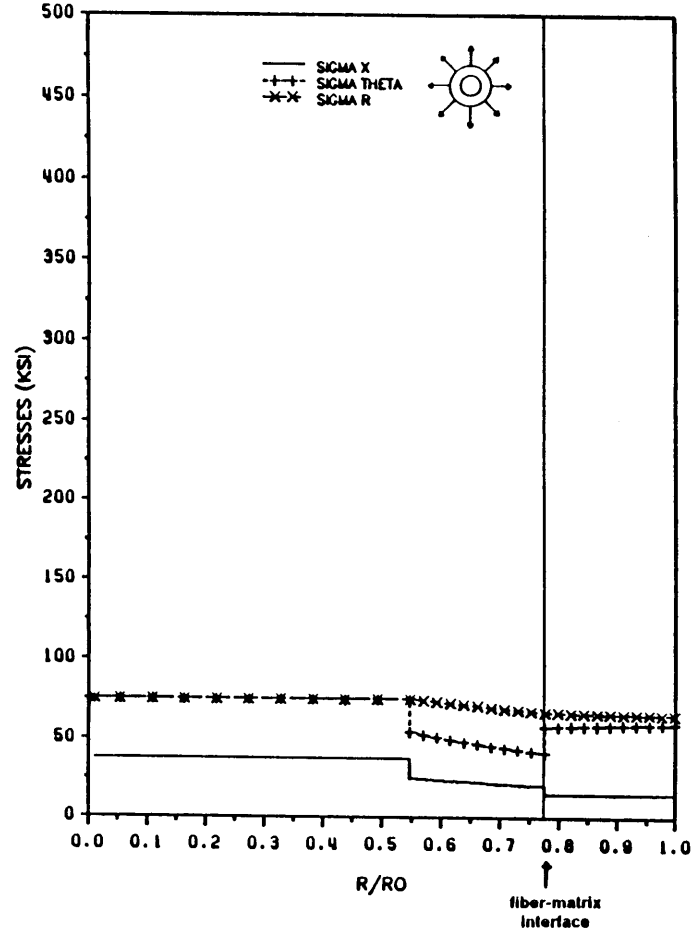

b) 50% transversely isotropic core

Figure 42. Stresses in a composite cylinder with a radially orthtoropic hybrid fiber for radial load.

core. As the core size increases the stresses in the core become more like the stresses in the purely transversely isotropic fiber. In the radially orthotropic fiber, increasing the size of the core reduces the tendency of the stresses near the core in the sheath to rise quickly. In all cases the stresses in the matrix are virtually undisturbed.

4.2.3 Shear Loading

For shear loading recall from Chapter 3 that the composite cylinders with circumferentially orthotropic fibers exhibit singular stresses at the center of the fiber. Inserting a transversely isotropic core into the center of the fiber removes the singularity. With a small transversely isotropic core the gradient of the stresses as $r \rightarrow 0$ is still quite high. As the size of the core increases the stress in the circumferentially orthotropic sheath becomes more stable and the stresses within the core decrease, approaching the stress level in the pure transversely isotropic fiber. Stresses near the fiber-matrix interface and in the matrix are not affected by the size of the transversely isotropic core. In the radially orthotropic fiber the transversely isotropic core does not affect the stress distribution in the fiber. Away from the core region stresses in either type of orthotropic are again unaffected by the core. The distribution of shear stresses in the composite cylinders with hybrid fibers are shown in Figure 43, Figure 44, Figure 45, and Figure 46.

4.2.4 Thermal Loading

A temperature change $\Delta T = 1°F$ causes the stress distributions illustrated in Figure 27 - Figure 31 in simple fibers. The stress distributions resulting in a circumferentially orthotropic

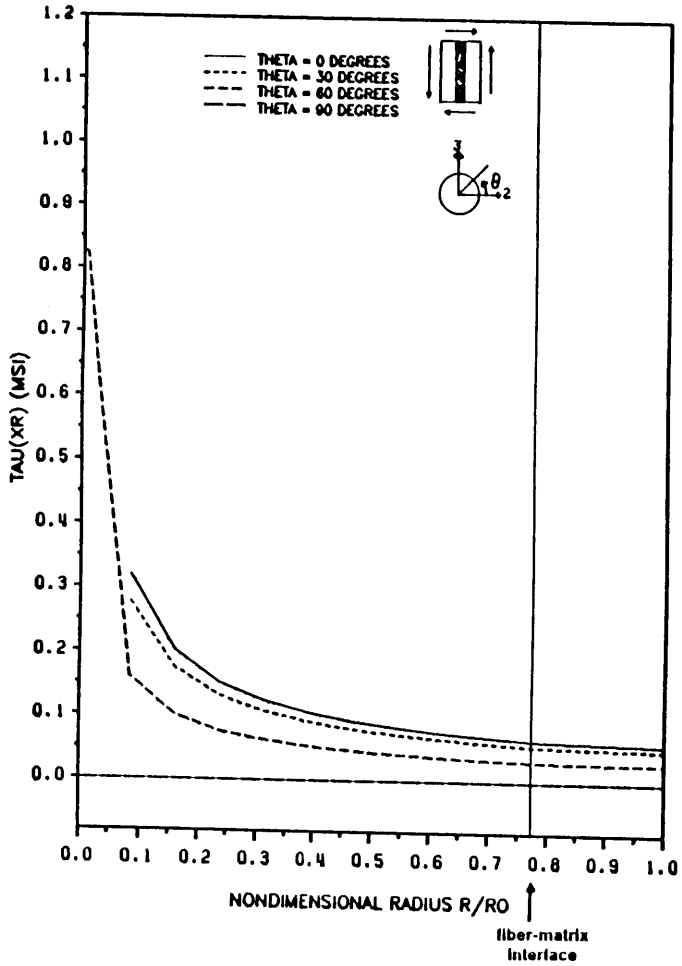

a) 0.01% transversely isotropic core

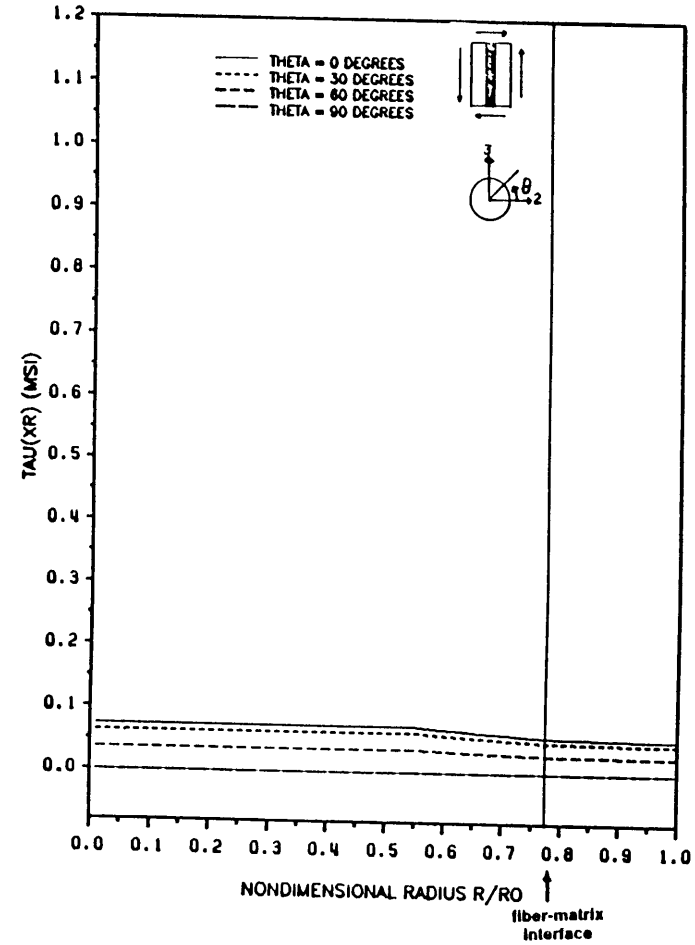

b) 50% transversely isotropic core

Figure 43. Stresses in a composite cylinder with a circumferentially orthotropic hybrid fiber for axial shear.

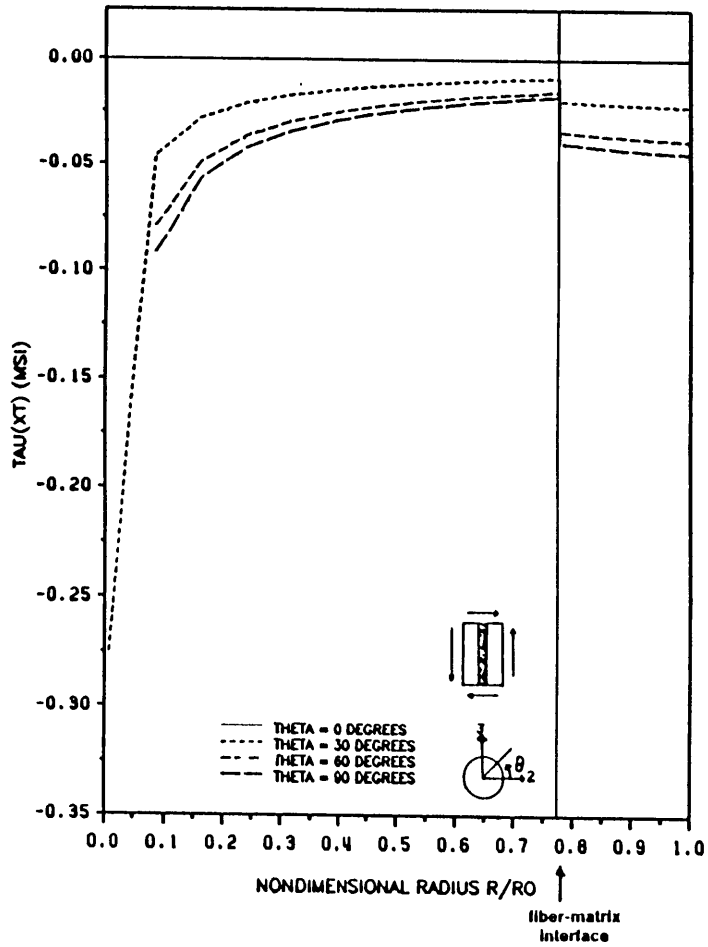

a) 0.01% transversely isotropic core

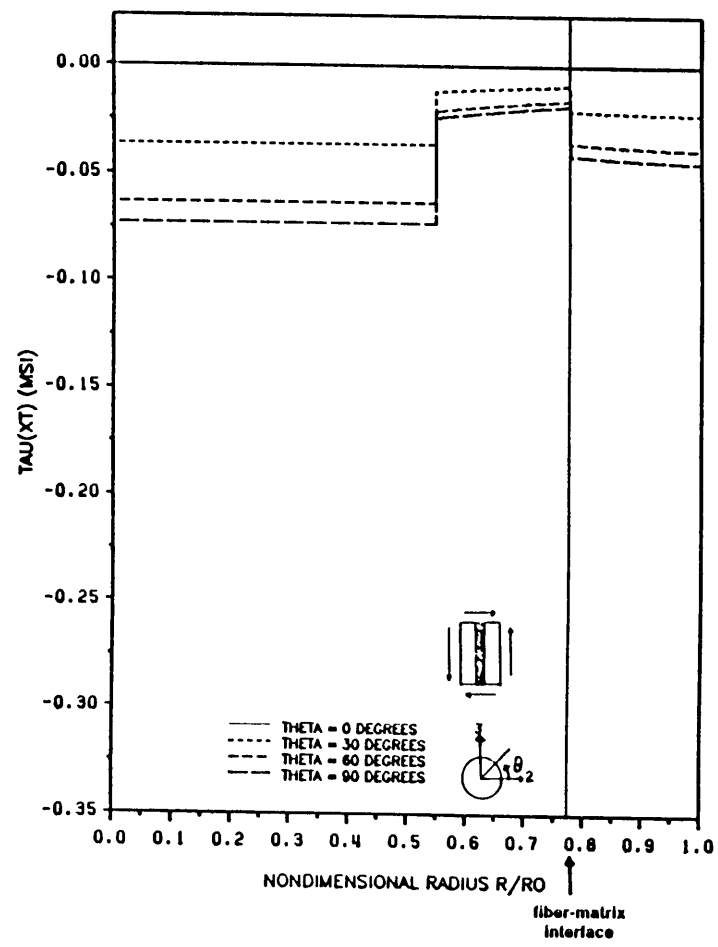

b) 50% transversely isotropic core

Figure 44. Stresses in a composite cylinder with a circumferentially orthotropic hybrid fiber for axial shear.

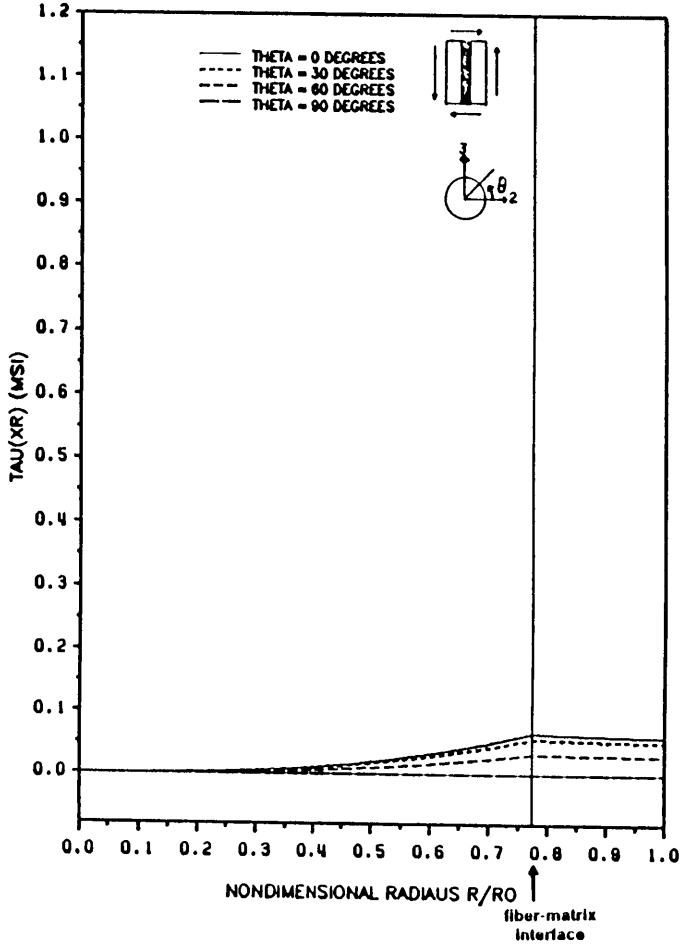

a) 0.01% transversely isotropic core

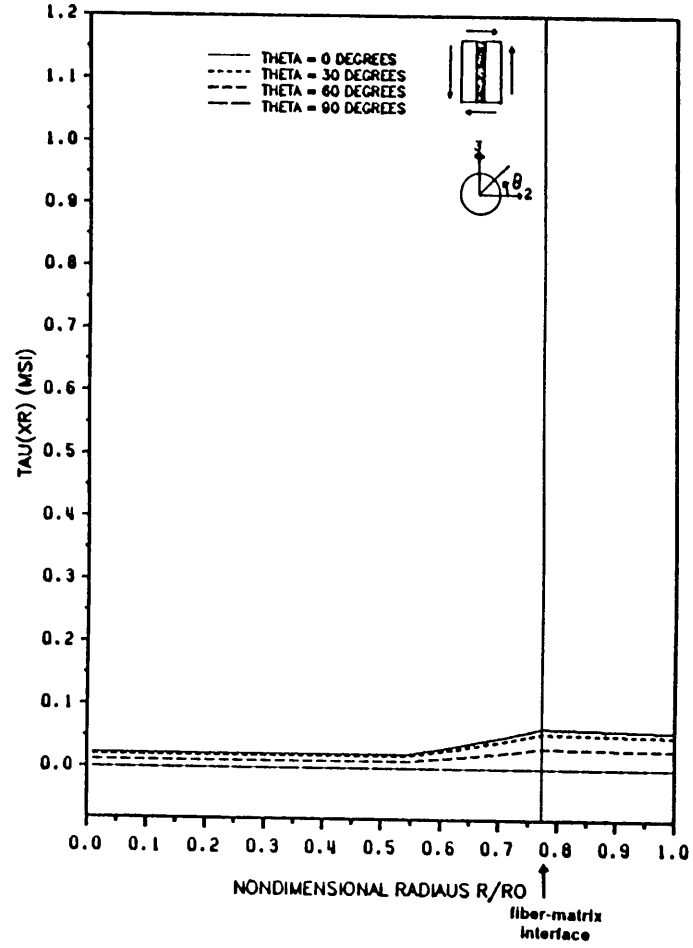

b) 50% transversely isotropic core

Figure 45. Stresses in a composite cylinder with a radially orthotropic hybrid fiber for axial shear.

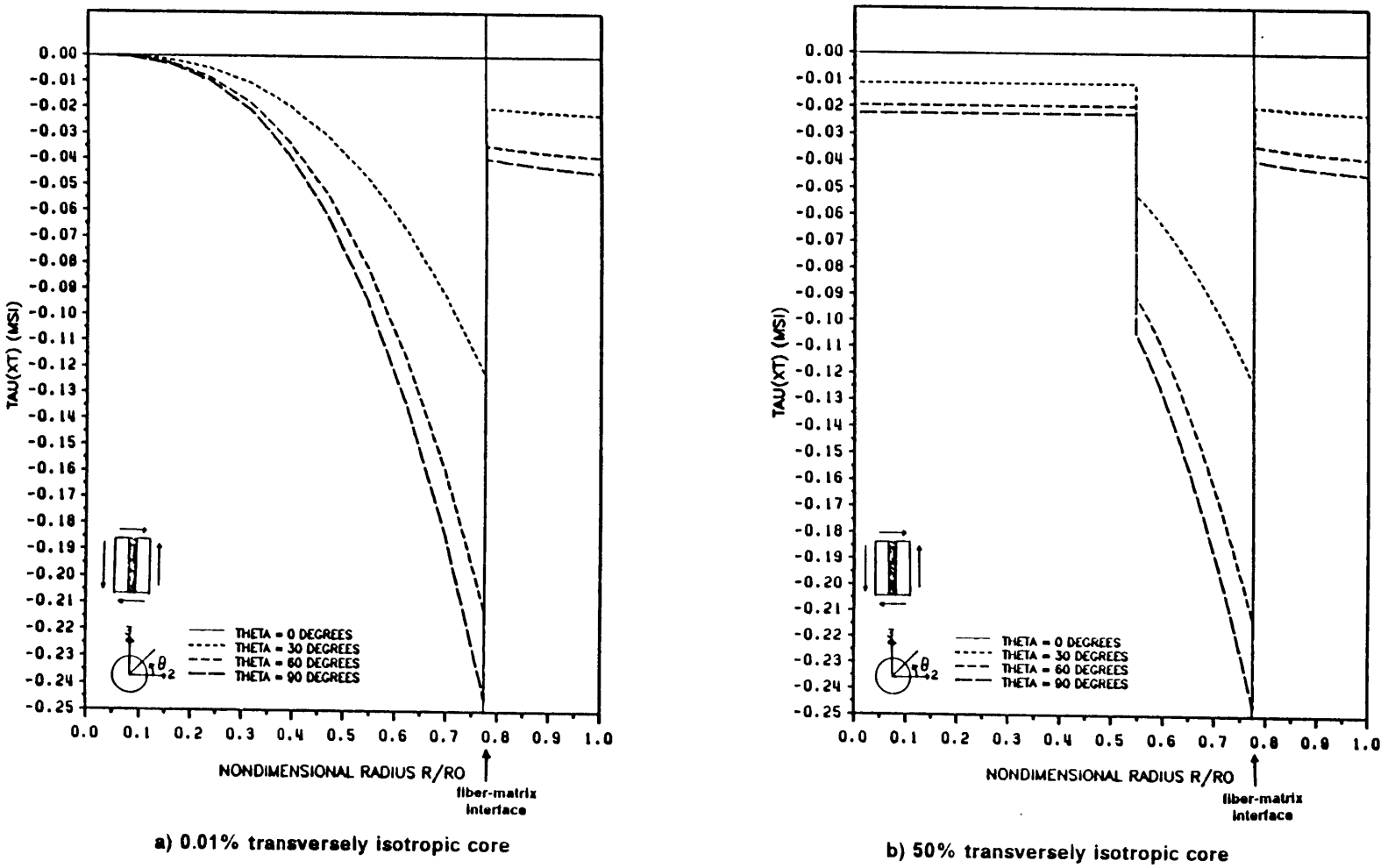

a) 0.01% transversely isotropic core

b) 50% transversely isotropic core

Figure 46. Stresses in a composite cylinder with a radially orthotropic hybrid fiber for axial shear.

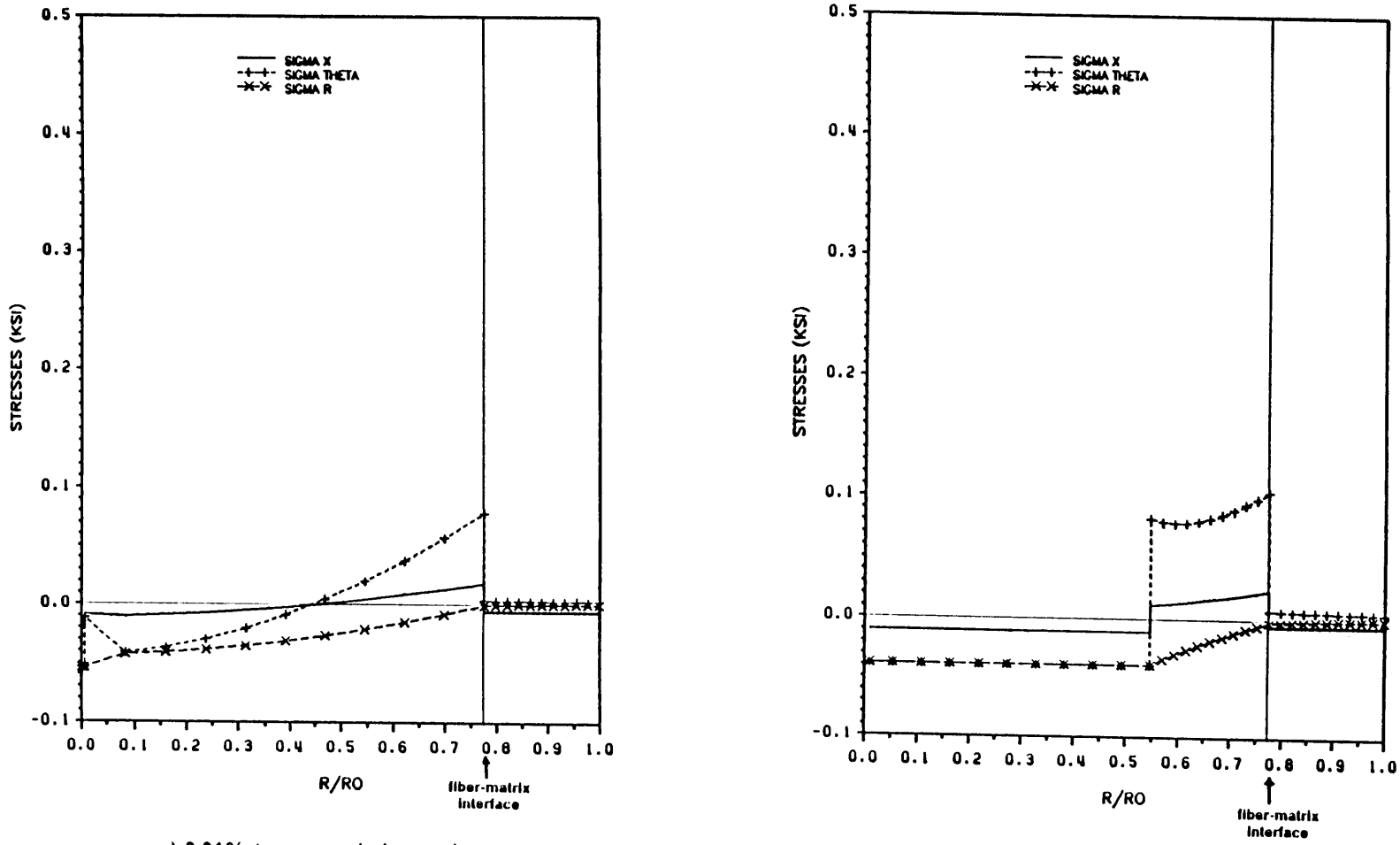

Figure 47. Stresses in a composite cylinder with a circumferentially orthotropic hybrid fiber for thermal loading.

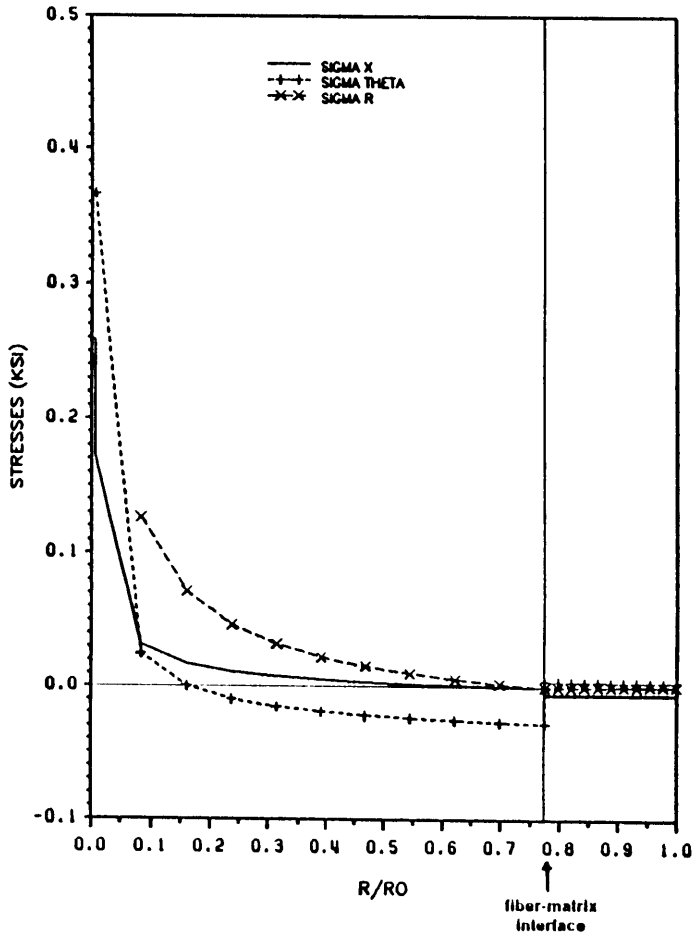

a) 0.01% transversely isotropic core

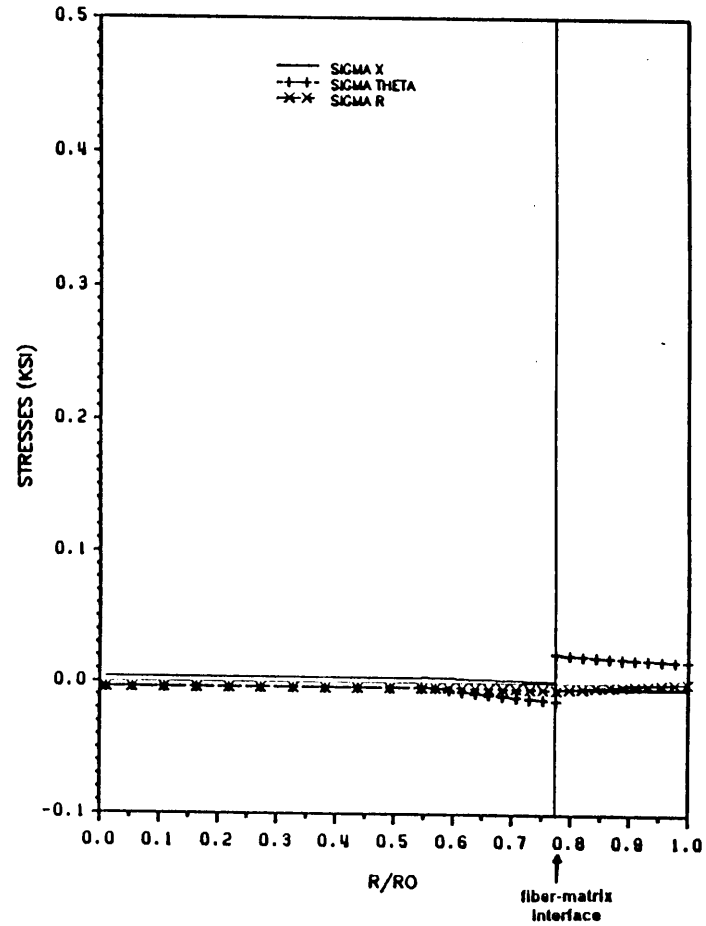

b) 50% transversely isotropic core

Figure 48. Stresses in a composite cylinder with a radially orthotropic hybrid fiber for thermal loading.

composite cylinder with a transversely isotropic core and in a radially orthotropic composite cylinder with a transversely isotropic core are shown in Figure 47 and Figure 48. In the radially orthotropic fibers the transversely isotropic core removes the singularity in the stresses at $r=0$. The smaller the core the higher the stress gradient at the inner radius of the annulus of radially orthotropic fiber. The stresses near the fiber-matrix interface are undisturbed by the presence of a transversely isotropic core. In the circumferentially orthotropic fiber the transversely isotropic core does not effect the stresses near the outer radius of the circumferentially orthotropic fiber or in the matrix. However, near the core region the stresses in the circumferentially orthotropic sheath do not have the same distribution as they would have in a pure circumferentially orthotropic fiber. The behavior of the stresses in the circumferentially orthotropic sheath illustrated in Figure 47 is caused by the change in relative magnitude of the first and second terms in Eqn 4.2 as the radius increases. In the purely circumferentially orthotropic fiber, since $A_2^f = 0$ this behavior is not seen.

4.3 Summary

The existence of a transversely isotropic core in the orthotropic fiber of a composite is beneficial. Under loadings which lead to singular stresses in an ideal circumferentially or radially orthotropic fibers the transversely isotropic core removes the singularity. However, if the core is small, the stress gradients in the fiber near the core are large. As the size of the transversely isotropic core increases the gradient is decreased. In fibers that do not have singular stresses there is essentially no effect of the transversely isotropic core on the stress distribution. In all fibers, the presence of a transversely isotropic core, of any size, does not effect the stress distribution in the matrix.

5.0 Relative Strength

The strength of a composite is a measure of the load that the composite can support before the stress within any phase of the composite exceeds the failure stress of that phase. It was seen in Chapters 3 and 4 that the stresses in the matrix of composite cylinders with orthotropic fibers were not dependent on the fiber morphology. The effect of fiber morphology on composite strength can therefore be addressed by considering only the stresses in the fiber. As discussed in the previous chapter, a real fiber cannot be purely orthotropic, but a transversely isotropic core must exist within the fiber. The relative strength of the circumferentially and radially orthotropic fibers with various sizes of transversely isotropic core and the purely transversely isotropic fiber is discussed in this chapter. The strength of the composite cylinder is analyzed using a maximum stress failure criterion.

The strength of a graphite fiber within the crystal basal plane is denoted X_t. Y_t is the strength of the fiber perpendicular to the basal plane. In all the fibers discussed in this work the basal planes line up along the axis of the fiber. The strength of each fiber in the axial direction is therefore X_t. The strength of the fiber in the transverse plane is dependent on the morphology of the fiber. In the circumferentially orthotropic fiber the basal planes align in an onionskin fashion around the center of the fiber. Thus the strength in the θ direction is X_t, while the strength in the r direction is Y_t. In the radially orthotropic fiber, since the basal planes line

up in a radial fashion the strength in the θ direction is Y_t and in the r direction X_t. In the transversely isotropic core and in a transversely isotropic fiber the basal plane orientation in the transverse fiber plane is random. The strength of the transverse fiber plane in both the r and θ directions in a transversely isotropic phase is denoted Y_{tl}.

The shear strength in the graphite basal plane is denoted S. The shear strength perpendicular to the basal plane is R. Due to the orientation of the basal planes in the circumferentially orthotropic fibers the shear strength in the $x-\theta$ plane is S, and in the x-r plane is R. In the radially orthotropic fiber the strength in the $x-\theta$ plane is R, while the strength in the x-r plane is S. The shear strength of the transversely isotropic fiber or core in both the x-r and $x-\theta$ planes is given by S_{tl}.

The strength of a graphite fiber varies greatly with the fiber precursor and manufacturing process. For the purpose of this study the strength in the basal plane X_t of the fiber is taken to be 200 ksi. Since the chemical bonds within the basal plane are stronger than the bonds between parallel rows of basal planes Y_t is considered to be less than X_t. To cover a range of possible values of Y_t, the ratio X_t/Y_t is varied from 2 to 20. The transverse strength of the transversely isotropic phase is taken to be the arithmetic mean of X_t and Y_t. Therefore, Y_{tl} ranges from 105 ksi to 150 ksi. The shear strength in the basal plane S is taken to be 10 ksi, one twentieth of X_t. The transverse shear strength R is varied from 0.5 ksi to 5 ksi. The shear strength of the transversely isotropic phase is taken to be the arithmetic mean of R and S and varies from 5.25 ksi to 7.5 ksi.

To complete the analysis of strength the compressive strength of the graphite fiber must be considered. For the purpose of this discussion the compressive strength in a given direction will be taken to be the negative of the tensile strength. Although this not likely to be the case it is a reasonable first assumption.

The relative strength of the radially orthotropic, circumferentially orthotropic, and transversely isotropic fibers is presented in terms of the applied load (strain or temperature) that causes the stresses in each phase of the fiber to reach the strength of that phase. This load is easily calculated by setting each stress component equal to the strength of the fiber in the corresponding direction, since the stresses in each phase of the composite cylinder are linear functions of the applied load. The failure load in the circumferentially orthotropic composite cylinder is found by setting

$$\begin{aligned} \sigma_x &= X_t \\ \sigma_\theta &= X_t \\ \sigma_r &= Y_t. \\ \tau_{x\theta} &= S \\ \tau_{xr} &= r \end{aligned} \tag{5.1}$$

Using a maximum stress failure criterion the component of stress which reaches its critical stress at the smallest applied strain will determine the failure mode and the strain at which that component reaches its critical stress is the failure strain. The failure strains in the composite cylinder with radially orthotropic fibers are determined by setting

$$\begin{aligned} \sigma_x &= X_t \\ \sigma_\theta &= Y_t \\ \sigma_r &= X_t. \\ \tau_{x\theta} &= R \\ \tau_{xr} &= S \end{aligned} \tag{5.2}$$

In the transversely isotropic composite cylinders failure strains are determined by setting

$$\begin{aligned} \sigma_x &= X_t \\ \sigma_\theta &= Y_{tl} \\ \sigma_r &= Y_{tl}. \\ \tau_{x\theta} &= S_{tl} \\ \tau_{x\theta} &= S_{tl} \end{aligned} \tag{5.3}$$

Because compressive and tensile strengths are considered to be the same in this study, the failure load for a given stress component is calculated at the radius which leads to the highest magnitude for that component. Results are presented in graphs of strain to failure, ε^f, or temperature to failure, T^f, versus $\frac{X_t}{Y_t}$ or $\frac{S}{R}$, the ratio of strength in the basal plane to strength perpendicular to it. Results for the two types of orthotropic morphologies are presented in separate graphs. The result for a purely isotropic fiber with the same properties as the core of the isotropic fiber (namely TI fiber A from Table 1) are also presented in each figure for comparison.

5.1 Axial Loading

For axial loading the stresses in the axial direction in the fiber are two orders of magnitude greater than the stresses in the transverse plane. Figure 49 and Figure 50 illustrates that the fiber fails by fiber breakage when the axial stress reaches X_t. Because all of the fibers have the same axial strength and the same axial properties, all of the fibers in this study, regardless of the morphology of the fiber fail at the same applied axial load. The only exception to this is the radially orthotropic fiber with a very small transversely isotropic core. Recall that in the radially orthotropic fiber as the transversely isotropic core tends to vanish the stresses in the fiber become singular. For a core size of 0.01% of the fiber volume, the circumferential stress in the orthotropic fiber becomes large enough that for low Y_t, the fiber will fail due to Y_t by splitting before the fiber fails by breaking. As Y_t increases to about 30 ksi ($\frac{X_t}{Y_t} = 8$) the failure mode changes to fiber breaking due to the axial stress. If the size of the transversely isotropic core is increased to 0.07% failure would occur due to X_t by fiber splitting for all values of $\frac{X_t}{Y_t}$ considered.

5.2 Radial Loading

For radial loading the predominant failure mode in the orthotropic fibers is fiber splitting due to Y_t, regardless of the size of the transversely isotropic core as depicted in Figure 51 and Figure 52. In the cylindrically orthotropic fibers this failure corresponds to σ_r reaching Y_t and in the radially orthotropic fibers to σ_θ reaching Y_t. In the cylindrically orthotropic fibers the failure mode switches to fiber splitting due to X_t for $\frac{X_t}{Y_t} < 3$. For small transversely isotropic cores the radially orthotropic fiber has lower strength than a circumferentially orthotropic fiber with the same size core. As the size of the core within the radially orthotropic fiber increases, so does its strength. When the core is 50% of the fiber the radially orthotropic fiber has greater strength than the circumferentially orthotropic fiber with a 50% core. The size of the transversely isotropic core does not affect the strength of the circumferentially orthotropic fiber greatly. For radial loading the orthotropic fibers have lower strength than the purely isotropic fiber.

5.3 Shear Loading

A fiber subjected to axial shear will fail due to R. In the circumferentially orthotropic fiber this corresponds to failure due to τ_{xr} , and in the radially orthotropic fiber to failure due to $\tau_{x\theta}$. The percentage of the fiber that is the transversely isotropic core does not affect the failure mode. However, as the size of the core is increased the strength of the circumferentially orthotropic fiber is increased. The size of the core does not affect the strength of the radially orthotropic fiber. For small cores, the circumferentially orthotropic fiber strength is less than the radially orthotropic fiber strength. For a core size equal to about 5% of the fiber volume the strengths of the two orthotropic fibers are equal. For large cores, the circumferentially orthotropic fiber

has greater strength than the radially orthotropic fiber. The strength of the orthotropic fiber is always less than the strength of a purely transversely isotropic fiber. Failure shear strains are shown in Figure 53 and Figure 54.

5.4 Thermal Loading

Except in the circumferentially orthotropic fiber with a large transversely isotropic core, the failure in an orthotropic fiber subjected to a temperature change is due to fiber splitting when Y_t is exceeded. For $\frac{X_t}{Y_t} > 2.5$, the failure mode in a cylindrically orthotropic fiber with a transversely isotropic core of 50% of the fiber volume switches to fiber splitting due to X_t. The strength of the radially orthotropic fiber is lower than the circumferentially orthotropic fiber when the transversely isotropic core is small. However, as the size of the core increases so does the strength, and for large cores the radially orthotropic fiber is stronger than the circumferentially orthotropic fiber. When the transversely isotropic core is approximately 1% of the fiber volume the strength of the two orthotropic fibers are the same. Regardless of the size of the transversely isotropic core, the orthotropic fibers have lower strength for thermal loading than the purely transversely isotropic fiber. The temperature changes needed to cause the different components of stress to exceed their respective failure level are shown in Figure 55 and Figure 56.

5.5 Summary

In summary, the strength of the composite cylinder with an orthotropic fiber is dependent on the size of the transversely isotropic core if the loading leads to singular stresses in the purely orthotropic fiber. If the stresses within the orthotropic fiber are well behaved (ie., do not become singular even if there is no transversely isotropic core), the size of the transversely isotropic core has no influence on fiber strength. In general the failure mode of the fiber is fiber splitting due to Y_t or R. However in a few instances, namely thermal and radial loading of cylindrically orthotropic fibers with large transversely isotropic cores, the failure mode switches to fiber splitting due to X_t for small $\frac{X_t}{Y_t}$. In the case of axial loading failure is due to fiber breakage except in the radially orthotropic fiber with small core, where fiber splitting due to Y_t is the mode of failure for low Y_t. In no case do the stresses in the transversely isotropic core cause failure before the orthotropic phase of the fiber fails, for the values of X_{ti} considered. In all cases, the purely transversely isotropic fiber has higher strength than either of the orthotropic fibers.

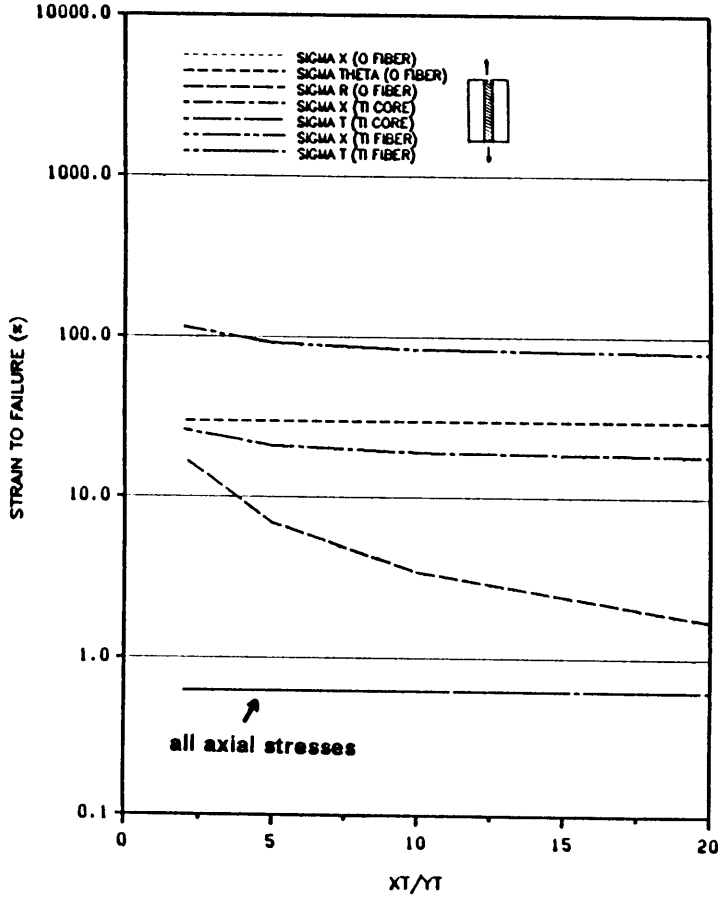

a) 0.01% transversely isotropic core

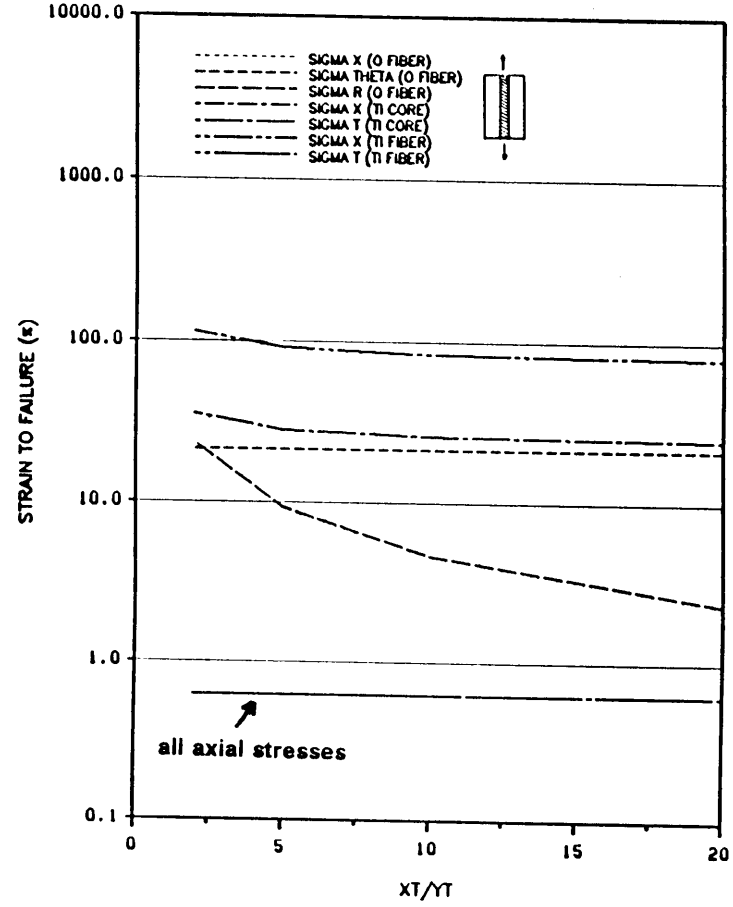

b) 50% transversely isotropic core

Figure 49. Strength of a Composite Cylinder with Circumferentially Orthotropic Fiber under Axial Load.

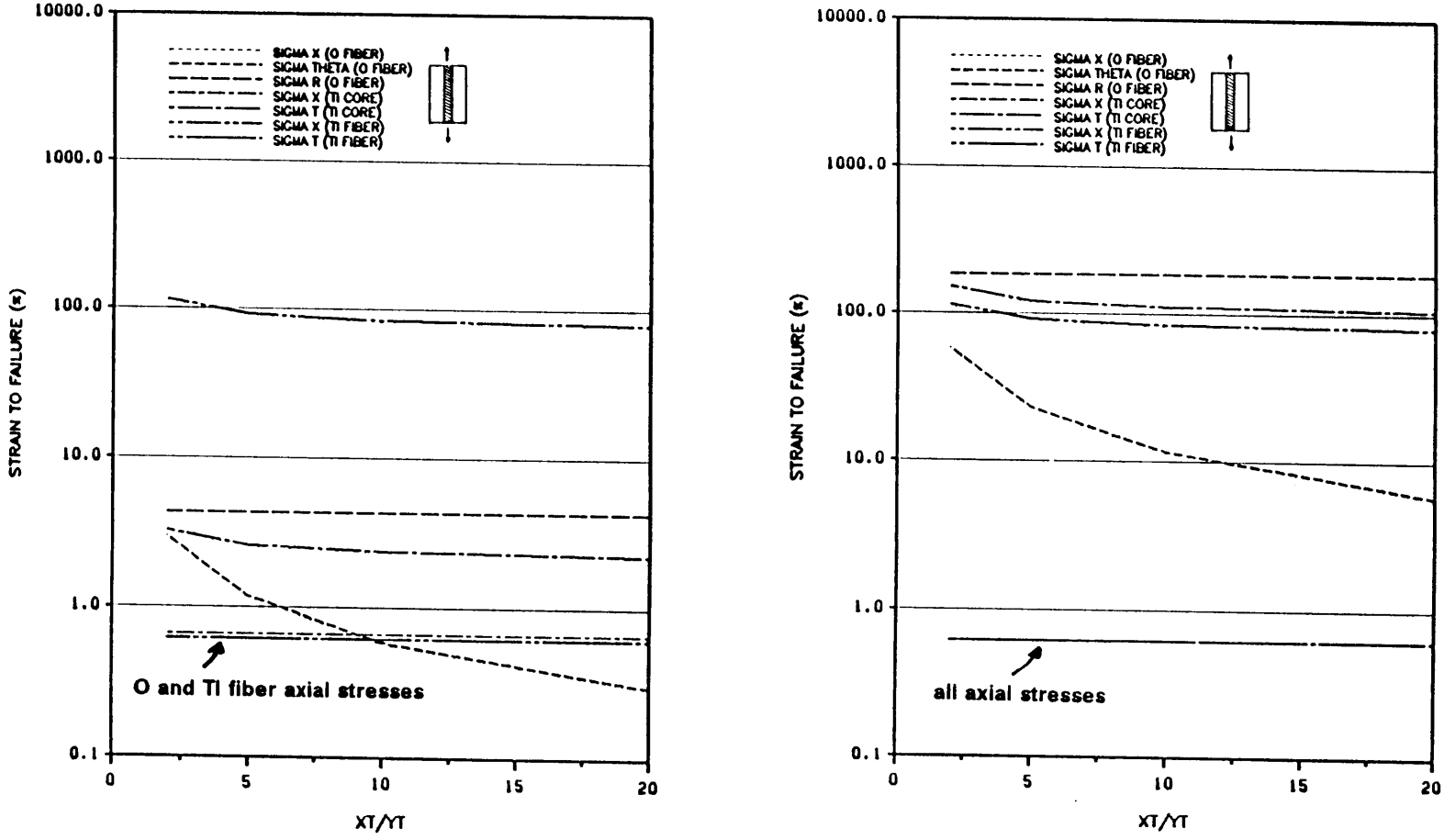

a) 0.01% transversely isotropic core

b) 50% transversely isotropic core

Figure 50. Strength of a Composite Cylinder with Radially Orthotropic Fiber under Axial Load.

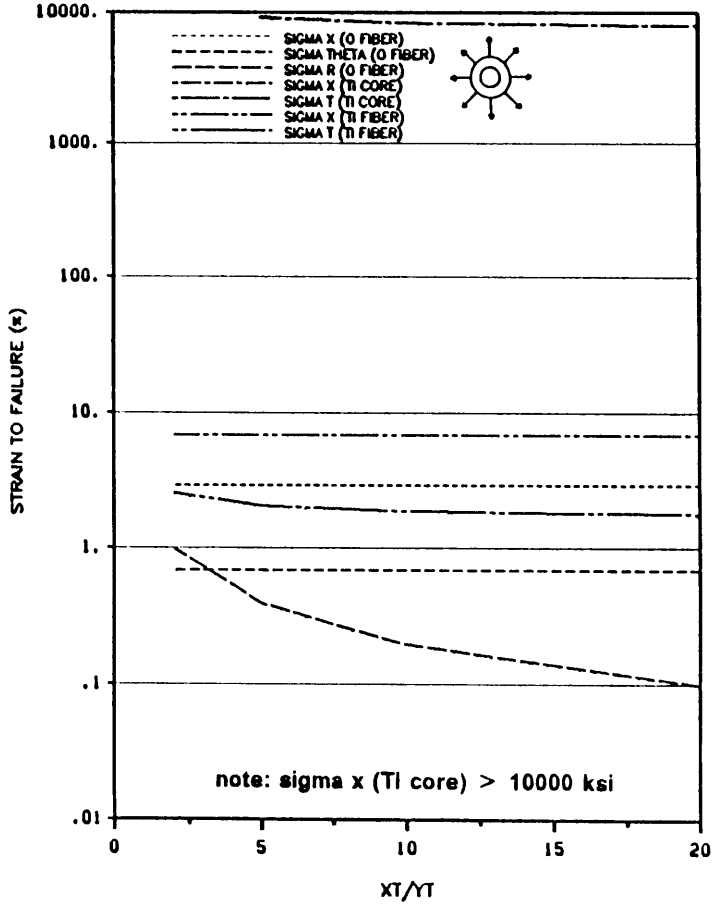

a) 0.01% transversely isotropic core

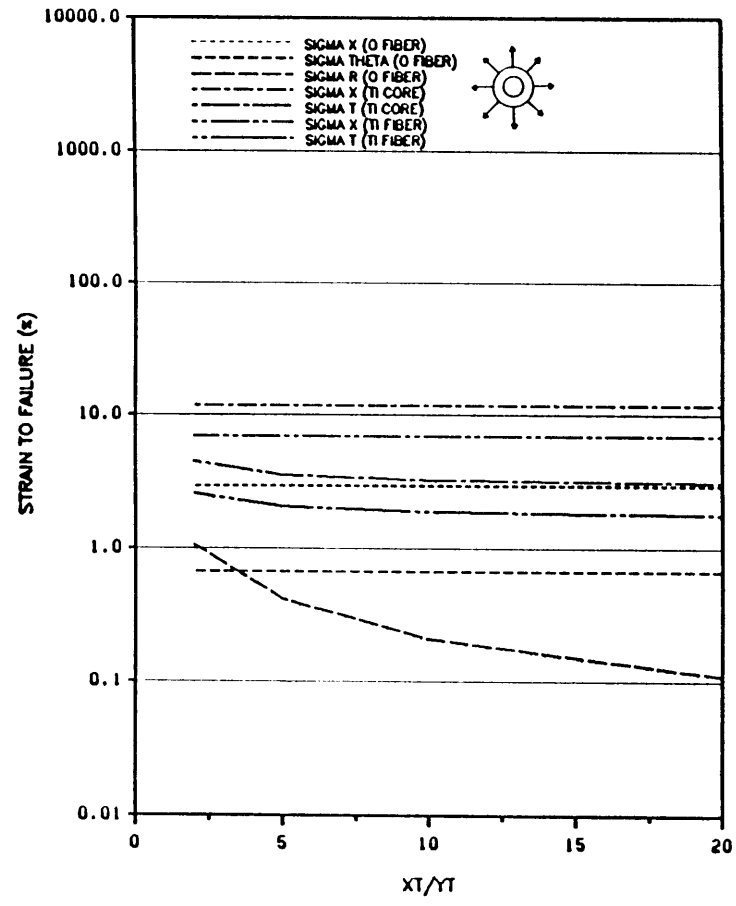

b) 50% transversely isotropic core

Figure 51. Strength of a Composite Cylinder with Circumferentially Orthotropic Fiber under Radial Load.

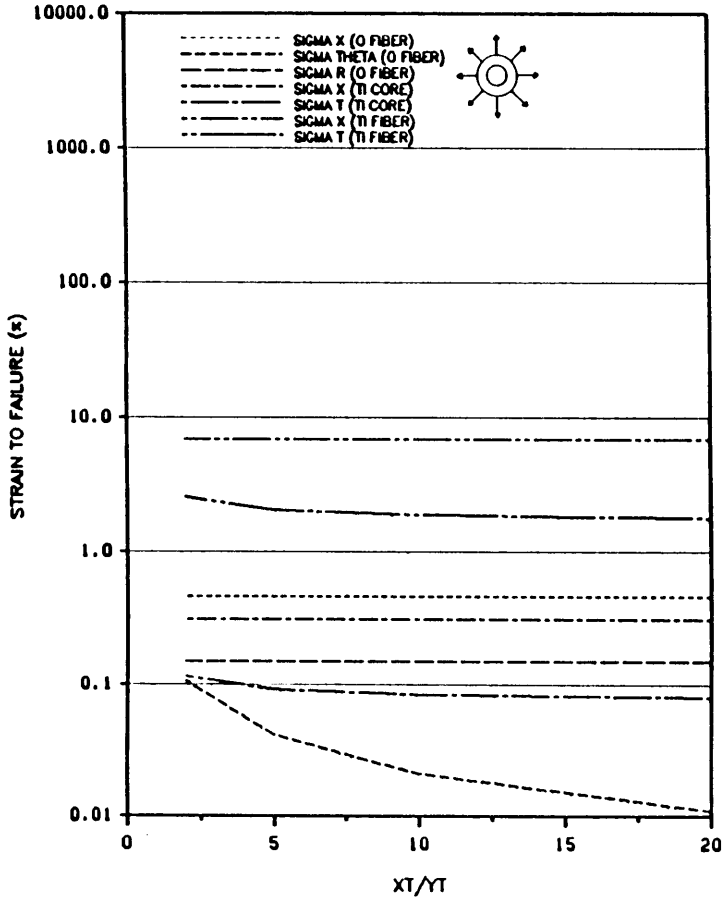

a) 0.01% transversely isotropic core

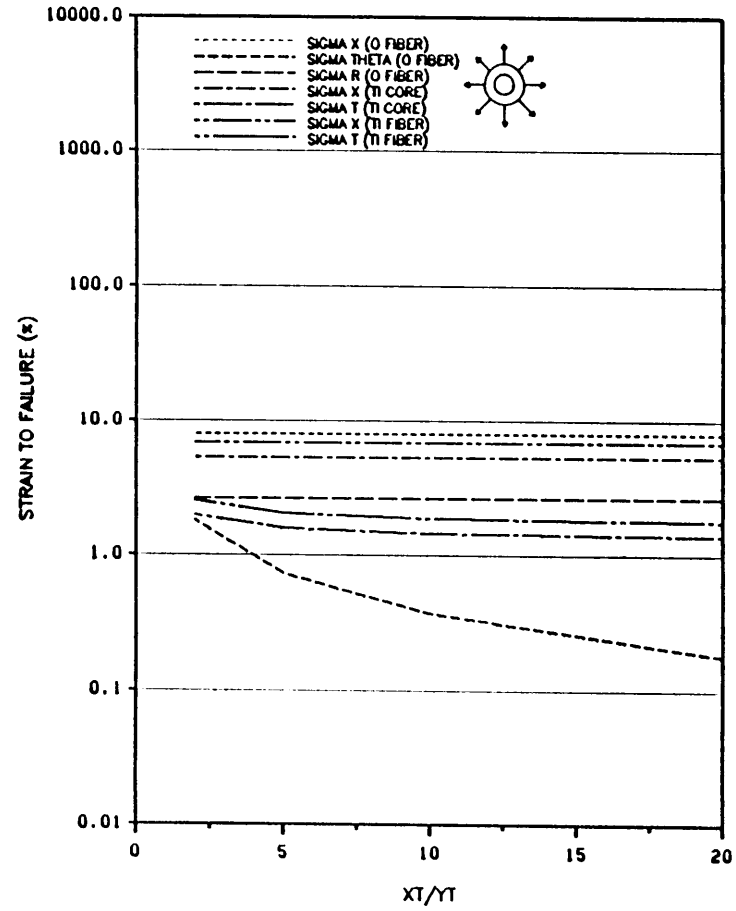

b) 50% transversely isotropic core

Figure 52. Strength of a Composite Cylinder with Radially Orthotropic Fiber under Radial Load.

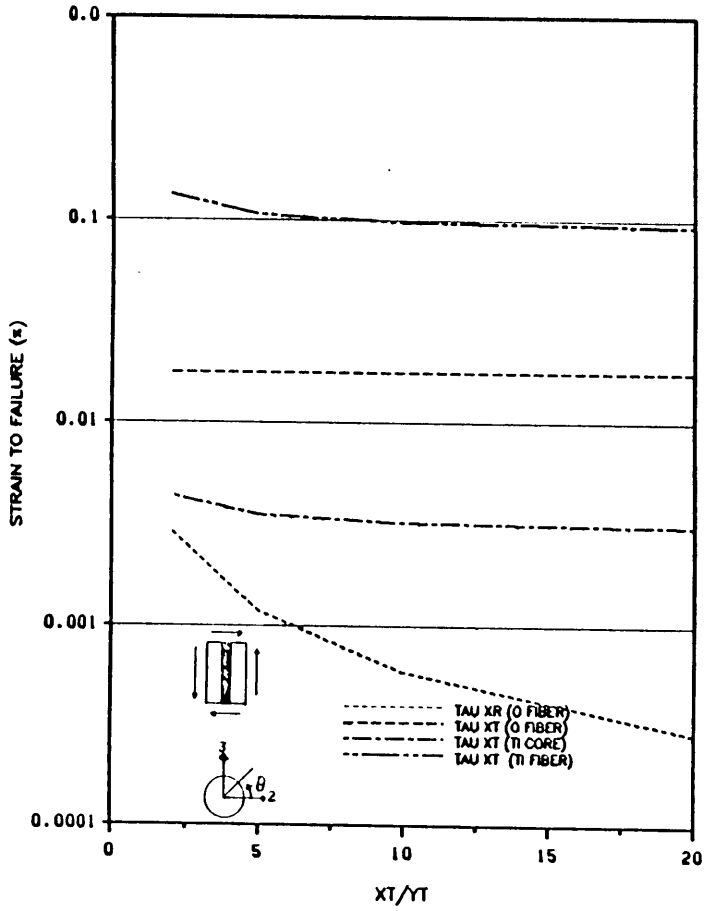

a) 0.01% transversely isotropic core

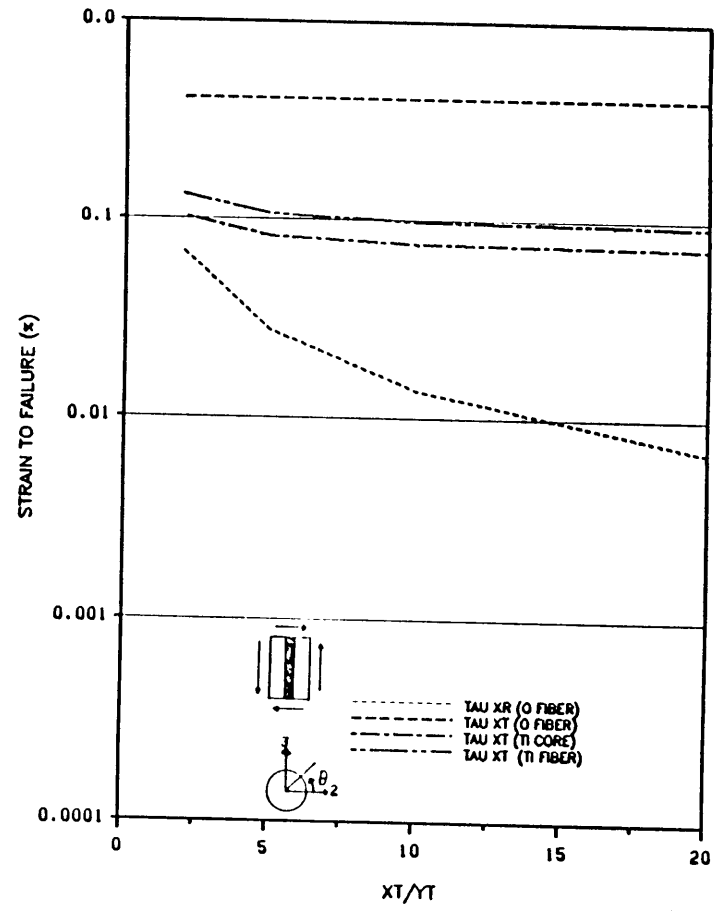

b) 50% transversely isotropic core

Figure 53. Strength of a Composite Cylinder with Circumferentially Orthotropic Fiber under Axial Shear Load.

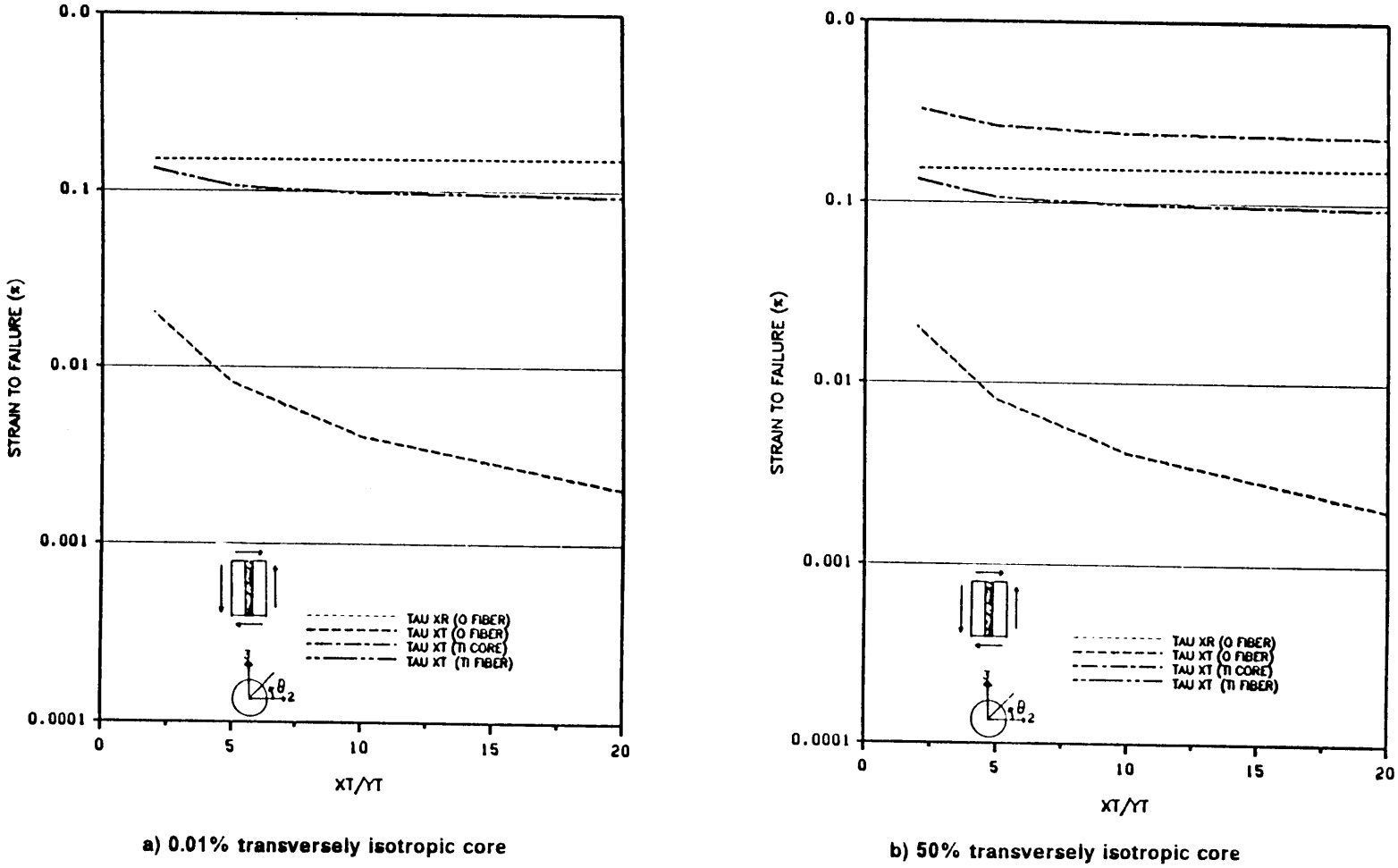

a) 0.01% transversely isotropic core

b) 50% transversely isotropic core

Figure 54. Strength of a Composite Cylinder with Radially Orthotropic Fiber under Axial Shear Load.

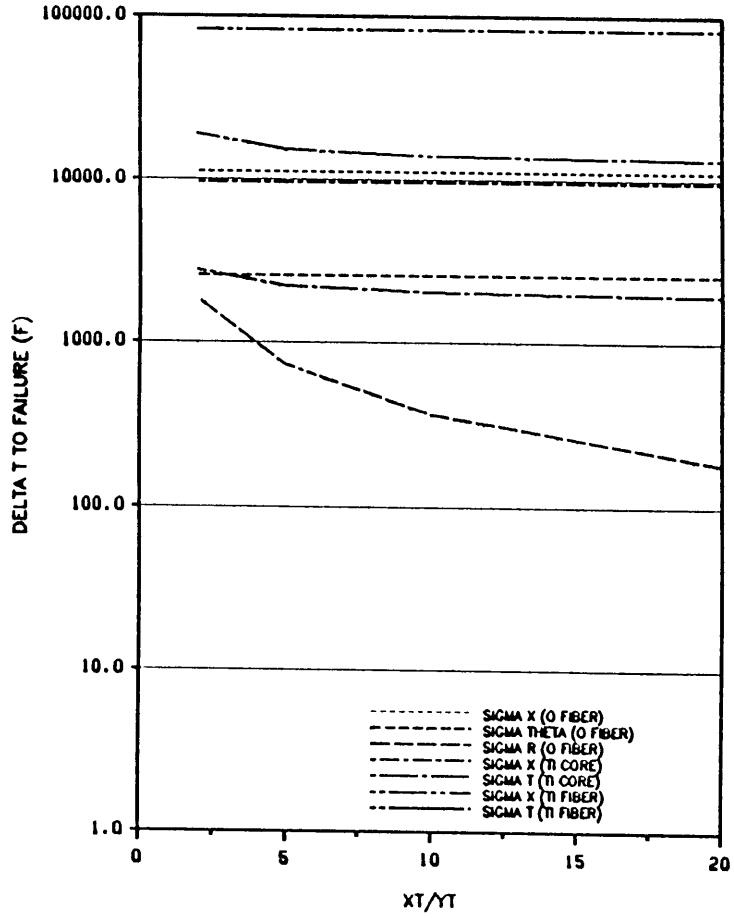

a) 0.01% transversely isotropic core

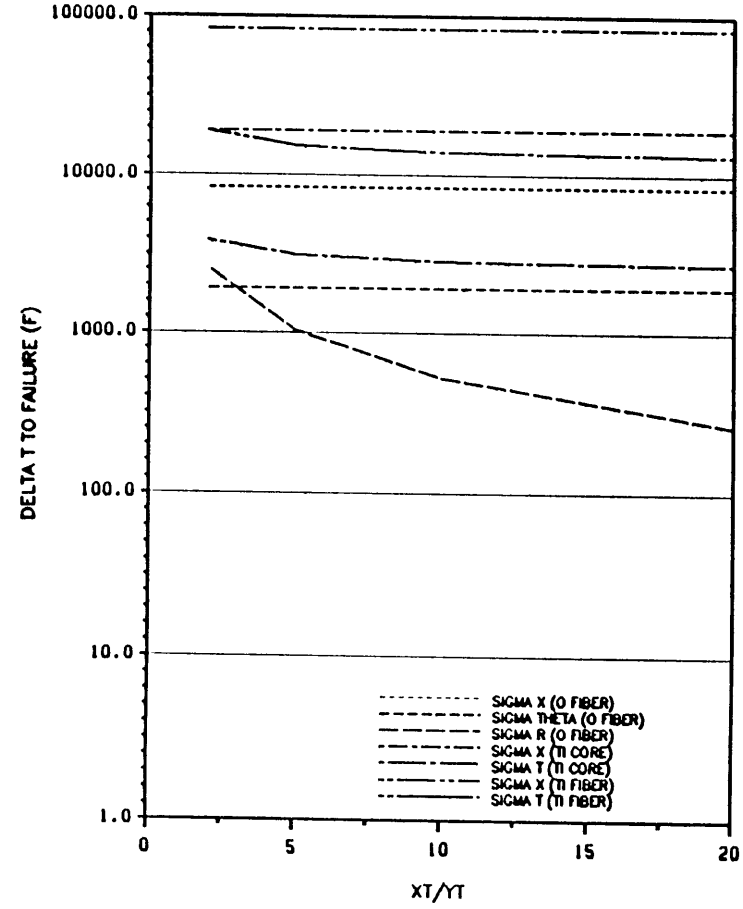

b) 50% transversely isotropic core

Figure 55. Strength of a Composite Cylinder with Circumferentially Orthotropic Fiber under Thermal Load.

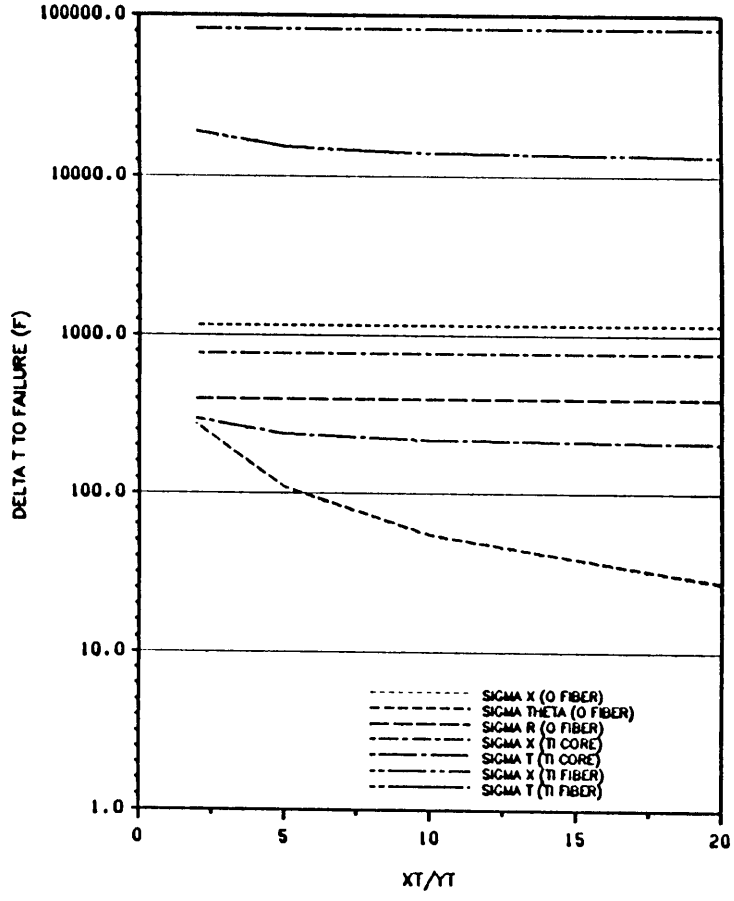

a) 0.01% transversely isotropic core

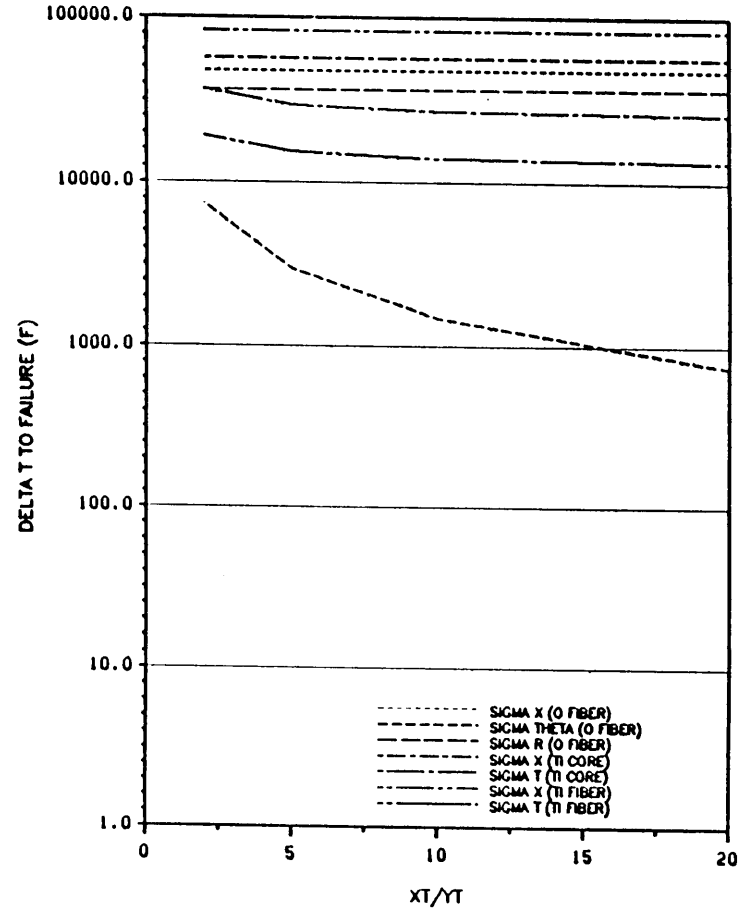

b) 50% transversely isotropic core

Figure 56. Strength of a Composite Cylinder with Radially Orthotropic Fiber under Thermal Load.

6.0 Conclusions

This study examined the effects of fiber morphology on the effective moduli of a composite material using the composite cylinder assemblage model. The effect of the morphology on the state of stress within a composite cylinder was also studied. Based on the state of stress within the composite cylinder the effect of fiber morphology on composite strength was also examined. The following conclusions may be drawn as a result of this study.

- Effect of fiber morphology on composite properties

    - For ideal orthotropic fibers with no transversely isotropic core, the radial and circumferential orthotropy of the fiber have the same effect on the properties of the composite. Transverse isotropy has a different effect.

    - For orthotropic fibers with a transversely isotropic core the properties of the composite are affected by the morphology of the sheath and the size of the core.

    - The effective axial modulus, transverse bulk modulus, and axial shear modulus decrease with increasing transversely isotropic core size. This effect is more pro-

nounced in the radially orthotropic fiber for E_A and k, and more pronounced in the circumferentially orthotropic fiber for G_A.

- The axial Poisson's ratio and the coefficients of thermal expansion increase with increasing core size. This effect is more pronounced in the radially orthotropic fibers.

- Effect of fiber morphology on stress distributions

  - Stress distributions within a composite cylinder are greatly affected by the morphology of the fiber.

  - For axisymmetric loads the stresses in the ideal radially orthotropic fiber at $r=0$ are singular.

  - For axial shear the stresses in the ideal cylindrically orthotropic fiber at $r=0$ are singular.

  - The presence of a transversely isotropic core in the orthotropic fiber removes the singular stresses at $r=0$. For small cores the gradient in the stresses as $r \rightarrow 0$ is high.

  - The stress distribution in the cylindrically orthotropic fiber for axisymmetric loads and in the radially orthotropic fiber for shear load is preserved within the sheath of the orthotropic fiber with a transversely isotropic core. As the size of the core increases the stresses within the core approach the level of stress in the purely transversely isotropic fiber.

- Effect of fiber morphology on strength.

The morphology of the sheath affects the strength of the composite cylinder as does the size of the transversely isotropic core.

- In the cylindrically orthotropic fiber for axial, radial, and thermal loads, and in the radially orthotropic fiber for axial shear loads, the size of the transversely isotropic core does not affect the strength of the fiber.

- In the radially orthotropic fiber for axial, radial, and thermal loads and in the circumferentially orthotropic fiber for shear load, the size of the transversely isotropic core does affect the strength of the composite cylinder. As the size of the core increases so does the strength.

- The orthotropic fibers have lower strength than the purely transversely isotropic fiber.

- The mode of failure in all fibers for axial load is fiber breaking, except in the radially orthotropic fiber with a small core in which case the mode of failure is fiber splitting.

- The mode of failure in all fibers for radial, shear, or thermal load is fiber splitting in the orthotropic sheath. Except in the thermal and radial loading of circumferentially orthotropic fibers with large transversely isotropic cores the fiber splitting is caused by Y_t rather than X_t.

7.0 References

1 Brydges, W.T., Badami, D.V., Joiner, J.C., and Jones, G.A., "The Structure and Elastic Properties of Carbon Fibers" *Applied Polymer Symposia*, vol. 9, pp. 255-261.

2 Otani, S., and Oya, A., "Status Report on Pitch-Based Carbon Fiber in Japan" *Composites '86: Recent Advances in Japan and the United States* K. Kawata, S. Umekawa, and A. Kobayashi, Ed., Proc. Japan-U.S. CCM-III, Tokyo, 1986.

3 Johnson, D.J., "Structure and Physical Properties of Carbon Fibers" *Chemistry and Industry*, 18 Sept. 1982, pp. 692-698.

4 Deifendorf, R.J., and Tokarsky, E., "High Performance Carbon Fibers" *Polymer Engineering and Science*, vol. 15, No. 3, pp. 150-159.

5 Wicks, B.J., and Coyle, R.A., "Microstructural Inhomogeneity in Carbon Fibers" *Journal of Materials Science*, vol. 11, pp. 376-383.

6 Barnet, F.R., and Norr, M.K., "A Three-Dimensional Structural Model for a High Modulus Pan-Based Carbon Fiber" *Composites* April 1976, pp. 93-99.

7 Guigon, M., and Oberlin, A., "Structure and Microtexture of some Pitch-Base Fibers" *Extended Abstracts and Program of the 16th Biennial Conference on Carbon*, p. 513.

8 Sawada, Y., and Shindo, A., "Torsional Behavior of Carbon Fibers" *??International Symposium on Carbon, Japan*, 1982.

9 Stewart, M., and Feughelamn, M., "Morphology of Carbon Fibers" *Nature*, vol. 4, p. 274.

10 Chamis, C. C. and Sendeckyj, G. P., "Critique on Theories Predicting Thermoelastic Properties of Fibrous Composites" *Journal of Composite Materials* vol. 2, no. 3, 1968, pp.332-358.

11 Christensen. R. M., *Mechanics of Composite Materials* John Wiley and Sons, Inc., 1979.

12 Hashin, Z., and Rosen, B. W., "The Elastic Moduli of Fiber-Reinforced Materials" *Journal of Applied Mechanics* June, 1964, pp.223-232.

13 Hashin, Z. *Theory of Fiber Reinforced Materials*, NASA CR-1974, March 1974.

[14] Hill, R., "A Self-Consistent Mechanics of Composite Materials," *Journal of the Mechanics and Physics of Solids,* vol. 16, 1965. pp. 213-222.

[15] Budiansky, B., "On the Elastic Moduli of Some Heterogeneous Materials," *Journal of the Mechanics and Physics of Solids,* vol. 13, 1965, pp. 223-227.

[16] Christensen, R.M., and Lo, K.H., "Solutions For Effective Shear Properties in Three Phase Sphere and Cylinder Models" *Journal of Mechanics and Physics of Solids,* vol. 27, pp. 315-330.

[17] Oshima, N. and Nomura, S., "A Method to Calculate Effective Modulus of Hybrid Composite Materials" *Journal of Composite Materials* vol. 19, 1985, pp.287-293.

[18] Aboudi, J. "A Continuum Theory for Fiber-Reinforced Elastic-Viscoplastic Composites" *International Journal of Engineering Science* vol. 20, no. 5, 1982, pp.605-621.

[19] Adams, D. F., and Doner, D. R., "Transverse Normal Loading of a Unidirectional Composite" *Journal of Composite Materials* vol. 1, 1967, pp.152-164.

[20] Adams, D. F., and Doner. D. R., "Longitudinal Shear Loading of a Unidirectional Composite" *Journal of Composite Materials* vol. 1, 1967, pp.4-17.

[21] Lekhnikskii, S.G., "Theory of Elasticity of an Anisotropic Body," 1950, Moscow, (Mir Publishers, 1981).

[22] Lekhnikskii, S.G., "Anisotropic Plates," 1957, Moscow, translations by Foreign Technology Division, Air Force Systems Command, FTD-HT-23-608-67.

[23] Cohen, D. and Hyer, M.W., "Residual Thermal Stresses in Cross-Ply Graphite-Epoxy Tubes," *Advances in Aerospace Sciences and Engineering* Eds. U Yuceoglu and R. Hesser, ASME Publication AD-08, 1984.

[24] Cohen, D. and Hyer M.W., "Residual Stresses in Cross-Ply Composite Tubes," CCMS-84-04, VPI&SU, Blacksburg, VA. 1984.

[25] Cohen, D., Hyer, M.W., and Tompkins, S.S., "The Effect of Thermal Cycling on Matrix Cracking and Stiffness Changes in Composite Tubes," CCMS-84-12, VPI&SU, Blacksburg, VA. 1984.

[26] Rousseau, C.Q., Hyer, M.W., and Tompkins, S.S., "Stresses and Deformations in Angle-Ply Composite Tubes" CCMS-87-04, VPI&SU, Blacksburg, VA. 1987.

[27] Avery, W.B., and Herakovich, C.T., "Effect of Fiber Anisotropy on Thermal Stresses in Fibrous Composites" *Journal of Applied Mechanics,* vol.53, 1986, pp. 751-756.

[28] Bowles, David, Personal Communication, Coefficients of thermal expansion of composites with transversely isotropic fibers.

The vita has been removed from the scanned document